Aalto University
School of Engineering

Sami Vallin

Modelling and optimization study on a high-temperature borehole thermal energy storage concept driven by power plant waste heat

Master's programme in Advanced Energy Solution – Sustainable Energy Conversion Processes

Master's thesis for the degree of Master of Science in Technology submitted for inspection.
Espoo, 27th August 2019

Supervisor: Ville Vuorinen
Advisor: Teppo Arola

Aalto University
School of Engineering

Aalto University, P.O. BOX 11000, 0076 Aalto
www.aalto.fi

Abstract of master's thesis

Author Sami Vallin

Title Modelling and optimization study on a high-temperature borehole thermal energy storage concept driven by power plant waste heat

Degree program Advanced Energy Solutions – Sustainable Energy Conversion Processes

Thesis supervisor Prof. Ville Vuorinen

Thesis advisor Dr. Teppo Arola

Date 27.8.2019	**Pages** 71+25	**Language** English

High-temperature borehole thermal energy storage has potential to increase energy conservation and therefore, decrease the amount of waste heat. Among the existing seasonal thermal energy storage technologies, borehole thermal energy storage is one of the most price-competitive and mature technology. Borehole thermal energy storage enables power plant to store waste heat during summer for later use during high demand winter season with efficiency of 40–65 %.

The effect of borehole spacing and length on the performance of borehole thermal energy storage has not been explored. This master's thesis studies how borehole spacing and depth affects large-scale storage performance and investment cost. In order to study the effect, a numerical model, based on the method proposed by Al-Khoury and Bonnier (2006), is created using COMSOL Multiphysics software. In the method, fluid flow is modelled in a single U-tube pipe in a one-dimensional (1D) heat pipe element and heat transfer in bedrock is in the three-dimensional (3D) domain.

In total, this study included 21 research cases. The created model was simulated with seven borehole spacings and three different ratios of storage width to height. Based on information found in the literature borehole spacing was varied at 0.5 meters interval from 2.0 m to 5.0 m. The storage width to depth –ratios used were 1.0, 0.67 and 0.5.

The results of this master's thesis indicate that the most economically optimal borehole spacing should be based on the determination of the optimal storage temperature drop and extraction of energy during discharging period within time t. Therefore, optimal spacing should be chosen based on the thermal properties of the storage medium, charging and discharging inlet temperatures of the fluid, required injected and extracted energy, and the length of the time period within which the power needs to be charged or discharged. Deeper boreholes do not seem to have a significant effect on storage performance or investment cost; however, this study did not consider increased heat losses due to suboptimal storage shape.

Based on simulation results, the same capacity (4.46 GWh) may cost 1.5 million € more in suboptimal case than in the optimal one (=550 boreholes, borehole spacing 3.5 m and depth 172 m). The BTES solution modelled in this thesis has the potential to yield 2-5 MW thermal energy continuously and 10 MW thermal energy for one-hour peaks.

Keywords: High-temperature borehole thermal energy storage, borehole heat exchangers, bedrock, underground heat, heat transfer, fluid flow, COMSOL Multiphysics

Aalto-yliopisto
Insinööritieteiden
korkeakoulu

Aalto yliopisto, PL 11000, 0076 Aalto
www.aalto.fi

Diplomityön tiivistelmä

Tekijä Sami Vallin		
Työn aihe Voimalaitoksen hukkalämmöllä toimivan korkean lämpötilan porareikälämpövaraston mallinnus- ja optimointitutkimus		
Maisteriohjelma Advanced Energy Solutions – Sustainable Energy Conversion Processes		
Työn valvoja prof. Ville Vuorinen		
Työn ohjaaja FT Teppo Arola		
Päivä 27.8.2019	**Sivut** 71+25	**Kieli** Englanti

Korkean lämpötilan porareikälämpövarastoratkaisulla voidaan parantaa energiatehokkuutta, sillä ratkaisu vähentää tuotetun hukkalämmön määrää. Porareikälämpövarasto on tällä hetkellä yksi kustannustehokkaimmista ja kehittyneimmistä kausilämpövarasto-teknologioista. Kesällä hukkalämpöä voidaan varastoida porareikälämpövarastoon, ja se voidaan hyödyntää talvella korkeamman kysynnän aikaan n. 40-65 % hyötysuhteella.

Porareikien syvyyden ja niiden välisten etäisyyksien vaikutuksia porareikälämpövaraston toimintaan ei ole juuri tutkittu. Tässä diplomityössä tutkitaan, kuinka porareiän syvyys ja niiden väliset etäisyydet vaikuttavat suuren lämpövaraston toimintaan ja investointi-kustannuksiin. Tämän työn numeerinen malli perustuu Al-Khouryn ja Bonnierin (2006) kehittämään menetelmään, ja se on tehty COMSOL Multiphysics –mallinnusohjelmalla. Menetelmässä, nesteen virtaus mallinnetaan yksittäisessä U-putkessa 1D-lämpöputki-elementissä ja kallioperän lämmönsiirtyminen 3D-kappaleena.

Tämän työn mallinnuksessa muodostettiin yhteensä 21 tapaustutkimusta, jossa käytettiin seitsemää eri porareiän välistä etäisyyttä sekä kolmea eri varaston leveyden ja syvyyden –suhdetta. Perustuen kirjallisuuteen, porareiän välistä etäisyyttä vaihdeltiin puolen metrin välein 2.0 m ja 5.0 m välillä. Varaston leveyden ja syvyyden –suhteet olivat 1.0, 0.66 ja 0.5.

Työn tulokset osoittavat, että tietyn ajan t sisään otettavat purkuenergiat ja sen aiheuttama lämpötilapudotus määrittävät taloudellisesti optimaalisimman porareikien väliset etäisyydet. Optimaalisen porareiän väliseen etäisyyteen vaikuttaa mm. kallion lämmönsiirto-ominaisuudet, nesteen sisäänmenolämpötilat lataus- ja purkuvaiheessa, lataus- ja purkuvaiheen energiamäärät sekä ajanjakson pituus, joissa lataus- ja purkuvaihe operoidaan. Syvemmät porareiät eivät tämän tutkimuksen mukaan vaikuttaisi merkittävästi varaston toimivuuteen tai investointikustannuksiin. Työ ei kuitenkaan ota huomioon muuttuvan geometrian vaikutusta lämpöhäviöihin.

Simulaation tulokset osoittavat saman kapasiteetin (4.46 GWh) voivan maksaa jopa 1.5 miljoonaa € enemmän suboptimaalisessa kuin optimaalisessa tapauksessa (550 porareikää, niiden välinen etäisyys 3.5 m ja syvyys 172 m). Tässä työssä mallinnetulla porareikävarasto-ratkaisulla on potentiaalia tuottaa 2-5 MW energiaa jatkuvasti ja 10 MW yksittäisiin piikkitehoihin.

Avainsanat: Korkean lämpötilan porareikälämpövarasto, porareikälämmönsiirrin, kallioperä, maalämpö, lämmönsiirto, nesteen virtaus, COMSOL Multiphysics

Foreword

This thesis is part of HUKATON –project, which studies new alternative solutions for utilizing waste heat. This project is cooperation among Turku University of Applied Sciences, Green Net Finland ry, Aalto University and Geological Survey of Finland.

I'd like to thank my advisor, PhD Teppo Arola, who suggested me this demanding but interesting topic. Some years ago, Teppo Arola introduced me geoenergy and its interesting aspects. I'd like to give special thanks to my supervisor, professor Ville Vuorinen and physicist Petri Hakala at the Geological Survey of Finland. Suggestions and comments made by them helped me a lot during this project. Without their advice, I'd be still struggling with the ideas behind created model. I'd like to thank also doctoral candidates Bulut Tekgül and Mateusz Janiszewski their comments and help.

I'd like to thank Lounavoima Oy and Petri Onikki for supporting this project and also providing data for simulations.

This was rather demanding but rewarding project.

Espoo, 27th August 2019
Sami Vallin

Table of Contents

Abbreviations

Abbreviation	Explanation
1D	One-dimensional
2D	Two-dimensional
3D	Three-dimensional
ATES	Aquifer thermal energy storage
BC	Boundary condition
BHE	Borehole heat exchanger
BTES	Borehole thermal energy storage
CTES	Cavern thermal energy storage
DST	Duct storage model
STES	Seasonal thermal energy storage
HT-BTES	High temperature borehole thermal energy storage
LT-BTES	Low temperature borehole thermal energy storage
MD-BTES	Medium-deep borehole thermal energy storage
PDE	Partial differential equation
TES	Thermal energy storage
UTES	Underground thermal energy storage

Nomenclature

Latin symbols	Explanation	Unit
A_h	Storage land area (hexagonal)	m^2
A_g	Grout cross-sectional area	m^2
A_p	U-tube pipe inner cross-sectional area	m^2
A_{sp}	Surface area of one leg of the U-tube pipe	m^2
A_{sg}	Surface area of grout	m^2
b_{ig}	Heat transfer coefficient between pipe-in and grout	$W\ m^{-2}\ K^{-1}$
b_{og}	Heat transfer coefficient between pipe-out and grout	$W\ m^{-2}\ K^{-1}$
b_{rg}	Heat transfer coefficient between grout and bedrock	$W\ m^{-2}\ K^{-1}$
f_s	Friction factor for smooth surfaces	-
f_r	Friction factor for rough surfaces	-
$H_{charging}(t)$	Enthalpy of BTES charging fluid at time t	$kJ\ kg^{-1}$
$H_{supply}(t)$	Enthalpy of district heating supply fluid at time t	$kJ\ kg^{-1}$
$H_{return}(t)$	Enthalpy of district heating return fluid at time t	$kJ\ kg^{-1}$
h_f	Fluid heat transfer coefficient	$W\ m^{-2}\ K^{-1}$
$c_{p,f}$	Specific heat capacity of fluid	$J\ kg^{-1}\ K^{-1}$
$c_{p,g}$	Specific heat capacity of grout	$J\ kg^{-1}\ K^{-1}$
$c_{p,\ r}$	Specific heat capacity of rock	$J\ kg^{-1}\ K^{-1}$
D/L	Storage width to depth -ratio	-
D_h	Hydraulic diameter	m
dS_{ig}	Derivative of surface area of inlet leg of the U-tube pipe	-
dS_{og}	Derivative of surface area of outlet leg of the U-tube pipe	-
dS_{rg}	Derivative of surface area of grout	-
dV_i	Derivative of volume of inlet pipe	-
dV_o	Derivative of volume of outlet pipe	-
dV_g	Derivative of volume of grout pipe	-
dz	infinitesimal depth	m
E_T	Error in outlet temperature	%
E_q	Error in power	%
f	Darcy's friction factor	-
k_f	Fluid thermal conductivity	$W\ m^{-1}\ K^{-1}$
k_g	Thermal conductivity of grout	$W\ m^{-1}\ K^{-1}$
k_p	U-tube pipe wall thermal conductivity	$W\ m^{-1}\ K^{-1}$
k_r	Thermal conductivity of rock	$W\ m^{-1}\ K^{-1}$

l_b	Borehole length (depth)	m
L	Storage depth	m
n	Number of boreholes in storage	-
n_{unit}	Number of boreholes in model unit	-
Nu	Nusselt number	-
$n_{boreholes}$	Number of boreholes	-
n_{serial}	Number of serial connections	-
$\dot{m}_{charging}(t)$	Total fluid mass flow rate during charging at time t	kg s^{-1}
$\dot{m}_{discharging}(t)$	Total fluid mass flow rate during discharging at time t	kg s^{-1}
$\dot{m}$	Fluid mass flow rate per borehole	kg s^{-1}
P	Price of storage	€
P_g	Perimeter of grout	m
P_{pi}	Inner perimeter of one leg of the U-tube pipe	m
Pr	Prandtl number	-
$Q_{storage}$	Storage capacity	MWh
Q_{unit}	Model unit capacity	MWh
$Q_{charging}(t)$	BTES heat capacity during charging at time t	MW
Q_{CHP}	Power plant heat capacity (34 MW)	MW
$Q_{demand}(t)$	Heat demand in district heating network at time t	MW
$Q_{discharging}(t)$	BTES heat capacity during discharging at time t	MW
$Q_{district}$	Total heat demand capacity in the district heating	MWh
Q_{FCG}	Flue gas condenser Heat capacity (4MW)	MW
q	Total heat flux	W
q_g	Heat flux grout	W
q_i	Heat flux pipe-in	W
$q_{charging}(t)$	Charged power into model at time t	W
$q_{discharging}(t)$	Discharged power from model at time t	W
q_o	Heat flux pipe-out	W
$q_s(t)$	Scaled BTES power production profile at time t	W
R_b	Borehole thermal resistance	m^2 K W^{-1}
R_g	Grout thermal resistance	m^2 K W^{-1}
R_p	Thermal resistance of one leg of the U-tube pipe	m^2 K W^{-1}
R_{pf}	Fluid convective thermal resistance	m^2 K W^{-1}
R_{pc}	Pipe wall conductive thermal resistance	m^2 K W^{-1}
r_b	Borehole radius	m
r_{pi}	Inner radius of one leg of the U-tube pipe	m

r_{po}	Outer radius of one leg of the U-tube pipe	m
r_s	Storage radius	m
Re	Reynolds number	-
S	Storage unit scale factor	-
s	U-tube pipe shaft spacing	m
s_b	Borehole spacing	m
s_h	The length of the size of hexagon	m
u	Fluid velocity	m s^{-1}
t	Time	s
T_b	Borehole wall temperature	°C
T_g	Grout temperature	°C
T_i	Pipe-in fluid temperature	°C
T_{inlet}	Fluid inlet temperature into storage	°C
T_{max}	Storage (bedrock) maximum temperature	°C
T_{min}	Storage (bedrock) minimum temperature	°C
T_o	Pipe-out fluid temperature	°C
$T_{outlet}(t)$	Fluid outlet temperature from storage at time t	°C
T_{r0}	Initial undisturbed bedrock temperature	°C
T_r	Bedrock temperature	°C
V_s	Volume of storage	m^3
$\dot{V}$	Volumetric flow rate	m^3 s^{-1}

Greek symbols	**Explanation**	**Unit**
α_f	Thermal diffusivity of fluid	m^2 s^{-1}
α_r	Thermal diffusivity of rock	m^2 s^{-1}
$\Delta T(\xi, t)$	Change in underground temperature	K
Δp	Pressure drop	bar
ξ	Distance between the point heat source and the point of interest	m
μ	Fluid viscosity	Pa · s
ρ_f	Density of fluid	kg m^{-3}
ρ_{gr}	Density of granite	kg m^{-3}
ρ_{hblgns}	Density of hornblende gneiss	kg m^{-3}
ρ_{rock}	Density of rock	kg m^{-3}

1 Introduction

In Finland, energy storage solutions are considered to play an important role in the country's future energy generation which will be produced entirely by renewable means (Child and Breyer, 2016). As the heating sector still produces a significant amount of CO_2-emissions in Finland (Energiateollisuus, 2018), thermal energy storage (TES) technology offers a solution to reduce them. (Reuss, 2015). TES decreases the required heat production by increasing energy efficiency; heat that was previously wasted, can be stored for later use (Reuss, 2015; Xu et al., 2014). Heat sources for storage systems include solar thermal panels or waste heat from combined heat and power (CHP) plants, industries or offices (Fisch et al., 1998; Banks, 2012). In the future, TES technologies have the potential to increase conserved energy, reduce dependency on fossil fuel -based technologies and decrease greenhouse gas -emissions (Fisch et al., 1998; Reuss, 2015).

According to Xu et al. (2014), seasonal thermal energy storage (STES) stores surplus thermal energy produced during the season with low heat demand and utilizes it during the season with high heat demand. The large amounts of energy that must be stored between seasons necessitates the use of high volume storage units (Xu et al., 2014; Alva et al., 2018). Therefore, storage material should have high heat and energy capacities, be cost-effective, environment-friendly and reliable in nature to decrease storage volume, environmental and economic costs (Alva et al., 2018). Although storage mediums for latent heat and thermochemical thermal energy storage systems offers high heat capacity and energy density, the materials lack reliability and are expensive (Xu et al., 2014). On the other hand, mediums for sensible heat storages thermal are cheap and reliable, but they have low energy density and problems with heat losses (Xu et al., 2014). Despite these disadvantages, underground thermal energy storage (UTES) has shown potential to be an economically and technically optimal STES alternative (Nordell, 2000; Reuss, 2014; Janiszewski et al., 2016; Shah et al., 2018).

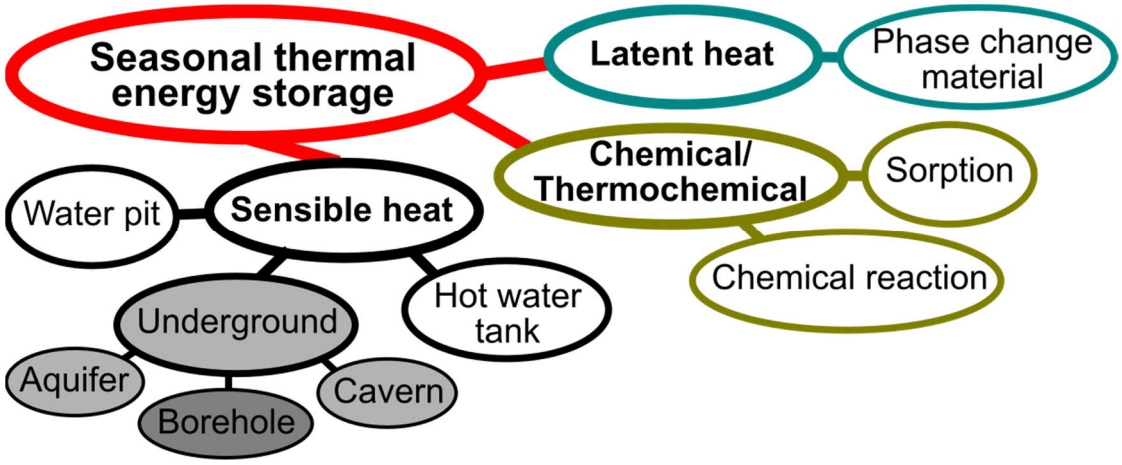

Figure 1. Seasonal thermal energy storage options. Borehole thermal energy storage belongs under the underground thermal energy storage concept.

There are three seasonal underground thermal energy storage technologies: aquifer thermal energy storage (ATES), borehole thermal energy storage (BTES) and cavern thermal energy storage (CTES) (Nordell, 2000). ATES systems are commonly utilized in large-scale applications in offices and industries. However, ATES technology is strongly site-dependent, requiring suitable hydrogeological conditions (Banks, 2012; Xu et al., 2014). On the other hand, BTES systems are less dependent on local conditions; therefore, they are applicable in most locations. BTES technology is sufficient for baseload purposes at relatively low price (Nordell, 2000; Reuss, 2015). Of UTES technologies, CTES systems are the most expensive alternative; however, CTES has shown potential to be price-competitive in grids with high fluctuations in power demand (Nordell, 2000). Janiszewski et al. (2016) concluded that BTES technology is one of the most suitable STES options in Finland due to favourable geology, simplicity and cost-effectiveness. However, Arola (2015) found that ATES may be locally cost-effective storage technology in suitable geological environment.

To date, most BTES systems operate at close to natural underground temperature and typically, utilize thermal energy for heating or cooling buildings, offices or industrial sites (Gehlin, 2016; Lanahan and Tabares-Velasco, 2017; Shah et al., 2018). However, Gehlin (2016) predicts a trend towards large-scale BTES systems connected with local or district heating network. Such systems are already assisting district heating networks in Drake Landing (Canada), Neckarsulm (Germany) and Crailsheim (Germany), to mention few (Nussbicker et al., 2007; Sibbitt et al., 2012; Bauer et al., 2016). Thus, thermodynamic feasibility of BTES have already been demonstrated; however, the feasibility of even larger BTES systems has not yet fully been examined. Such larger systems face a new economic challenge to be price-competitive with peak load plants or other heat storage systems (Gadd and Werner, 2015).

Investment decisions are supported by simulations to predict the cost and ensure thermodynamic feasibility of the BTES project (Lanahan and Tabares-Velasco, 2017). Cui et al. (2018) review available 2D and 3D models for vertical borehole heat exchangers (BHEs). Of these models, the analytical duct storage (DST) model developed by Hellström (1989) is the most commonly used tool for BTES simulations (Nussbicker et al., 2006; Sibbitt et al., 2012; Sørensen et al., 2012; Nordell et al., 2015; Malmberg, 2017). This model allows only cylindrical geometry with uniformly positioned boreholes. Additionally, DST assumes constant heat transfer at each borehole; therefore, the model does not consider heat transfer driven by temperature difference between fluid and bedrock. For that reason, DST overestimates long-term heat recovery of BHEs (Picard and Helsen, 2014). Numerical methods have been developed that can accommodate any geometry and provide more accurate heat transfer analyses of BTES (Lanahan and Tabares-Velasco, 2017). One of the most widely used numerical methods for borehole heat exchangers simplifies fluid flow in a one-dimensional (1D) line source to minimize computational time. Heat

transfer in underground material is defined in 3D blocks. (Al-Khoury et al., 2005; Al-Khoury and Bonnier, 2006; Diersch et al., 2011). Lanini et al. (2014) and Rapantova et al. (2016) have validated this numerical method using experimental results. However, a drawback of the numerical method is a high computational cost, while analytical DST models offer fast but restricted solutions (Lanahan and Tabares-Velasco, 2017; Park et al., 2018).

A waste incineration power plant in Korvenmäki, near the town of Salo (see page 25, Figure 19 for location), is seeking new economical and environment-friendly solutions to assist their power production during peak demand periods. As the waste heat produced by power plant significantly exceeds heat demand during peak periods, discharging period is considered the key factor in determining the required storage size. This master's thesis optimizes borehole spacing between 2 and -5 m and width-to depth -ratio between 0.5 and -1 using developed BTES model and studies their effects on storage performance and cost. Optimal borehole pattern is based on literature survey.

The feasibility of large-scale high-temperature borehole thermal energy storage is studied by simulation using COMSOL Multiphysics software. This thesis employs similar modelling environment for borehole heat exchangers (BHEs) that Saied et al. (2013) and Ozudoguru et al. (2014) introduced for COMSOL Multiphysics but develops an efficient numerical model for estimating the required size of a BTES. According to Reuss (2015) and Rinkjøb (2018), resolution of at least should be used to avoid inaccurate results which overestimate the capacity of the renewable sources and underestimate required investment. The integration of renewable energy sources increases the volatility of the energy production (Hirth, 2013) that may add the requirement modelling storages in finer temporal resolution. Furthermore, Reuss (2015) recommends a resolution of hour in order to simulate varying temperatures and dynamic system behaviour realistically. As this thesis studies the feasibility of BTES technology in highly variating peak power production, considering dynamic system behaviour becomes important to find out BTES potential to provide power in hourly-based demand. Therefore, this thesis focus on hour-based resolution and considers only one year of operation, neglecting long-term system performance. One-hour resolution increases computational cost; therefore, the model geometry is simplified. For that reason, the model neglects heat losses at the domain boundaries.

The main objectives of this master's thesis are:

1) To find out how borehole spacing and storage width to depth -ratio affects BTES capacity, size, performance and cost. Optimal spacing and depth are given as a result.
2) Study whether BTES technology can produce enough power for peak power production cost-effectively. Literature considers BTES sufficient only in baseload purposes.

2 Background

2.1 Physical background

Heat conduction in bedrock can be described one-dimensionally by Fourier's law and convective heat transfer inside of a pipe, by Newton's law.

2.1.1 Fourier's law

Heat transfer in a solid material is driven by temperature differences and heat conduction. In bedrock, minerals with higher energy level randomly transfers energy to the less energetic minerals. Therefore, heat is conducted in the direction of decreasing temperature. Physically, Fourier's law describes the rate of conduction through a plane in solid materials. In the steady state condition, the amount of transferred energy (q) through a plane of area (A) depends on the temperature difference (ΔT) between heat source and the point of interest (ξ), which consist of material with thermal conductivity (k) (Bergman et al., 2011):

$$q = -kA\frac{\Delta T}{\xi}. \tag{2.1}$$

2.1.2 Newton's cooling law

Fluid transfers heat by diffusion but also by macroscopic motion. The latter mechanism creates convective heat transfer with temperature differences and fluid flow. Fluid with velocity (u) creates convection, while heat diffusion is dominant close to the pipe wall surface, where fluid velocity is low. In turbulent flow, convective heat transfer becomes significant. Boundary layers originate at the regions with a low fluid velocity and significant viscous forces. The boundary layer develops because low velocity fluid particles near the pipe surface interact with particles with higher velocity in the next layer. Convective heat transfer may be described physically by Newton's cooling law, which describes the amount of energy transferred from fluid to the environment or vice versa:

$$q = hA\left(T_s - T_f\right), \tag{2.2}$$

where temperature difference between pipe surface (T_s) and fluid (T_f) through the heat transfer surface area (A) causes heat flux (q). The convective heat transfer coefficient (h) is dependent on the thickness of boundary layer, surface roughness and geometry of pipe, fluid flow and its thermodynamic properties. (Bergman et al., 2011).

2.2 Borehole thermal energy storage

According to Gehlin (2016), BTES systems utilize underground material (rock or soil) to store thermal energy in the form of heat. The definition of BTES includes often only vertical borehole systems (Nordell, 2000; Reuss, 2014; Gehlin, 2016); however it was originally defined as a system having closed-loop borehole heat exchangers (BHEs), which includes both vertical and horizontal boreholes (Gehlin, 2016).

Borehole thermal energy storage systems can be classified according to temperature and size. For example, IEA ECES (1998) divides UTES systems according to temperature. A high-temperature UTES (HT-UTES) systems have a storage loading temperature of greater than 50°C. Applications having lower loading temperatures are low-temperature UTES (LT-UTES) systems. Nordell (2000) classifies BTES systems according to their size: a small-scale application includes only one borehole, a large-scale application is a system of boreholes extracting heat by heat pumps, and a seasonal application is a system that stores heat for later demand. More precisely, seasonal BTES systems must provide thermal energy at least three months after the end of loading (IAE ECES, 1998).

2.2.1 Storage medium: thermal properties

Storage capacity, power and heat losses depend on the thermal properties of the storage medium. The thermal properties of rock (or soil) are density (ρ), specific heat capacity (c_p) thermal conductivity (k) and thermal diffusivity. (Gehlin, 2016). Of these properties, thermal conductivity is one of the most important factors determining the overall performance of the storage medium. A rock with high thermal conductivity is preferable for efficient heat transfer between the rock and the borehole (Gehlin, 2016). On the other hand, a rock with low thermal conductivity decreases heat losses (Reuss, 2015). Therefore, mineralogical composition, porosity and water saturation play essential role, as these factors define the thermal conductivity of the rock or soil (Eppelbaum et al., 2014).

Mineralogical composition is one of the main factors that define a rock type. The composition and content of minerals can vary significantly among rock types; for that reason, each rock type has a characteristic range for thermal conductivity (Eppelbaum et al., 2014). For example, as shown in Figure 2, the major mineralogical components of granite are quartz (7.04 W m^{-1} K^{-1}), feldspar (2.40 W m^{-1} K^{-1}), plagioclase (2.00 W m^{-1} K^{-1}) and biotite (1.17 W m^{-1} K^{-1}) (Cermak and Rybach, 1982; Gill, 2010). However, mineral content in granite varies regionally, creating a known range for thermal conductivity. It has been established that high quartz content is a key reason for the high thermal conductivity of rock (e.g. granite) (Banks, 2012). Thermal conductivity can also be

increased by other abundant silica based minerals such as olivines (3.16-5.06 W m^{-1} K^{-1}) and pyroxenes (3.82-5.02 W m^{-1} K^{-1}) (Cermak and Rybach, 1982). Therefore, different mixtures of mineral components create different values for thermal conductivity (Eppelbaum et al., 2014). However, some minerals have orientation (foliation), which creates different thermal conductivity in the direction of foliation as in the normal of foliation (Eppelbaum et al., 2014). According to Clauser and Huenges (1995), minerals, which are located randomly within the rock, may affect anisotropically in the thermal conductivity of rock. In regional scale, folding, faults and displacements causes anisotropy for rock masses.

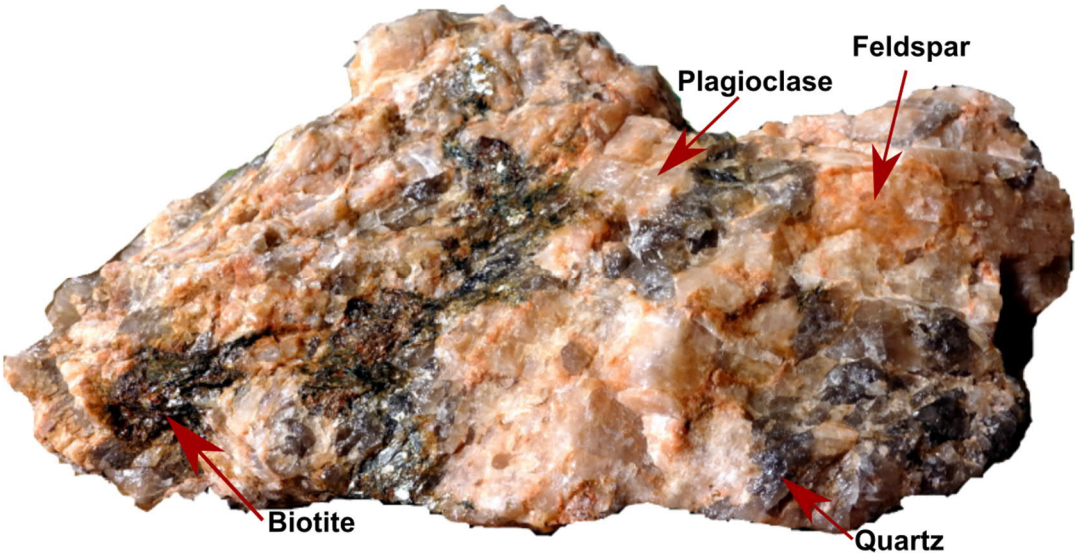

Figure 2. Granite composing mainly of feldspar, plagioclase, quartz and biotite. These mineral components create most of thermal properties of the rock. Due to homogenous material, a rock has highly anisotropic thermal properties. Picture: Sami Vallin.

Two other important factors affecting the thermal conductivity of rock are porosity and water saturation. Void space in the rock can be filled with air (0.03 W m^{-1} K^{-1} at 20 °C) or groundwater (0.6 W m^{-1} K^{-1} at 20 °C) (Eppelbaum et al., 2014). Because both have a lower thermal conductivity than the rock, the thermal conductivity of the rock decreases in response to increased porosity. (Poelchau et al., 1997). However, if void space is filled with groundwater instead of air, the thermal properties of the rock are enhanced due to the thermal properties of groundwater (Cho et al., 2009). For that reason, the presence of groundwater increases the thermal conductivity and heat capacity of the rock samples with the same porosity. Nevertheless, the presence of groundwater does not necessarily have positive impacts on heat transfer (Gehlin, 2016). Cracks, fractures and faults provide access to groundwater flow in the bedrock (Banks and Robins, 2002). If the groundwater flow rate is high relative to storage size, increased convective heat transfer can cause significant heat losses. Such hydrogeological conditions are not advisable for BTES operation. (Reuss, 2015). Only in the case of a low groundwater flow rate can the presence of groundwater improve storage performance (Gehlin, 2016). However, convective heat losses have been found to be negligible in

hard and non-permeable bedrock (Åberg and Johansson, 1988). Figure 3 summarizes key factors effecting for BTES design.

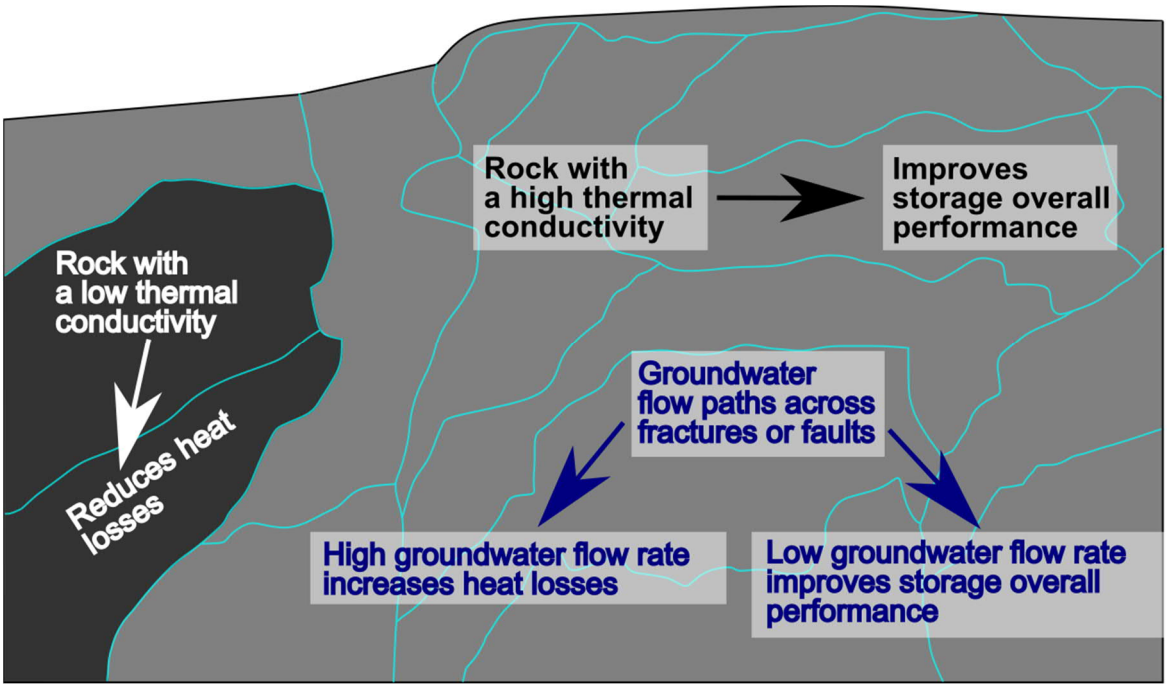

Figure 3. Schematic figure of storage medium showing key factors effecting to the performance of BTES (Grey coloured medium is a rock with a high thermal conductivity, dark grey is a rock with a low thermal conductivity and blue colour represents groundwater flow).

While thermal conductivity describes the ability of the material to transfer heat, density ρ_r and specific heat capacity $c_{p,r}$ describe how much energy a specific volume can store given a specific temperature change (Bergman et al., 2011). In general, high volumetric heat capacity $\rho_r c_{p,r}$ should be sought in order to maximize the amount of energy within the storage volume (Banks, 2012; Gehlin, 2016). The capacity of rock typically varies between 1.8 – 3.0 MJ m^{-3} K^{-1} (Gehlin, 2016). However, increased storage volumetric capacity has the drawback of decreasing thermal diffusivity α, as illustrated by Equation (2.1.)

$$\alpha_r = \frac{k_r}{\rho_r c_{p,r}}. \tag{2.1}$$

Thermal diffusivity defines how rapidly material will react to thermal changes (Bergman et al., 2011). This physical property limits the available power a storage system can yield given a specific heat exchanging surface area. High thermal diffusivity decreases the requirement for large heat exchanging surface area (Kotzé et al., 2013). Because rock and soil have low thermal diffusivity, they require large heat exchanging surface area to provide large amount of power; therefore, underground materials perform usually sufficiently as a base load purposes (Nordell, 2000). Table 1 (see page 9) summarizes the thermal properties of chosen rock types at room temperature.

The thermal properties of materials are always temperature-dependent (Bergman et al., 2011). When considering underground materials such as rock or soil, according to Vosteen and Schellescmidt (2003) specific heat capacity increases in response to increased temperature while thermal conductivity and thermal diffusivity decline. However, the density of rock does not significantly affect the response of thermal properties to increased temperature. As previously mentioned, temperature dependence of rock depends on its mineralogical composition. At lower temperatures (< 200 °C), some minerals such as quartz and olivines are strongly dependent on temperature, whereas most of the minerals show only minor temperature dependence (Cermak and Rybach, 1982; Vosteen and Schellschmidt, 2003). Therefore, depending on the rock type, decreased thermal conductivity and diffusivity may impact on the storage overall performance at 50-100 °C. Figure 4 and Figure 5 demonstrate the effect of temperature on thermal conductivity and diffusivity on chosen rock types.

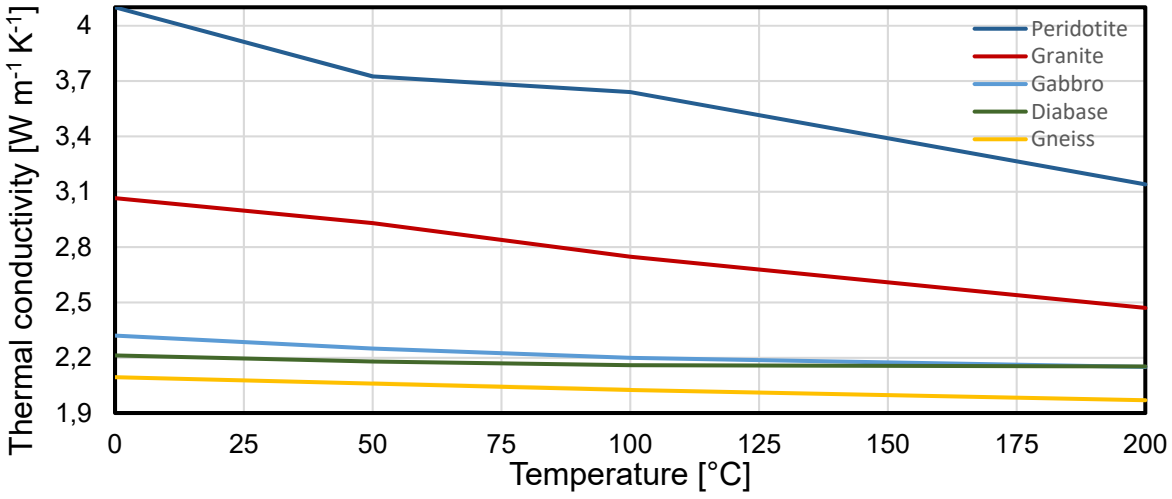

Figure 4. Thermal conductivity of chosen rock types in response to increased temperature. Thermal conductivity of rocks shows almost linear correlation as a function of temperature at these temperatures (Cermak and Rybach, 1982).

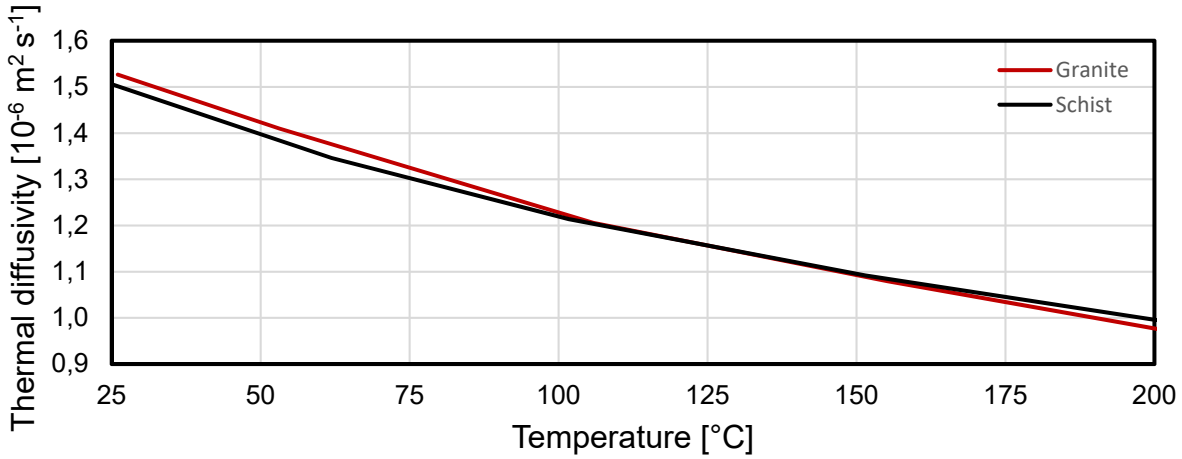

Figure 5. Thermal diffusivity of chosen rock types as a function of temperature (Whittington et al., 2009).

Table 1. Thermal properties of typical igneous and metamorphic rocks. (Cermak and Rybach, 1982 [1]; Schön, 2015 [2], Waples and Waples, 2004 [3]; Kukkonen and Lindberg, 1998 [4]; Schärli and Rybach, 2001 [5]; Whittington et al., 2009 [6]). These rock types are typical in Finland based on Lehtinen et al. (1998).

Rock type	Thermal conductivity k_r (W m^{-1} K^{-1})			Density ρ_r (kg m^{-3})	Specific heat capacity $c_{p,r}$ (J kg^{-1} K^{-1})			Thermal diffusivity α_r (10^{-6} m^2 s^{-1})		
	Mean	Range	n		Mean	Range	n	Mean	Range	n
Igneous rocks										
Anorthosite	1.75	1.60 – 2.09	14 [1]	2700-2740 [2]	–	–	–	–	–	–
Diabase	2.63	1.55 – 4.30	115 [1]	2700-3100 [2]	910	750 – 1000	22 [1]	0.97	0.85 – 1.12	22 [1]
Diorite	2.91	1.72 – 4.14	50 [1]	2700-2950 [2]	1029	775 – 1117	4 [1,5]	0.68	0.54 – 0.86	3 [1]
Granite	3.05	1.25 – 4.45	356 [1]	2500-2800 [2]	960	670 – 1550	102 [1]	1.18	0.56 – 2.11	89 [1,6]
Granodiorite	2.65	1.35 – 3.40	89 [1]	2730-2840 [3]	1065	752 – 1860	12 [1,5]	0.77	0.50 – 1.18	11 [1]
Gabbro	2.63	1.62 – 4.05	71 [1]	2800-3100 [2]	1010	880 – 1130	9 [1]	0.97	0.97 – 1.22	9 [1]
Monzonite	3.06	–	1 [1]	2640 [1]	743	742 – 743	2 [5]	1.02	0.93 – 0.11	2 [1]
Peridotite	3.81	3.78 – 4.85	23 [1]	3100-3275 [2]	992	855 – 1090	15 [1,5]	1.33	1.19 – 1.41	14 [1]
Syenite	2.31	1.35 – 5.20	50 [1]	2625-2900 [2]	460	–	1 [3]	0.63	–	1 [1]
Tonalite	2.75	2.51 – 3.11	3 [1,3]	2674-2740 [4]	-	826 – 829	2 [1,3]	1.31	1.12 – 1.40	2 [4]
Metamorphic rocks										
Quartzite	5.26	3.10 – 7.60	186 [1]	2575-2650 [2]	1014	710 - 1340	8 [1]	2.00	1.48 – 2.95	8 [1]
Gneiss	2.44	1.20 – 4.80	308 [1]	2500-2900 [2]	770	460-920	68 [1]	0.97	0.59 – 1.57	124 [1]
Migmatite	2.17	2.00 – 2.40	3 [1]	2750 [3]	840	840	3 [1]	–	–	–
Schist	3.80	2.20 – 5.20	122 [1]	2500-2900 [2]	800	670-1050	18 [1]	1.00	0.78 – 1.83	41 [1,6]
Mica schist	2.71	2.50 – 2.92	8 [1]	–	1130	1050-1210	5 [1]	0.77	0.64 – 0.88	5 [1]
Amphibolite	2.46	1.35 – 3.90	78 [1]	2675-3200 [2]	940	757-1260	18 [1,5]	0.69	0.46 – 0.82	25 [1]

2.2.2 Borehole heat exchanger

A large BTES system includes multiple BHEs, which consist of four components as shown in Figure 6: a borehole with given radius r_b and length l, pipes, grout or backfilling groundwater and an insulation layer on the top (Gehlin, 2016). The most common BHEs utilize single U-shaped pipe to circulate heat exchanging fluid at velocity u to exchange thermal energy between grout (or backfilling groundwater) and rock material (or soil) (Chiasson, 2016). Other pipe geometries include double U-tube, concentric and coaxial pipe (Chiasson, 2016; Gehlin, 2016). In a BHE, fluid enters a pipe inlet (pipe-in) at given temperature T_i, releases or extracts thermal energy q to or from underground material through grout and exits the pipe outlet (pipe-out) at temperature T_o. In other words, borehole with a single U-tube pipe exchanges thermal energy per unit depth in closed-loop system. (Chiasson, 2016). As already mentioned, the thermal energy released or extracted thermal energy changes the naturally occurring underground temperature T_{r0} to the disturbed temperature T_r (Reuss, 2015; Chiasson, 2016). The system also includes grouting or backfilling material, with the given temperature T_g. The most common material for grouting a borehole is a bentonite-cement mixture, but non-grouting materials such as naturally occurring groundwater are typically used in applications in northern Europe. (Reuss, 2015; Chiasson, 2016). Finally, the top of the BTES system is covered by the insulation layer to minimize heat losses (Chiasson, 2016; Gehlin, 2016).

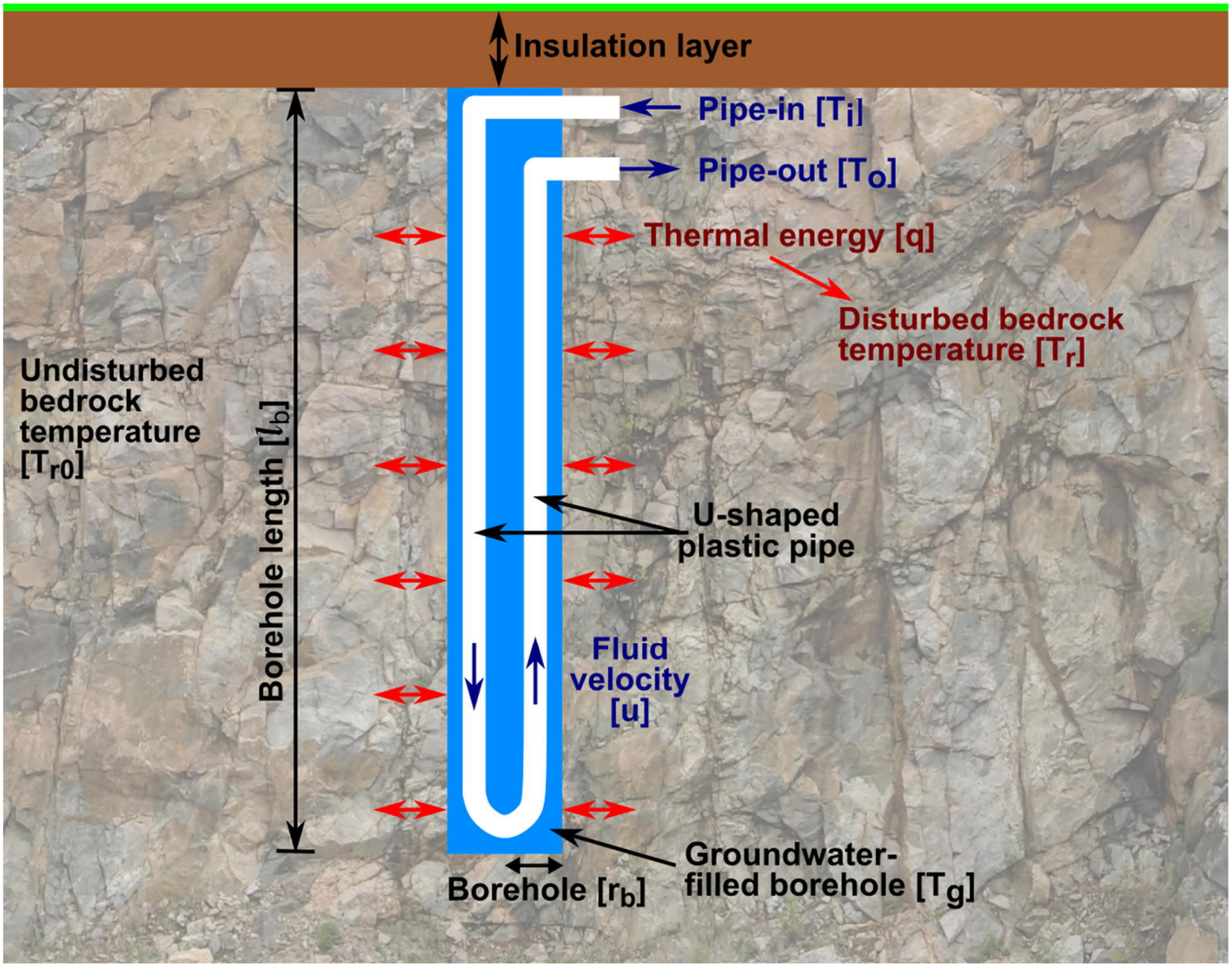

Figure 6. Schematic diagram of single U-tube BHE in a groundwater-filled borehole.

Typically, BHEs include plastic polymer pipes due to their high resistance to corrosion (Reuss, 2015). However, each type of plastic pipe type has a different ability to resist heat aging; therefore, the average yearly temperature of the heat exchanger fluid and its operational pressure determine the required polymer material for pipes (Liebel and Reuss, 2006). Plastic pipes also have operational pressure and temperature limits, which cannot be exceeded without causing permanent damage to the pipes. These operational limits depend on pressure: at higher the pressures, lower the average yearly temperatures of the heat exchanger fluid can be used (Reuss, 2015). It is recommended to increase pipe wall thickness under high temperature and pressure conditions to enhance the heat aging properties of the pipe material. (The Nordic Plastic Pipe Association, 2011; Reuss, 2014). Among polymer materials, only polybutene (PB) and cross-linked polyethylene (PE-X) have proven to be capable of withstanding occasional fluid temperatures up to 90°C with high life-expectancy, and both materials are successfully utilized in HT-BTES systems (Nussbicker et al., 2006; Reuss, 2015; Malmberg, 2017). According to Liebel and Reuss (2006) PE-X polymer pipe has shown the best resistance against heat aging, external actions and joint failure.

Table 2. Properties of heat resistant pipe materials used in BHEs. Sources: (Reuss, 2015 [1], Lehikoski, 2019 [2]).

Material	Thermal conductivity k_p [W m^{-1} K^{-1}]	Continuous operating temperature for 34 years	Peak temperature
PE-100	0.42 [1]	NA	60 °C [3]
PE-RT	0.42 [1]	80 °C at 2.0 bar [2]	95 °C at 4.0 bar [2]
PB	0.22 [1]	NA	99 °C [3]
PE-X	0.41 [1]	NA	99 °C [3]

The effective operation of BHEs requires efficient heat transfer between the U-tube pipe and the borehole wall. In theory, heat transfer in BHEs is increased by minimizing total borehole thermal resistance (Chiasson, 2016), thus minimizing the temperature difference between the borehole wall and fluid (Bergman et al., 2011; Chiasson, 2016). Borehole thermal resistance can be lowered by choosing grouting material with high thermal conductivity (Chiasson, 2016; Gehlin, 2016). For example, groundwater enhances heat transfer properties in the borehole due to natural convection (Gustafsson and Gehlin, 2008). However, although the heat transfer properties of the bentonite-cement mixture typically used as grouting material are inferior to those of groundwater, its ability to seal void spaces and improve the mechanical properties of rock or soil optimizes benefits in most geological environments (Gehlin, 2016; Santhoshkumar et al., 2016).

According to Javed and Spitler (2017), total borehole thermal resistance (R_b) is described as a circuit, where grout resistance (R_g) is connected in series with a parallel connection of pipe resistances (R_p) (see Figure 7). Pipe resistances are the sum of convective fluid resistance (R_{pf}) and conductive pipe wall resistance (R_{pw}). While convective heat transfer occurs within the cross-sectional area determined by the inner radius (r_{pi}) of the pipes, conductive heat transfer occurs within the pipe wall, which is determined by the thickness between outer radius (r_{po}) and inner radius. To simplify mathematical descriptions, geometrical symmetry is assumed between the inlet and outlet pipe. These simplifications presume also one-way heat transfer between grout and borehole wall (from grout to borehole wall during the charging phase, and the reverse during the discharging phase). As fluid has a different temperature in the inlet and outlet pipe, both grout and borehole wall have slight temperature variation at each cross-section. However, the assumption of one thermal circuit neglects temperature variation and assumes uniform borehole wall mean temperature (T_b) at each cross-section (Chiasson, 2016). In order to evaluate borehole total thermal resistance accurately, Claesson and Helsström (2011) developed the analytical multipole method. So far, the method has been proven to be one of the most accurate to estimate borehole total resistances in a system that contains U-tube pipe (Javed and Spitler, 2017).

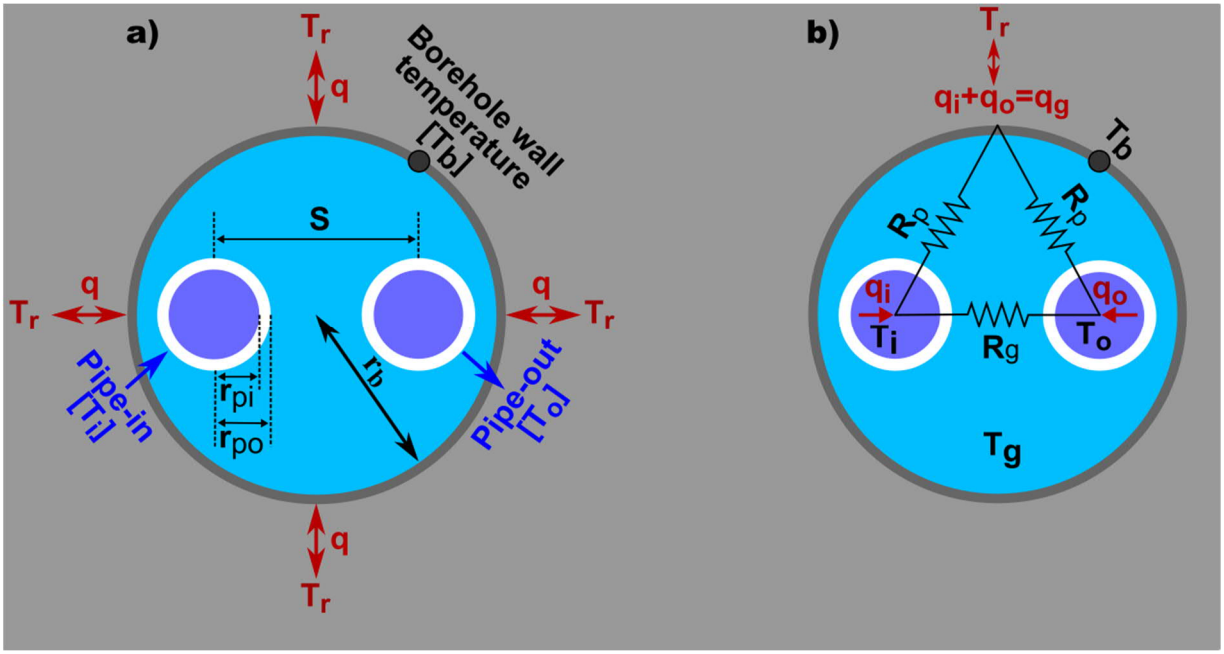

Figure 7. a) Borehole cross section defining pipe and borehole parameters. b) Thermal circuit for a borehole with a single U-shaped pipe with stationary heat flow.

The solution of the borehole thermal resistance provides a basis for evaluating the temperature distribution of BHE with the single U-tube pipe. As illustrated in Figure 7, in the steady state condition, thermal energy released by U-tube pipe (inlet: $q_i(z)$; outlet: $q_o(z)$ equals heat flux flowing through the grout $q_g(z)$:

$$q_i(z) + q_o(z) = q_g(z). \tag{2.2}$$

Only local steady-state condition with known borehole wall temperature has an analytical solution. One comprehensive analytical solution is based on calculating dimensionless temperature response factors - the so called g-functions (Eskilson, 1987; Eskilson and Claesson, 1988). Another analytical solution can be derived from the equation for internal flow emitting constant heat flux (q) given by Bergman et al. (2011). This equation can be used to determine the temperature distribution in the inlet $T_i(z)$ and outlet $T_o(z)$ legs of the single U-tube pipe as a function of depth z:

$$T_i(z) = T_i + \frac{P_p}{\dot{m}c_{p,f}} b_{ig}\left(T_i - T_g(z)\right) \cdot dz$$
$$T_0(z) = T_o + \frac{P_p}{\dot{m}c_{p,f}} b_{og}\left(T_o - T_g(z)\right) \cdot dz. \tag{2.3}$$

where P_p is the inner perimeter of one leg of the U-tube pipe, T_i and T_o are temperatures at previous depth, $\dot{m}$ is mass flow rate of fluid, $c_{p,f}$ is specific heat capacity of fluid, and dz infinitesimal depth,

and b_{ig} and b_{og} are known heat transfer coefficients between the inlet or outlet pipe and grout, respectively. Inlet and outlet pipes require prescribed boundary conditions for the surface (z = 0) and bottom (z = l) as follows:

$$T_i(0) = T_{inlet}$$
$$T_o(l) = T_i(l). \quad (2.4)$$

Thermal energy released by inlet and outlet pipes can be calculated from equation for heat capacity. Energy transferred through the grout is calculated from Newton's cooling law equation:

$$q_i(z) = \dot{m} c_{p,f}\left(T_i - T_i(z)\right)$$
$$q_o(z) = \dot{m} c_{p,f}\left(T_o - T_o(z)\right)$$
$$q_g(z) = b_{rg}\left(T_g(z) - T_r\right). \quad (2.5)$$

where b_{rg} is the heat transfer coefficient between the rock and grout, and T_r is the given rock temperature. Finally, Equations 2.3 can be substituted into Equations 2.5. $T_g(z)$ must be calculated iteratively in order to find a grout temperature that satisfies the energy balance from equation 2.2. This set of equations can be solved simultaneously from each depth z, and the solution thus yield a temperature distribution of grout, inlet and outlet pipes as demonstrated in Figure 8. All parameters are given in Table 3.

Table 3. All parameters given in Feflow White papers (Diersch et al., 2010).

Parameter	Value
l	100 m
r_b	0.065 m
r_{po}	0.032 m
r_{pi}	0.0291 m
T_r	10 °C
T_{inlet}	80 °C
$\dot{m}$	0.25 kg s^{-1}
$c_{p,f}$	4180 J kg^{-1} K^{-1}
b_{ig}	31.9 W m^{-2} K^{-1}
b_{og}	31.9 W m^{-2} K^{-1}
b_{rg}	95.1 W m^{-2} K^{-1}

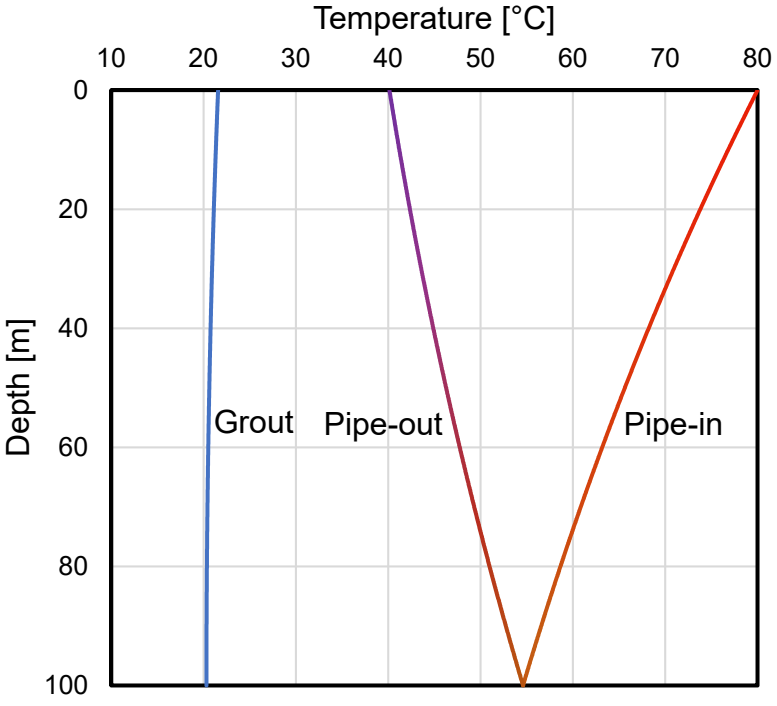

Figure 8. Analytical solution for a stationary problem given in Feflow White papers using Equations 2.2.-2.5.

Al-Khoury et al. (2005) derived the first efficient numerical solution for a stationary condition of BHEs. As many of problems related to BTES are transient, stationary equations may not be valid (e.g. Catolico et al., 2016; Tordrup et al., 2017; Korhonen et al., 2018). Al-Khoury and Bonnier (2006) derived a set of equations to achieve accurate solutions to transient BHE problems.

2.2.3 Storage design

Thermal energy storage design parameters are site-specific and depend on the storage medium's thermal properties and heat demand (capacity and power) (Reuss, 2015; Gehlin, 2016). Required storage capacity Q depends on storage volume, volumetric heat capacity $\rho_r c_{p,r}$ of the storage medium andthe difference between maximum T_{max} and minimum T_{min} temperatures as can be seen from Equation 2.6:

$$Q = V_s \rho_r c_{p,r} (T_{max} - T_{min}). \quad (2.6)$$

Thus, 1 m^3 rock material with heat capacity of 1.9 MJ m^{-3} K^{-1} holds 5.6 kWh energy after being heated by 10°C. As shown in Figure 9, higher storage capacity requires the higher storage volume and storage radius.

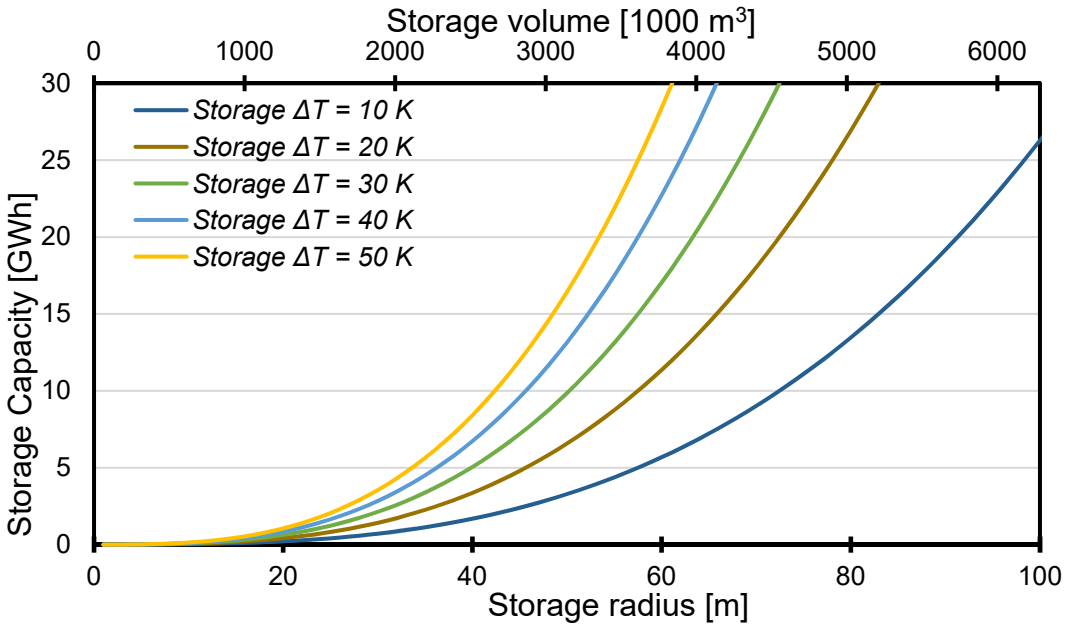

Figure 9. Storage capacity as a function of storage radius r_s and storage volume in case of cylindrical storage geometry with length $L=2r_s$. Storage ΔT defines the difference between minimum and maximum temperatures. Heat losses of 20 % and volumetric heat capacity of 1.9 MJ m^{-3} K^{-1} are assumed.

As storage capacity and volume increase, heat losses also increase due to greater storage surface area (Gehlin, 2016; Reuss, 2015). Although larger storage capacity increases absolute heat losses, it enhances storage efficiency relatively. Furthermore, the geometry of the storage affects storage

efficiency. (Gehlin, 2016). Spherical storage geometry has the lowest surface-area-to-volume ratio, and for that reason, it minimizes heat losses caused by geometry. In engineering applications, spherical geometry is challenging to implement, and so cylindrical storage shape is favoured (see Figure 10). (Reuss, 2015). The storage width-to-depth –ratio also affects heat losses. According to Ritola (1988) heat losses are minimized when the ratio of width (D) to depth (L) is between 1 and 2. Lanini et al. (2014) proved D/L -ratio should be close to 2 in small scale applications, while Janiszewski et al. (2018) concluded that larger storages require the D/L –ratio to be 1. However, Bär et al. (2015) and Welsch (2019) have argued that medium-deep borehole thermal energy storage (MD-BTES, L > 500 m) is the optimal solution for storage with high heat demand. Another benefit of MD-BTES is that groundwater flow decreases in response to increased depth in crystalline bedrock (Bär et al., 2015).

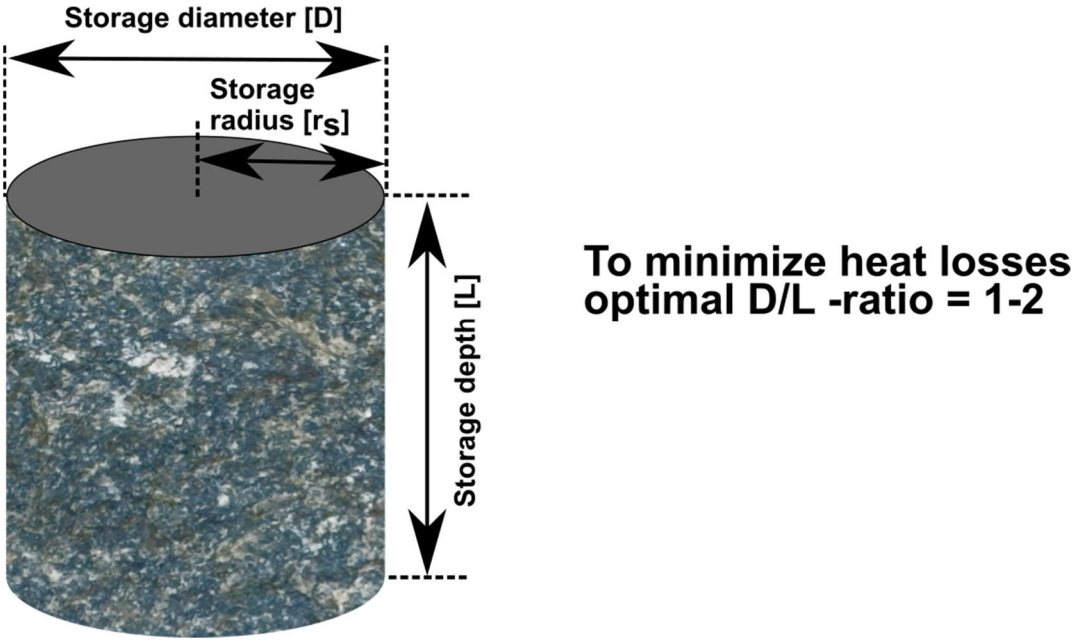

Figure 10. Optimal cylindrical storage geometry

The storage medium requires boreholes with certain spacing and pattern as shown in Figure 11. Typically, boreholes are spaced 2-5 meters apart in either in quadratic or hexagonal pattern (Reuss, 2014; Gehlin, 2016). Both optimal spacing and pattern depend on the thermal properties of the storage medium α_{rock} and k_{rock} and the required charging and discharging power q and duration (t). This can be demonstrated using an equation (2.7) derived by Marcotte and Pasquier (2009) that shows how point heat source with a constant heat flux change temperature at given time (t) and distance (ξ):

$$\Delta T(\xi, t) = \left(\frac{q}{4\pi k_{rock}\xi}\right) erfc\left(\frac{\xi}{2\sqrt{\alpha t}}\right). \quad (2.7)$$

Additionally, storage maximum and minimum temperatures restrict storage total capacity. Storage temperature change is dependent on borehole spacing and pattern and therefore the distance of the boreholes to the middle point of the pattern. As shown in Figure 12, temperature change decreases in response to greater distance between heat source and the circumcentre point of the pattern (in a hexagonal pattern). For that reason, storage total capacity may be increased by decreasing spacing. On the other hand, the heat required can be extracted in less time when using lighter spacing. Therefore, lighter spacing provides access to more power. As Figure 11 demonstrates, the hexagonal pattern has a shorter distance to the middle point of the pattern than quadratic patter, and therefore, hexagonal pattern is more efficient. Additionally, hexagonal pattern has lower top surface area, and for that reason, it reduces heat losses. (Reuss, 2015).

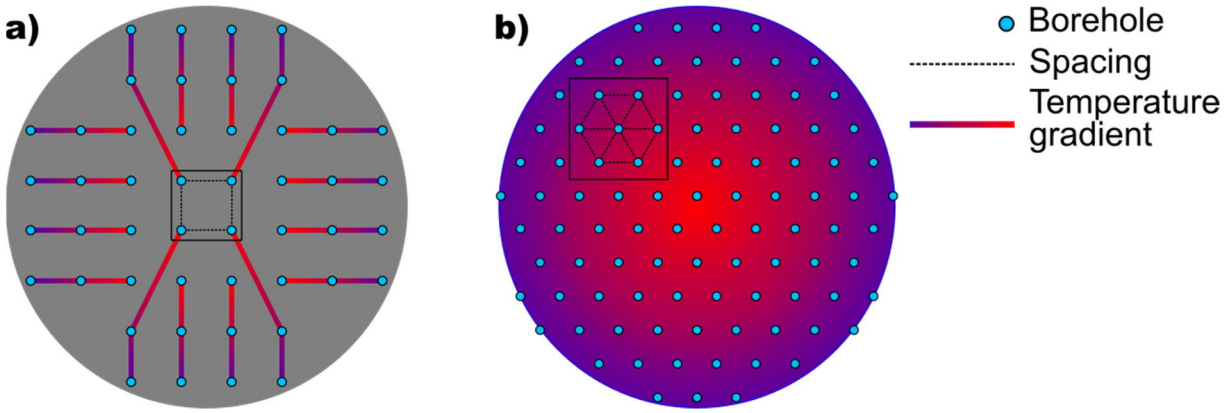

Figure 11. a) Quadratic pattern. Three BHEs connected in series showing approximate fluid flow temperature distribution (modified after Janiszewski et al., 2018). *b) Hexagonal pattern. Approximate temperature distribution in the storage medium.*

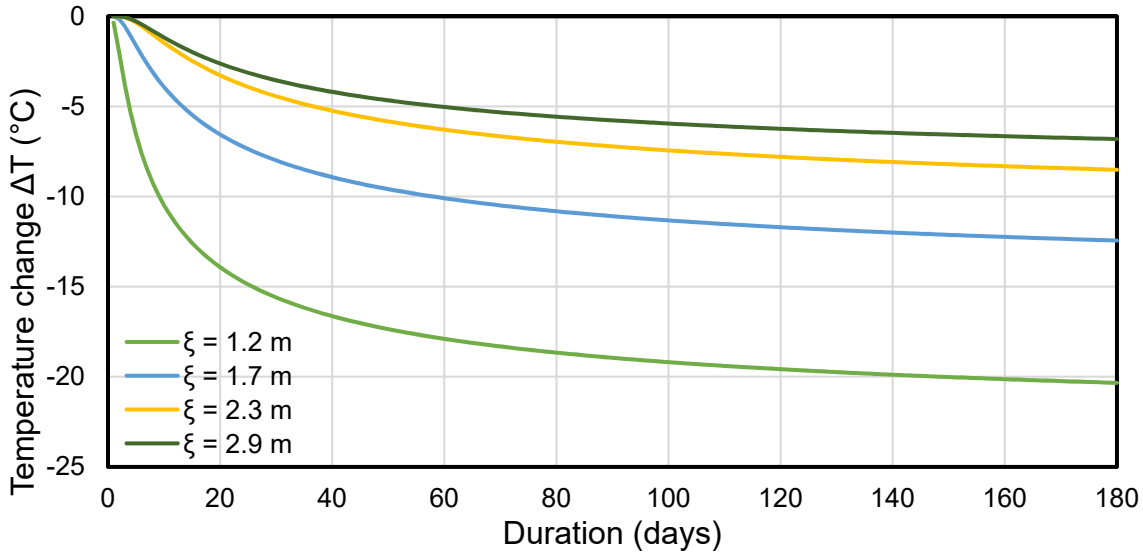

Figure 12. The temperature change of rock medium at distance ξ in response to constant 1 kW heat extraction with a point heat source (Equation 2.7). Assumptions of k_{rock} *= 2.90 W* m^{-1} K^{-1}, $\alpha = 1.3 \cdot 10^{-6}$ m^2 s^{-1}. *Each distance represents circumcentre point of the triangle in the hexagonal pattern when spacing is 2 m (ξ = 1.2 m), 3 m (ξ = 1.7 m), 4 m (ξ =2.3 m), 5 m (ξ = 2.9 m).*

Storage design is a complex economic and operational optimization, and its objective is to satisfy heat demand by minimizing heat losses and storage cost (Gao et al., 2015). While heat losses are minimized by specific storage width-to-depth –ratio, storage cost is minimized by decreasing the required land area and total borehole length (Nordell, 1994). On the other hand, maximum power and capacity is achieved by choosing denser spacing and a hexagonal rather than quadratic pattern, but such solution increase storage cost due to the increased total borehole length (Manonelles, 2014).

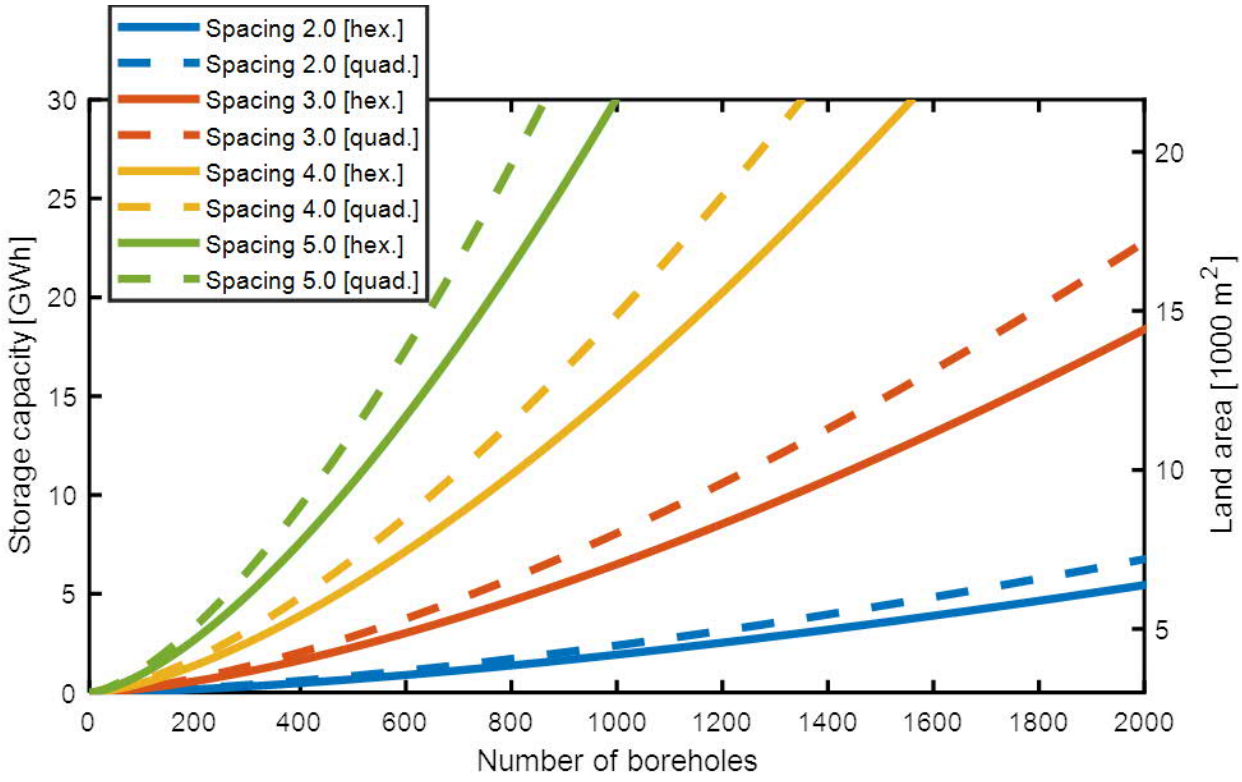

Figure 13. Storage capacity and land area in response to the number of boreholes when borehole spacing and pattern ins varied. Storage geometry is assumed cylinder and its height $H=2r_s$. Storage $\Delta T = 20$ K

Additionally, storage design may require boreholes connected in series in addition to parallel connections (Reuss, 2015; Gehlin, 2016; Malmberg, 2017). The number of parallel connections may be restricted by the mass flow rate; for that reason, the combination of parallel and serial connections is required to satisfy planned storage capacity (see Figure 14). In the case of multiple serial connections, heat exchanging fluid can release or extract more thermal energy within one cycle than in the case of only parallel connections. (Gehlin, 2016). The approach with the combination of parallel and serial connections concentrates more thermal energy on the centre of the storage than the system of parallel connections (Reuss, 2015). However, the number of serial connections is limited by the required power of the pump and pressure drop (Δp) in one cycle. As shown in equation 2.8, pressure drop depends on fluid velocity (u) and total length of boreholes in one series (Bergman et al., 2011):

$$\Delta p = f \frac{\rho u^2}{2} \frac{l_b}{2r_{pi}}. \quad (2.8)$$

The pressure level must be kept above 1 bar to avoid the dissolution of gases (Nordell et al., 2015). Typically, existing HT-BTES systems have 2-6 boreholes connected in series (Malmberg, 2017).

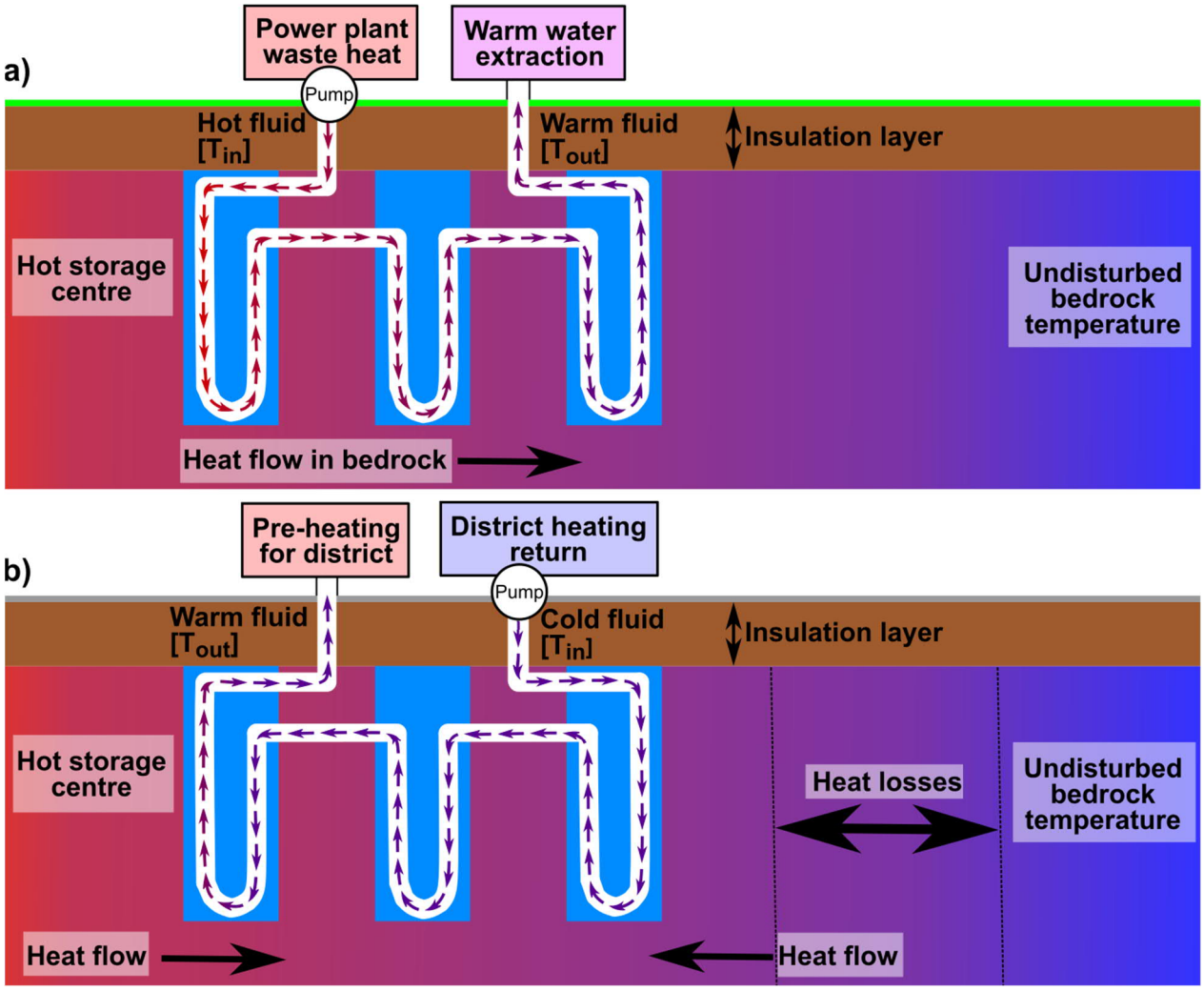

Figure 14. Schematic diagram of serial connections during a) charging period and b) discharging period.

A BTES system can be connected to either in a local or district heating system (Reuss 2015; Gehlin, 2016). In district heating systems, BTES is designed to be one of the pre-heaters before the condenser as shown in Figure 15 (Malmberg, 2017; Xu et al., 2018). In the CHP unit, a flue gas condenser is the first pre-heater in the district heating system due to its low cost (Mäkelä and Tuunanen, 2015; Malmberg, 2017). Therefore, additional pre-heaters are advisable to connect after the flue gas condenser. In Finland, typical district heating fluid return temperature varies between 40 and 60 °C and its required heating power depends on the heat demand in the district heating system (Energiateollisuus, 2014; Malmberg, 2017). If the condenser of the CHP unit alone is not

enough to satisfy the heat demand, pre-heaters are used to provide extra power (Mäkelä and Tuunanen, 2015) Additionally, the heating power of the BTES may be enhanced by connecting adsorption or compression heat pumps to the system. During the summer, the waste heat of power plant condenser is used to charge the BTES. (Malmberg, 2017; Xu et al., 2018).

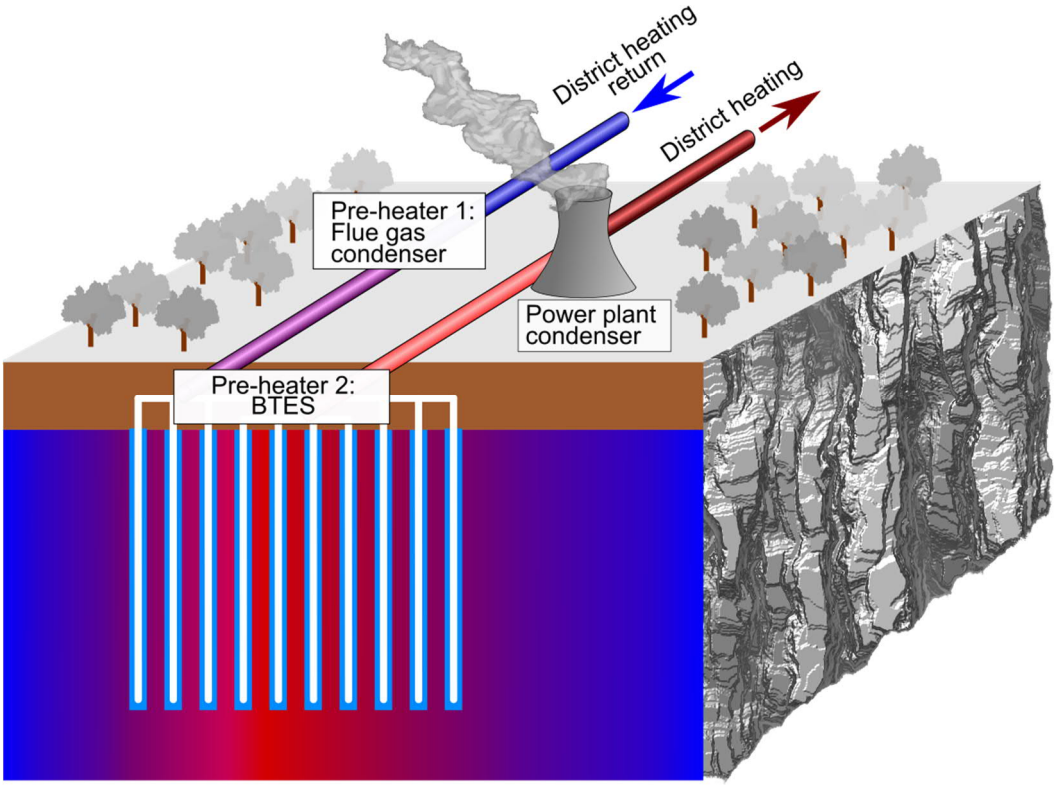

Figure 15. Schematic figure showing how flue gas condenser, BTES and power plant condenser are connected in the district heating system.

2.2.4 High-temperature borehole thermal energy storage applications

To date, nine known HT-BTES applications have been constructed in the world, as shown in Table 4 (Malmberg, 2017; Xu et al., 2018; Hakala et al., 2019). Six of the BTESs are currently in operation (Malmberg, 2017), while two storage facilities has no results available from the operation (Xu et al., 2018; Hakala et al., 2019). The pilot storage facility in Luleå (Sweden) was in operation in the 1980s (Malmberg, 2017).

Industrial waste heat assisted experimental BTES projects Emmaboda and Luleå faced difficulties as a result of using open coaxial BHEs. At first, both systems used pressure below 1 bar, which led to problems with gas dissolution into the heat carrier fluid. (Nordell, 1994; Nordell et al., 2015). The high concentrations of gases caused problems with the precipitation of oxides in the system (Nordell et al., 2015). Additionally, both experiments recognized higher heat losses than expected (Nordell, 1994; Nordell et al., 2015). So far, the BTES experiment in Luleå has been cancelled due

to errors made in design and construction, but the BTES experiment in Emmaboda is the ongoing (Malmberg, 2017). Nordell et al (2015) recommended using only closed-loop BHEs to avoid the problems encountered in these experiments.

The BTES experiment in Paskov is the first BTES connected to a CHP unit. So far, the experiment has been a scientific optimization project to determine the optimal lengths of injection and extraction periods and to estimate the efficiency of the storage. Simulations revealed that under optimal conditions 65 % heat recovery can be achieved in full-scale operation. At this stage, only measured injection power is available from Paskov. (Rapantova et al., 2016). Another small-scale pilot storage system connected to a CHP is in Brædstrup. At the full-scale operation, the storage is expected to include 480 boreholes and provide 3.6 MW thermal energy (Sørensen et al., 2012). The temperature will be boosted by the heat pump or electric heater as shown in the schematic in Figure 16 (Bach, 2012).

Among already existing BTES projects Drake Landing, Crailsheim and Neckarsulm are solar-assisted and successfully connected with the district heating system. These BTES systems, together with solar panels, supply heat to 52 homes in Drake Landing (Sibbitt et al., 2011; Sibbitt et al.2012), 260 homes in Crailsheim (Bauer et al., 2016) and 700 homes in Neckarsulm (Reuss, 2015). Industrial waste heat and solar assisted BTES in Chifeng is planned to connect with the district heating system that provides heat for one million residents (Guo et al., 2017). BTES in Toholampi started its operation in spring 2019 and it is connected with the local heating system.

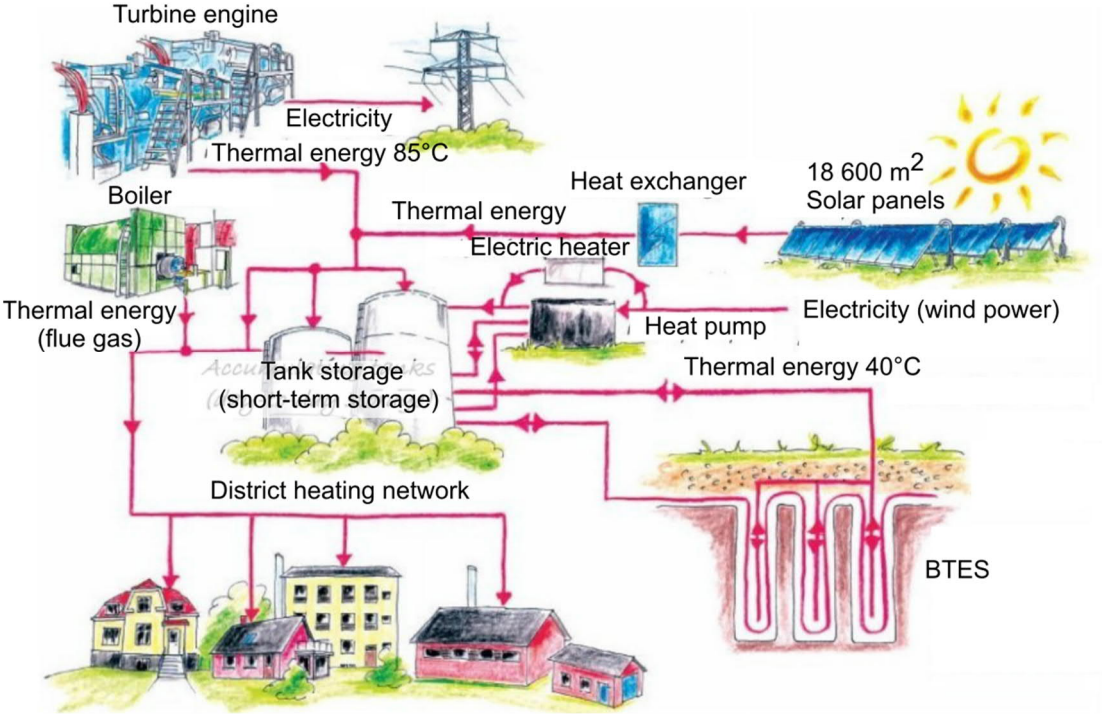

Figure 16. Schematic figure showing heating network of CHP for district heating in Brædstrup (modified after Bach, 2012)

Table 4. Review of high temperature borehole thermal energy storages connected in district heating system. (Malmberg, 2017 [1]; Schmidt and Sørensen, 2018 [2]; Sørensen and Schmidt, 2018 [3]; Sibbitt et al., 2012 [4]; Sibbitt et al., 2011 [5]; Bauer et al., 2016 [6]; Philippe et al., 2009 [7]; Nussbicker et al., 2006 [8]; Nussbicker et al., 2007 [9]; Nordell et al., 2015 [10]; Nordell, 1994 [11]; Rapantova et al., 2016 [12]; Guo et al., 2017 [13]; Xu et al., 2018 [14]; Arola et al., 2019 [15])

Parameters	**Unit**	**Brædstrub** [1,2,3]	**Chifeng** [13,14]	**Toholampi** [15]	**Drake Landing** [1,4,5]	**Crailsheim** [1,6,7]	**Neckarsulm** [1,7,8,9]	**Emmaboda** [1,10]	**Luleå** [1,11]	**Paskov** [1,12]
Country		Denmark	China	Finland	Canada	Germany	Germany	Sweden	Sweden	Czech Republic
Operation		2012-	2018-	2019-	2007-	2008-	1999-	2010-	1983-89	2011-
Source of heat		Waste heat +solar	Waste heat +solar	Waste heat +solar	Solar	Solar	Solar	Waste heat	Waste heat	Waste heat
Storage medium		Soil (clay)	Soil	Rock	Soil	Soil	Soil	Rock	Rock	Rock
BHE type		Double U-tube	Single U-tube	Single U-tube	Single U-tube	Double U-tube	Double U-tube	Open coaxial	Open coaxial	Double U-tube
BHE material		PE-X	-	PE-RT	PE-X	PE-X	PB		-	PE-RT
No. of BHs		48	468	61	144	80	528	140	120	16
Storage shape		Cylindrical	Hexagon	Hexagon	Cylindrical	Cylindrical	Rectangular	Rectangular	Rectangular	Rectangular
Dimensions	m	r = 15	r = 52 m	r = 12.1	r = 17.5	r = 13.9	30x48/24x28	40x56	36x44	10x10
Land area	m^2	707	7025	380	962	607	2112	2240	1584	100
BHE length	m	45	80	45	37	55	30	45	65	60
Storage volume	m^3	19 000	500 000	17 100	37 500	34 000	63 360	323 000	115 000	6 000
D/L –ratio		0.67	1.3	0.54	0.83-0.97	0.5	0.8-1.6	0.27-0.37	0.55-0.67	0.17
BH spacing	m	3	4	2.5	2.25	2.25	2	4	4	2.5
BH Pattern		Hexagonal	Hexagonal	Hexagonal	Quadratic	Quadratic	Quadratic	Quadratic	Quadratic	Quadratic
BH Diameter	m	0.15	-	0.115	0.15	0.13	0.15	0.115	0.152	0.12
BHEs in series		6	6	4	6	2	6	2	5	2
Thermal diffus.	m^2s^{-1}	$0.75 \cdot 10^{-6}$		$0.52 \cdot 10^{-6}$	$0.87 \cdot 10^{-6}$	$1.03 \cdot 10^{-6}$	$0.77 \cdot 10^{-6}$	$1.28 \cdot 10^{-6}$	$1.50 \cdot 10^{-6}$	$0.94 \cdot 10^{-6}$
Charging temp.	°C	35-80	75*	70*	40-67	32-50	50-63	30-60	32-50	70-97
Storage temp.	°C	12-50	43-60*	20-70*	50-63	32-50	50-63	37-43	39-68	39-78
Extracted energy	MWh	226.8	2170*	-	250	382	321.5	89	1000	-
Injected energy	MWh	360	3290*	-	700	707	734.5	3271	2300	2000
Efficiency	%	63	66*	-	36	54	44	3	44	-
Max power	MW	0.600	-	-	-	0.530	0.500	-	0.500	-

**Simulated values, no monitored values available.*

2.2.5 Economical aspects

To make STES competitive in district heating systems, price and demand variations are required. Waste heat is stored when the price and demand are low, and therefore, some of the heat generated in summer can be stored and extracted later during the colder season when the price and demand are high. Previously, waste heat created no revenues for a power plant, but seasonal storage offers the possibility of higher revenues. Base load plants have a low seasonal price variation in current district heating systems, but peak load plants are expensive to operate and generate seasonal price variations. Due to expensive operation, they are the main competitor to STES. Therefore, the cost-effectiveness of seasonal energy storage must be economical in comparison to the peak load plant to make it attractive investment for the district heating system. (Gadd and Werner, 2015).

In terms of the storage cost per water equivalent volume, BTES is one of the most competitive STES options (Tveit et al., 2009; Rossi Espagnet, 2016; Welsch et al., 2018). However, the competitiveness of the storage type depends on its size. Often, relative storage losses decrease as storage volume increases, making the larger storage units an attractive choice compared with medium-scale units (Gadd and Werner, 2015). For that reason, larger storage units cost less per volume or kilowatt hour (kWh) in comparison to smaller storages, but this price behaviour depends strongly on the storage type (Tveit et al., 2009). However, such straightforward conclusions cannot yet be drawn for BTES due to lack of experiments with various storage sizes. So far, HT-BTES consistently costs between 0.65-2.6 € kWh^{-1} (thermal energy) (Sibbitt et al., 2011; Rossi Espagnet, 2016).

The cost of BTES arises from the investment, maintenance and operational costs as well as from the storage efficiency (Manonelles, 2014). The initial investment cost of BTES is high, which is mostly attributable to drilling (Lanahan and Tabares-Velasco, 2017). The cost of drilling is directly proportional to the borehole length and number of boreholes (Lanini et al., 2014; Manonelles, 2014). If HT-BTES is used, extra cost is incurred because it requires heat-resistant pipes. Heat resistant materials with thicker pipe walls are more expensive than pipe materials required for LT-BTES. (Sibbitt and McClenahan, 2015). When BTES systems are connected with CHPs and district heating systems, they may require additional heat pumps and heat exchanger investments, which also increase cost (Malmberg, 2017; Xu et al., 2018). On the other hand, cost savings can be achieved in hydrogeologically feasible regions by choosing natural groundwater over bentonite to backfilling U-tube pipes (Gehlin, 2016). After all initial investments, BTES has a low maintenance and operational costs, making it competitive storage option (Lanahan and Tabares-Velasco, 2017; Manonelles, 2014). Figure 17 summarizes factors effecting the price of BTES

According to Welsch et al. (2018), a BTES unit connected into a CHP unit is not economically optimal if the unit consumes electricity from the grid due to the transmission costs of electricity. They determined that the economically optimal solution includes an additional renewable energy source in the same site connected to the BTES unit to produce electricity for it. However, the authors did not consider a fluctuating electricity market, which could have led to a different outcome.

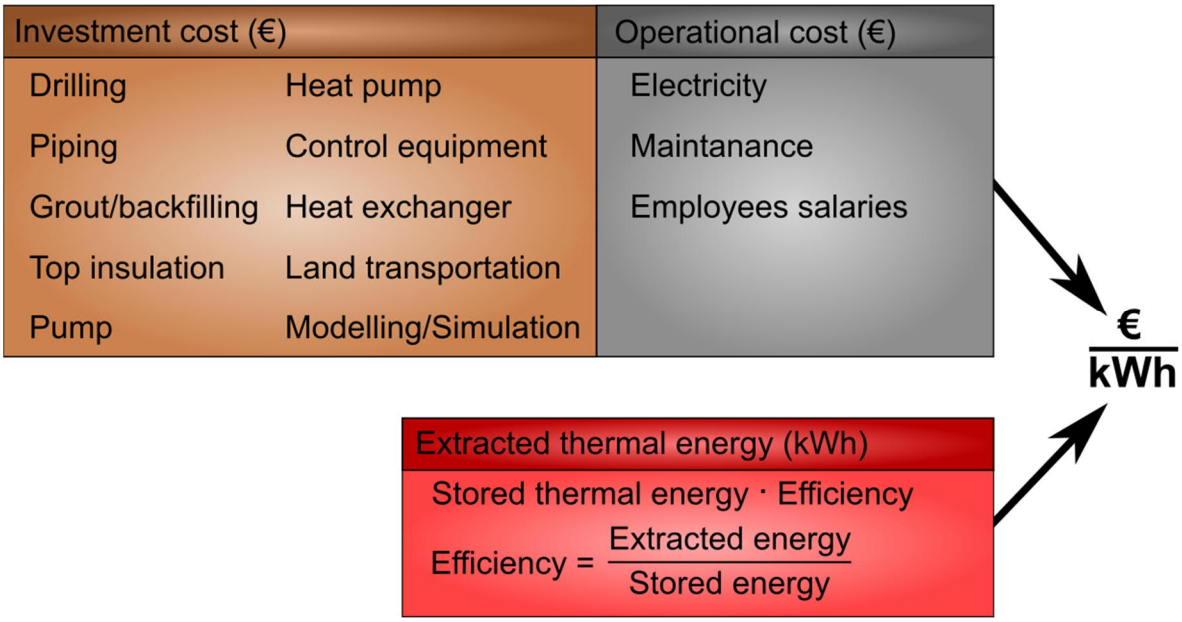

Figure 17. Economic factors effecting the price of BTES per kWh.

2.2.6 Environmental aspects

According to Bakema et al. (1995) UTES has an indirect positive environmental impact. Heat that was previously produced from the peak load plant operated by fossil fuels could instead be produced from stored waste heat. For that reason, UTES may replace fossil fuels and reduce CO_2, NO_x and SO_2 –emissions. However, because UTES requires electricity for pumping, the environmental impact of UTES depends on the source of electricity. A clean electricity source for UTES may reduce emissions significantly. Although UTES may have a clear beneficial impact on the environment, its positive impact has been questioned if the storage is connected into the CHP unit. Storage losses and electricity generated from the grid may cancel out CO_2-benefits achieved with UTES (Welsch et al., 2018).

Risks of UTES relate to disturbing subsurface ecology, degrading groundwater quality and contaminating drinking water (see Figure 18) (Bonte et al., 2011). However, the risks of BTES are dependent on the geological environment. Regions with sedimentary rocks have the higher risks than regions with igneous or metamorphic rocks. Nevertheless, BTES posts some common risks to

groundwater in all environments, including the growth of micro-organisms, algae production, leaching of heavy metals (e.g. As, Ni, Cd, Zn) or chlorides, oxidation of organic compounds and changing natural groundwater temperature. These may have a negative impact on groundwater quality; therefore, special attention is required in case of the storage locates close to regions with the important groundwater resource (Bonte et al., 2011; Brielmann et al., 2009). Especially increased groundwater temperature will affect by decreasing pH and oxygen saturation and by increasing oxidation of heavy metals and organic compounds (Saito et al., 2016; Riedel, 2019). In high-temperature BTES applications, mineral weathering may increase due to hydrothermal alteration. Warm groundwater (> 50 °C) may leach, transport and precipitate minerals as a result of changing geological conditions (Pirajno, 2009). However, the environmental impacts of BTES have not been fully explored (Brielmann et al., 2009).

The environmental risks related to heat transfer fluid or drilling are higher in regions with sedimentary rocks; therefore, appropriate sealing is required (Brielmann et al., 2009; Gehlin, 2016). BHEs sealed with groundwater are common in the regions with the hard igneous or metamorphic rocks (Gehlin, 2016). The most important environmental risks are summarized in Figure 18.

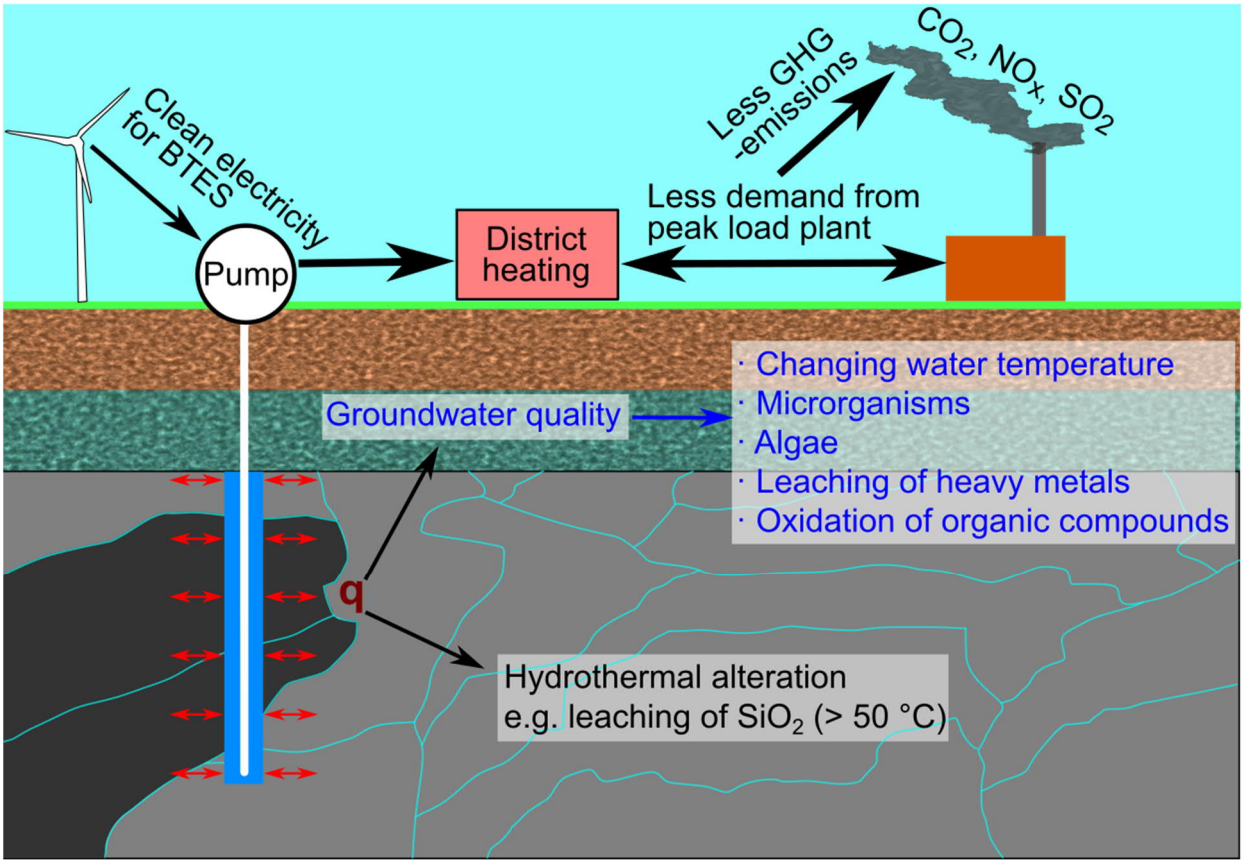

Figure 18. Environmental impacts of BTES. Positive environmental impacts decrease greenhouse gas emissions due to less demand from peak load plant. Negative environmental impacts decrease groundwater quality.

3 Methods

3.1 Location

The location of planned BTES system connected with waste incineration power plant is in Korvenmäki landfill area (see Figure 19), in the town of Salo, in southwest Finland (N = 6699696, E = 292390, ETRS-TM35FIN). Therefore, the simulations utilized data provided by power plant company. According to Lounavoima (2019), the power plant produces 34 MW of heat for 10,000 residents in the district heating network of Salo. This site-specific data was used to calculate the amount of waste heat the power plant produces during summer. Heat demand data is based on estimated demand in the district heating network during the winter season.

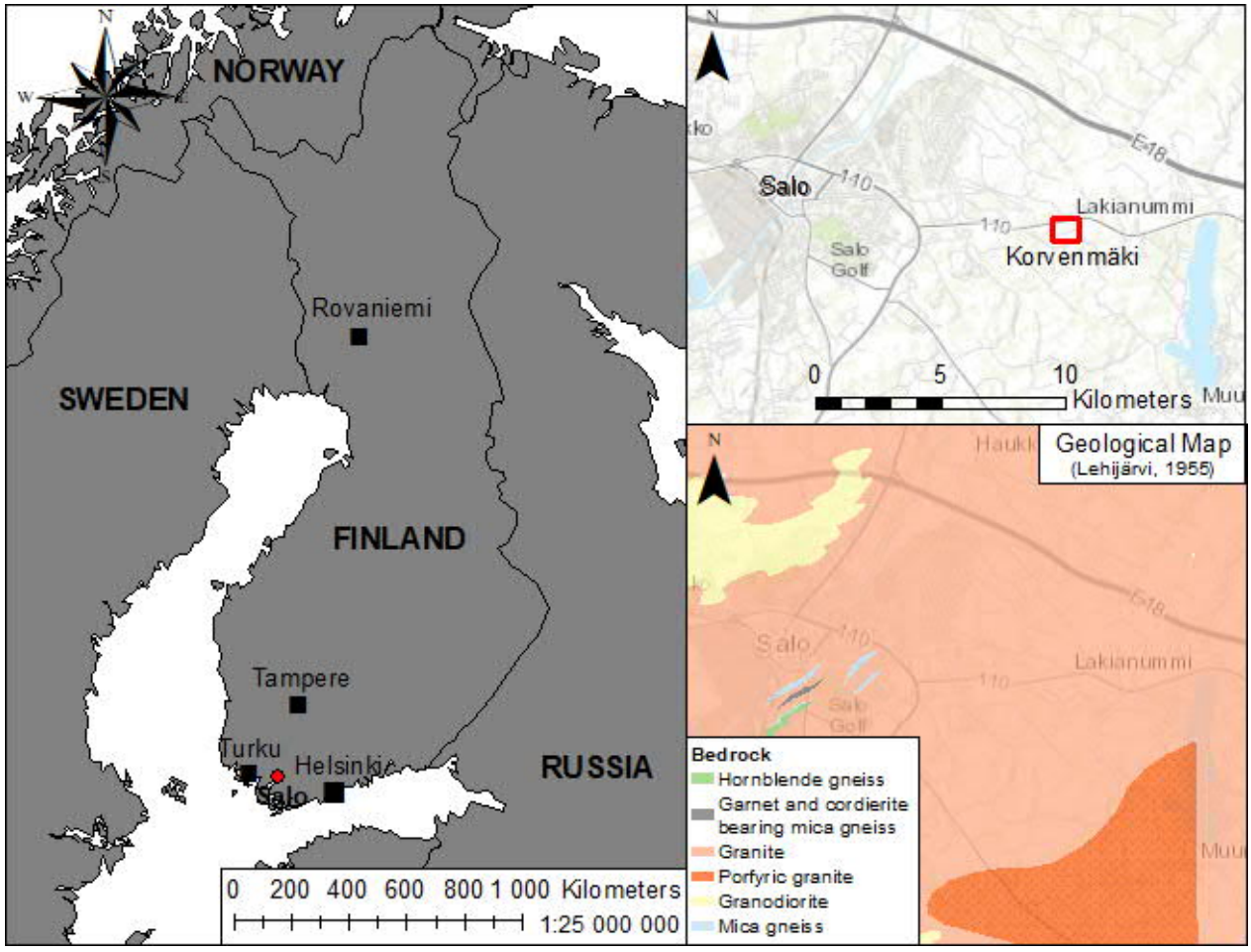

Figure 19. The location of the BTES system, which is in the planning stage. The bottom right corner shows a geological map of the region.

3.1.1 Geology

According to Lehijärvi (1955), the Salo region is mostly covered by granitic rocks. However, such migmatites, different gneisses, metavulcanic and metasedimentary rocks are also typical for the region (Aho, 2015). These rocks formed 1.90 Ga ago in Svecofennian orogeny and subsequently metamorphosed 1.83 Ga ago (Lahtonen et al., 2005)

Soil cover is extremely thin, and granite and hornblende gneiss are the main rock types in Korvenmäki landfill area. Their contents have been estimated to be distributed equally in the bedrock. Thermal properties of both rock types were analysed in the laboratory of the Geological Survey of Finland and the results are presented in Table 5.

Figure 20. Landscape picture of the rock cutting located below the planned BTES. Black-coloured rocks are mostly hornblende gneiss and red-coloured rocks granite Picture: Sami Vallin.

Table 5. Thermal properties of rock samples taken from Korvenmäki. Rock samples were analysed in the laboratory of the Geological Survey of Finland at room temperature.

Parameter		**Unit**	**Value**	**Value**	**Value**
			Granite	**Hornblende gneiss**	**Average**
Thermal conductivity	k_r	W m^{-1} K^{-1}	2.90	2.04	2.47
Density	ρ_r	kg m^{-3}	2610	2883	2746.5
Specific heat capacity	$c_{p,r}$	J kg^{-1} K^{-1}	676	695	685.5
Thermal diffusivity	α_r	m s^{-2}	$1.64 \cdot 10^{-6}$	$1.02 \cdot 10^{-6}$	$1.31 \cdot 10^{-6}$

3.2 Finite element method

The numerical model was created using the commercial software package COMSOL Multiphysics (version 5.4) and solved utilizing the finite element method. In order to develop scientific valid numerical model, the simulation language in COMSOL Multiphysics was verified by comparing simple solutions with those obtained using two other software packages. The method used was validated by comparing simulation results to results of experimental thermal response test results conducted by the Geological Survey of Finland.

The simplified and efficient model created in this thesis is based on the method derived by Al-Khoury and Bonnier (2006). In this method, heat transfer is modelled in 3D domain to simulate

heat flow in underground material. As thermal conductivity is assumed to be constant, a heat equation can be simplified as shown by Bergman et al. (2011):

$$\frac{\partial^2 T_r}{\partial x^2}+\frac{\partial^2 T_r}{\partial y^2}+\frac{\partial^2 T_r}{\partial z^2}+\frac{q}{k_r}=\frac{1}{\alpha_r}\frac{\partial T_r}{\partial t}. \tag{3.1}$$

Simplified fluid flow and heat transfer in BHEs is described by three partial differential equations (PDE) derived for the transient BHE problem (Al-Khoury and Bonnier, 2006). The equations simplify BHEs in 1D heat pipe element with pseudo 3D heat transfer, as illustrated in Figure 21. These equations describe the inlet pipe (subscript i), outlet pipe (subscript o) and grout (subscript g), respectively:

$$\rho_f c_{p,f}\frac{\partial T_i}{\partial t}dV_i-k_f\frac{d^2T_i}{dz^2}dV_i+\rho_f c_{p,f}u(t)\frac{dT_i}{dz}dV_i=b_{ig}\left(T_i-T_g\right)dS_{ig}$$

$$\rho_f c_{p,f}\frac{\partial T_o}{\partial t}dV_o-k_f\frac{d^2T_i}{dz^2}dV_o-\rho_f c_{p,f}u(t)\frac{dT_o}{dz}dV_o=b_{og}\left(T_o-T_g\right)dS_{og}$$

$$\rho_g c_{p,g}\frac{\partial T_g}{\partial t}dV_g-k_g\frac{d^2T_g}{dz^2}dV_i=b_{ig}\left(T_g-T_i\right)dS_{ig}+b_{og}\left(T_g-T_i\right)dS_{og}+b_{rg}\left(T_g-T_i\right)dS_{rg}. \tag{3.2}$$

In this study, net heat conduction is assumed negligible in the z-direction. Therefore, the equations can be simplified as follows:

$$\rho_f c_{p,f}\frac{\partial T_i}{\partial t}dV_i+\rho_f c_{p,f}u(t)\frac{dT_i}{dz}dV_i=b_{ig}\left(T_i-T_g\right)dS_{ig}$$

$$\rho_f c_{p,f}\frac{\partial T_o}{\partial t}dV_o-\rho_f c_{p,f}u(t)\frac{dT_o}{dz}dV_o=b_{og}\left(T_o-T_g\right)dS_{og}$$

$$\rho_g c_{p,g}\frac{\partial T_g}{\partial t}dV_g=b_{ig}\left(T_g-T_i\right)dS_{ig}+b_{og}\left(T_g-T_o\right)dS_{og}+b_{rg}\left(T_g-T_r\right)dS_{rg}. \tag{3.3}$$

Additionally, the finite element model requires these equations to be derived to weak formulation (Al-Khoury et al., 2005). Therefore, the equations must be modified by using Galerkin's method:

$$\int_V \rho_f c_{p,f}\frac{dN^T}{dt}\frac{dT_i}{dt}dV_i+\int_V \rho_f c_{p,f}u(t)\frac{dN^T}{dz}\frac{dT_i}{dz}dV_i=\int_S N^T b_{ig}\left(T_i-T_g\right)dS_{ig}$$

$$\int_V \rho_f c_{p,f}\frac{dN^T}{dt}\frac{dT_o}{dt}dV_o+\int_V \rho_f c_{p,f}u(t)\frac{dN^T}{dz}\frac{dT_o}{dz}dV_o=\int_S N^T b_{og}\left(T_o-T_g\right)dS_{og}$$

$$\int_V \rho_g c_{p,g} \frac{dN^T}{dt} \frac{dT_g}{dt} dV_g =$$

$$\int_S (N^T b_{ig}(T_g - T_i) dS_{ig} + N^T b_{og}(T_g - T_o) dS_{og} + N^T b_{rg}(T_g - T_r) dS_{rg}) . \quad (3.4)$$

As suggested by Ozudogru et al. (2014), physics module for weak form edge PDE is used to model line elements as BHEs in COMSOL MultiPhysics. In these equations, ρ_f and $c_{p,f}$ represent the density and specific heat capacity of heat exchanger fluid, and ρ_g and $c_{p,g}$ represent the density and specific heat capacity of grout. Average fluid velocity is denoted by u, temperature as a function of time is dT/dt and as a function of depth dT/dz. Derivatives of volume dV_i and dV_o describe cross-sectional surface areas of inlet and outlet legs of the U-tube pipe A_p, and derivatives of surface areas dS_{ig} and dS_{og} are perimeters of inlet and outlet legs of the U-tube pipe P_{pi}. The derivative of volume of grout dV_g is a cross-sectional area of the borehole A_g and derivative of surface area of grout dS_{rg} is the perimeter of the borehole P_g.

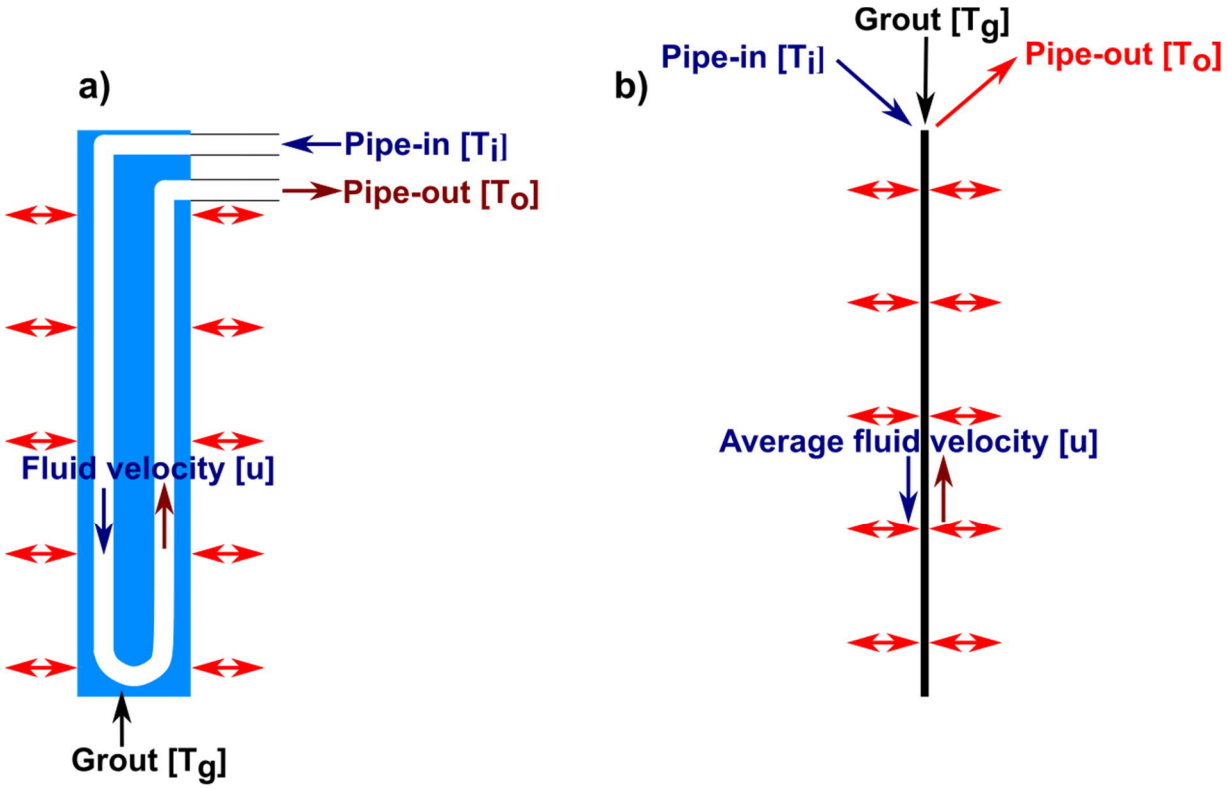

Figure 21. a) Schematic illustration of single U-tube pipe. b) Simplification of the single U-tube pipe as a heat pipe element.

The unknown heat transfer coefficients b_{ig}, b_{og} and b_{sg} represent heat flux constant between the inlet pipe and grout, outlet pipe and grout, and grout and underground material, respectively. The relationship between the heat transfer coefficients and thermal resistances of BHEs can be derived using Fourier's law and Ohm's law, as demonstrated by Diersch et al. (2010):

$$b_{ig} = b_{og} = \frac{1}{2\pi r_{po} R_p}$$

$$b_{rg} = \frac{1}{2\pi r_b R_g}, \tag{3.5}$$

in which r_{po} is the outer radius of one leg of the single U-tube pipe, r_b is the radius of the borehole, R_p is the thermal resistance of pipe, and R_g is the thermal resistance of the grout. The inlet and outlet pipes are assumed to have geometrical and thermal symmetry. According to Javed and Spitler (2017), the thermal resistance of the pipe can be divided into conductive resistance of the pipe wall (R_{pc}) and convective resistance of the heat exchange fluid (R_{pf}):

$$R_p = R_{pc} + R_{pf}, \tag{3.6}$$

and thermal resistance of pipe wall can be calculated, as follows:

$$R_{pc} = \frac{1}{2\pi k_p} \ln\left(\frac{r_{po}}{r_{pi}}\right), \tag{3.7}$$

where k_p is the thermal conductivity of the pipe material and r_{pi} is the inner radius of one leg of the single U-tube pipe. The thermal resistance of the heat exchanging fluid can be calculated using Equation 3.8:

$$R_{pf} = \frac{1}{2\pi r_{pi} h_f}. \tag{3.8}$$

Furthermore, total borehole resistance must be calculated in order to determine thermal resistance of grout and the heat transfer coefficient between grout and soil. Total borehole resistance can be calculated using the first-order multipole method derived by Claesson and Hellström (2011):

$$R_b = \frac{1}{4\pi k_g}\left[\beta + \ln\left(\frac{\theta_2}{2\theta_1(1-\theta_1^4)^{\sigma}}\right) - \frac{\theta_3^2\left(1-\frac{4\sigma\theta_1^4}{1-\theta_1^4}\right)^2}{\frac{1+\beta}{1-\beta} + \theta_3^2\left(1+\frac{16\sigma\theta_1^4}{(1-\theta_1^4)^2}\right)}\right]. \tag{3.9}$$

In this method, k_g is thermal conductivity of grout and θ_1, θ_2, θ_3, σ and β are defined as follows:

$$\theta_1 = \frac{s}{2r_b}, \qquad \theta_2 = \frac{r_b}{r_{po}}, \qquad \theta_3 = \frac{r_{po}}{s}, \qquad \sigma = \frac{k_g - k_r}{k_g + k_r}, \qquad \beta = 2\pi k_g R_p, \tag{3.10}$$

in which s is the shaft spacing and r_b and r_{po} are borehole radius and outer pipe radius, respectively. R_p is the thermal conductivity of the single U-tube pipe and k_r is the thermal conductivity of the rock. As the legs of the single U-tube pipe are connected in parallel and the U-tube pipe and grout are connected in series, the thermal resistance of the grout can be solved as follows (Javed and Spitler 2017):

$$R_g = R_b - \frac{R_p}{2}. \tag{3.11}$$

The heat transfer coefficient of heat exchanging fluid h_f is dependent on the Nusselt number Nu, thermal conductivity of theheat exchanger fluid k_f and thehydraulic diameter of the pipe D_h as described by Bergman et al. (2011):

$$h_f = \frac{Nuk_f}{D_h}, \tag{3.12}$$

in which the dimensionless Nusselt number describes convective heat transfer at the surface. It is calculated using Gnielinski correlation (Bergman et al., 2011)

$$Nu = \frac{\left(\frac{f_s}{8}\right)(Re - 1000)Pr}{1 + 12.7\left(\frac{f_s}{8}\right)^{\frac{1}{2}}\left(Pr^{\frac{2}{3}} - 1\right)}. \tag{3.13}$$

The Gnielinski correlation is valid only for smooth surfaces with Prandtl numbers (Pr) between 0.5 and -2000 and Reynolds number (Re) between 3,000 and -5,000,000. The Reynolds number, which describes the ratio of viscous and inertial forces, depends on the density of the heat exchanger fluid (ρ_f), average velocity of the fluid (u), hydraulic diameter of the pipe (D_h) and dynamic viscosity of the fluid (μ_f) (Bergman et al., 2011):

$$Re = \frac{\rho_f u D_h}{\mu}. \tag{3.14}$$

As Nusselt number correlation is valid only for smooth surfaces, friction factor (f_s) must be calculated using the equation for smooth surfaces derived by Petukhov (1970):

$$f_s = (0.790 * \ln(Re) - 1.64)^{-2} \qquad 3000 \lesssim Re \lesssim 5{,}000{,}000. \tag{3.15}$$

Fluid average velocity is calculated by converting fluid mass flow rate ($\dot{m}$) into velocity as follows:

$$u(t) = \frac{\dot{m}(t)}{\rho_f} \cdot A_p. \tag{3.16}$$

The BHE element includes Dirichlet type boundary conditions, and the BHE has prescribed inlet temperature that is defined as follows (Al-Khoury et al., 2005):

$$T_i = T_{inlet}(z = 0). \tag{3.17}$$

The rest of the BHE requires numerical calculation using the set of Equations 3.4. The second boundary condition describes the bottoms of inlet and outlet pipes to having the same temperature:

$$T_i = T_o(z = l_b). \tag{3.18}$$

3.2.1 Code verification

According to Sargent (2013), verification ensures that simulation software calculates the appropriate equations correctly. Therefore, verification refers to the mathematical correctness of the software or model (Oberkampf and Roy, 2011). The simulation language in COMSOL Multiphysics was verified by comparing the solution of the 2D heat equation (Eq. 3.1) between COMSOL MultiPhysics and MATLAB, from which MATLAB code utilized code written by Vuorinen (2018). It solves the 2D heat equation on Cartesian grid utilizing the second-order finite difference method and Euler time stepping. In both software, the simulations for verification were carried out in a domain that has a circular heat source at the centre (see Figure 22). In these simulations, the heat source represents a borehole that has a constant wall temperature and the rest of the domain represents bedrock that has average thermal properties of Korvenmäki region bedrock that has periodic boundary conditions. Table 6 provides all parameters used for the verification.

Table 6. Parameters used for verifying implementation of heat equation

Parameter	Unit	Value
Mesh		200 · 200
Time step	s	1.9446
r_b	m	0.115
T_b	°C	85
T_{r0}	°C	6
k_r	W m^{-1} K^{-1}	2.47
ρ_r	kg m^{-3}	2746.5
c_r	J kg^{-1} K^{-1}	685.5
α_r	m s^{-2}	1.31 · 10^{-6}

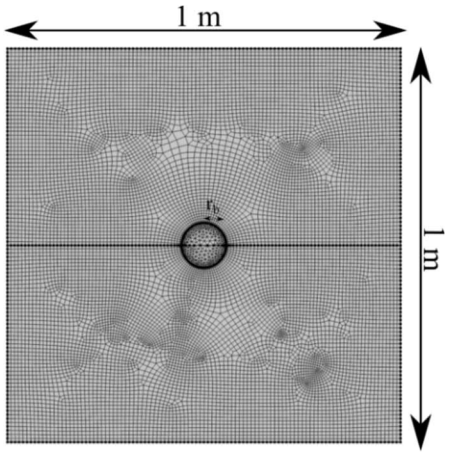

Figure 22. Geometry of the simulated domain.in the code verification

In addition to, the implementation of COMSOL MultiPhysics, the set of Equations 3.3 was verified using an analytical Excel solution. In order to verify the simulation language, only the geometry of the borehole with a BHE element was modelled, as shown in Figure 22. This solution was compared to the Excel-based analytical solution, that was derived in Section 2.1.1 (Equations 2.2-2.5). As the analytical solution requires a prescribed borehole wall temperature, the boundary condition of the borehole wall T_b equals the initial bedrock temperature. In order to copy the solution of BHE element throughout the borehole geometry, thermal diffusivity of the borehole domain is set as a large value ($\alpha_r > 100$ m^2 s^{-1}). All essential parameters are provided in Table 7.

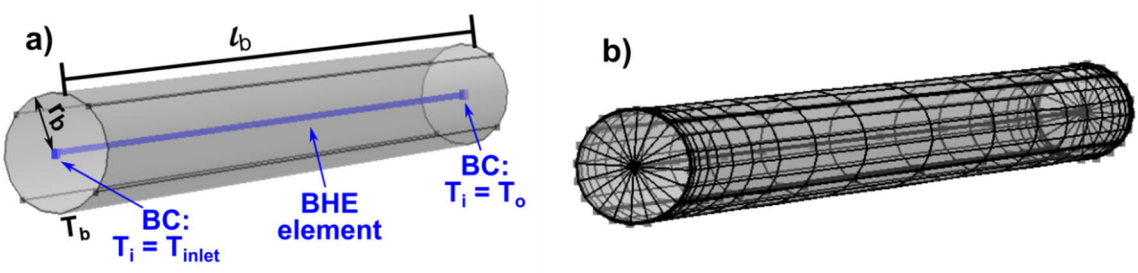

Figure 23. a) Dimensions of simulated borehole in the code verification. Boundaries of inner borehole have prescribed temperature of T_b. b) Mesh. Borehole includes 16 elements per layer and 100 elements in z-direction

Table 7. All parameters for verification of set of Equations 3.3

Parameter	Unit	Value
l	m	100
r_b	m	0.115
r_{po}	m	0.0250
r_{pi}	m	0.0205
s	m	0.0590
k_f	W m^{-1} K^{-1}	0.656
ρ_f	kg m^{-3}	977.32
$c_{p,f}$	J kg^{-1} K^{-1}	4214.29
α_f	m s^{-2}	$4.21 \cdot 10^{-6}$
Pr		2.76
k_g	W m^{-1} K^{-1}	1.88
ρ_g	kg m^{-3}	2225
$c_{p,g}$	J kg^{-1} K^{-1}	1071
α_g	m s^{-2}	$0.79 \cdot 10^{-6}$
k_r	W m^{-1} K^{-1}	2.47
b_{ig}	W m^{-2} K^{-1}	81.256
b_{rg}	W m^{-2} K^{-1}	84.635

3.2.2 Al-Khoury and Bonnier's method validation

According to Sargent (2013), a method validation determines the representation of theories and assumptions for a modelled system at reasonable accuracy. Therefore, validation refers to the physical correctness of a method or model (Oberkampf and Roy, 2011). The transient method derived by Al-Khoury and Bonnier (2006) was validated by comparing simulation results from COMSOL MultiPhysics with data from in -situ thermal response tests (TRT) measured by the Geological Survey of Finland. According to Reuss (2015), a TRT is an in situ experiment that determines the thermal performance of BHEs, and its temperature recovery is evaluated during injection or extraction of energy.

The Geological Survey of Finland provided two TRT-measurements from Espoo (southern Finland, near Helsinki) and Rovaniemi (northern Finland) (see Figure 19 for location); therefore, the method was validated in two separate simulation models. Fluid inlet temperature was prescribed based on TRT data, and the output data of the simulations includes fluid outlet temperature and two separate values for power—one released by fluid to the surroundings and one flowing through the borehole wall. The results are shown in error plots, where the error for outlet temperature and power are calculated using Equations 3.19 and 3.20, respectively:

$$E_T = \frac{T_{outlet,sim} - T_{outlet,meas}}{T_{outlet,meas}} \cdot 100 \tag{3.19}$$

$$E_q = \frac{q_{sim} - q_{meas}}{q_{meas}} \cdot 100. \tag{3.20}$$

In both cases, the error is calculated from the last time moment. Boundary conditions are predefined on six boundary surfaces. The top surface is thermally insulated and therefore, there is no heat flux through the upper boundary:

$$q = 0. \tag{3.21}$$

The boundary conditions of the vertical domain edges are periodic where opposite edges are prescribed as having no temperature difference, as follows:

$$\Delta T = 0. \tag{3.22}$$

The bottom boundary of the domain is defined as representing geothermal flux. According to Kukkonen (1989), geothermal flux is 0.040 W m^{-2} in Finland. All essential parameters for method validation are given in Table 8. In model validation, the borehole geometry shown in Figure 23 is connected in the underground domain (Figure 24).

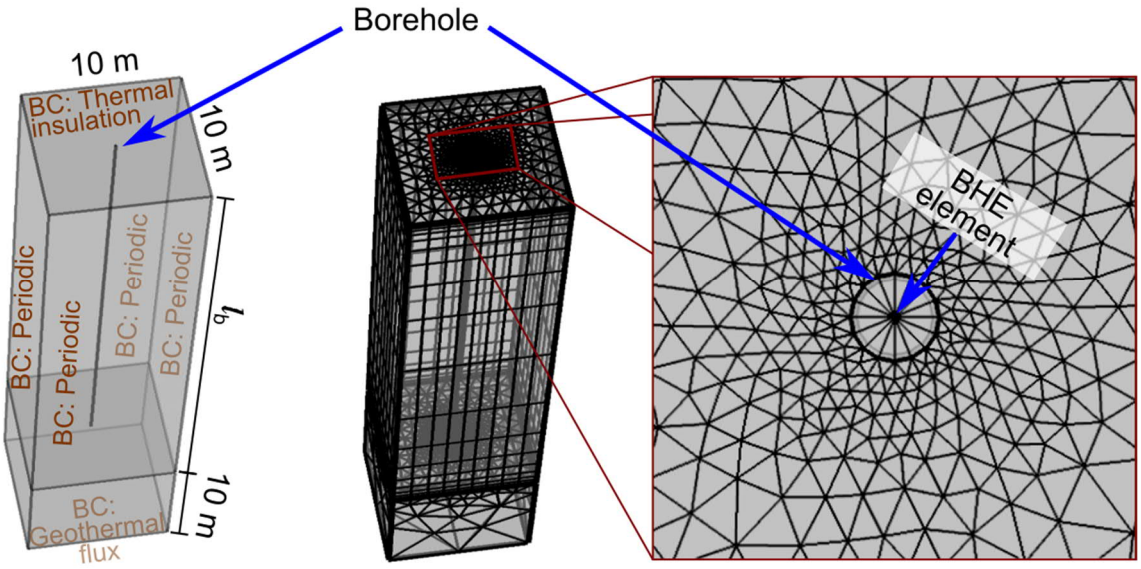

Figure 24. The model used for method validation and verification.

Table 8. All essential parameters for method validation and verification.

		Espoo	Rovaniemi
Parameter	**Unit**	**Value**	**Value**
l_b	m	287.5	246.1
Domain	m	10 · 10	10 · 10
Mesh	xy · z	2400 · 500	2400 · 500
r_b	m	0.0572	0.0572
r_{po}	m	0.020	0.020
r_{pi}	m	0.018	0.018
k_p	W m^{-1} K^{-1}	0.39	0.39
s	m	0.075	0.075
$\dot{m}$	kg s^{-1}	0.64	0.66
T_{r0}	°C	8.76	5.30
q_{geo}	W m^{-2}	0.042	0.042
k_f	W m^{-1} K^{-1}	0.656	0.656
ρ_f	kg m^{-3}	950	950
$c_{p,f}$	J kg^{-1} K^{-1}	4021.05	4021.05
μ_f	m s^{-2}	3.279 · 10^{-3}	3.279 · 10^{-3}
Pr		31.393	31.393
k_g	W m^{-1} K^{-1}	1.6	1.6
ρ_g	kg m^{-3}	1000	1000
$c_{p,g}$	J kg^{-1} K^{-1}	4200	4200
k_r	W m^{-1} K^{-1}	3.2	3.2
$\rho_r c_{p,r}$	J m^{-3} K^{-1}	2.40 · 10^{6}	2.40 · 10^{6}
R_b	m^2 K W^{-1}	0.067	0.0720

3.2.3 Al-Khoury and Bonnier's method verification

According to Oberkampf and Roy (2011), the most common way to verify numerical models is to increase mesh densities and calculate convergence rate. This procedure enables one to approximate error caused by mesh. In fluid dynamics, model error is considered to be acceptable if the difference between the measured and predicted values is less than 10 % (Zhang et al., 2007); therefore, the effort is made to keep mesh error below 10 %. In order to determine a sufficient grid for a final numerical BTES model, convergence rates of pipe-out temperature and integration of power through the borehole wall were solved using the same model and parameters as in the method validation.

3.3 BTES model: Applying Al-Khoury and Bonnier's BHE method to BTES

The objective was to create an efficient numerical model that can be used to estimate the feasibility of the BTES system for peak power production, optimal borehole spacing and depth. The following sections discuss input data handling, the model parameters used, developed model and output data handling.

3.3.1 Input data

Input data is used to calculate mass flow rates within the BTES system and, later, per borehole. Calculations are based on the power plant's estimated hourly heat production, district heating return and supply temperatures and pressures from 2017. In total, there is a demand for 12 MW peak power and 4.46 GWh extra capacity. As Figure 25 demonstrates, the power plant's maximum heat capacity Q_{CHP} (34 MW) is compared with the estimated power plant heat production for the district heating network $Q_{demand}(t)$ to calculate available waste heat $Q_{chaging}(t)$ for the BTES charging period each hour:

$$Q_{charging}(t) = Q_{CHP} - Q_{demand}(t). \tag{3.23}$$

The amount of waste heat each hour, determines the total mass flow rate $\dot{m}_{charging}(t)$ for BTES charging. Fluid for waste heat extraction returns at the same enthalpy H_{return} as district heating return fluid and collects waste heat until the fluid has the enthalpy $H_{charging}$ at 85 °C and 2 bar:

$$\dot{m}_{charging}(t) = \frac{Q_{charging}(t)}{H_{charging}(t) - H_{return}(t)} \tag{3.24}$$

Each hour, the maximum available mass flow rate is assumed to charge the BTES system. Therefore, the mass flow rate is divided among the boreholes connected in parallel, which is determined by dividing number of boreholes $n_{boreholes}$ by serial connections n_{serial}:

$$\dot{m}(t) = \frac{\dot{m}_{charging}(t)}{\left(\frac{n_{boreholes}}{n_{serial}}\right)} \tag{3.25}$$

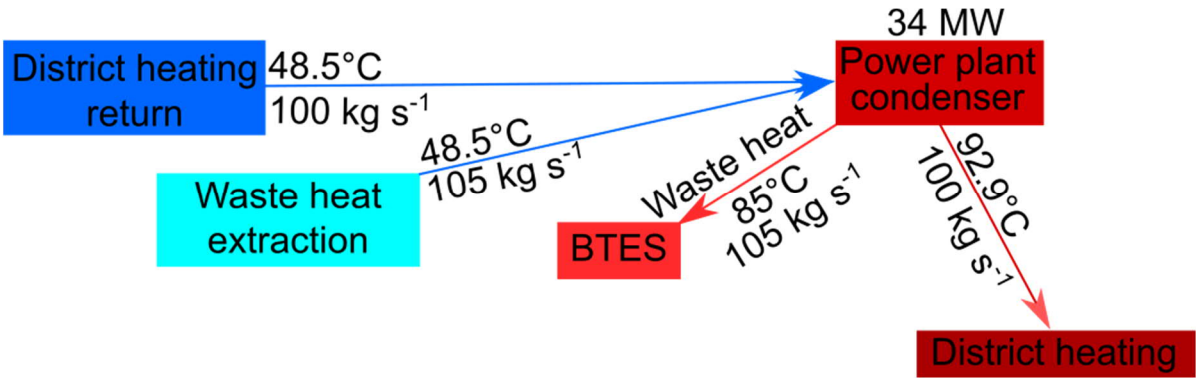

Figure 25. Flow chart of the charging period. Waste heat is used to charge the BTES system. Mass flow rate for BTES is total the mass flow to the system, and it is divided among the parallel connections. Mass flows and temperatures are average values for the period.

During the discharging period, heat demand $Q_{demand}(t)$ is compared with estimated flue gas condenser capacity (Q_{FCG} = 4 MW) and power plant condenser heat capacity to calculate available required BTES heating power $Q_{discharging}(t)$ per hour:

$$Q_{discharging}(t) = Q_{demand}(t) - Q_{CHP} - Q_{FGC} \tag{3.26}$$

During peak demand periods, the required maximum heating power is estimated to be 50 MW, of which flue gas and the power plant condenser contribute 38 MW as shown in Figure 26. The objective is to satisfy the rest of the heat demand by adding BTES into the system.

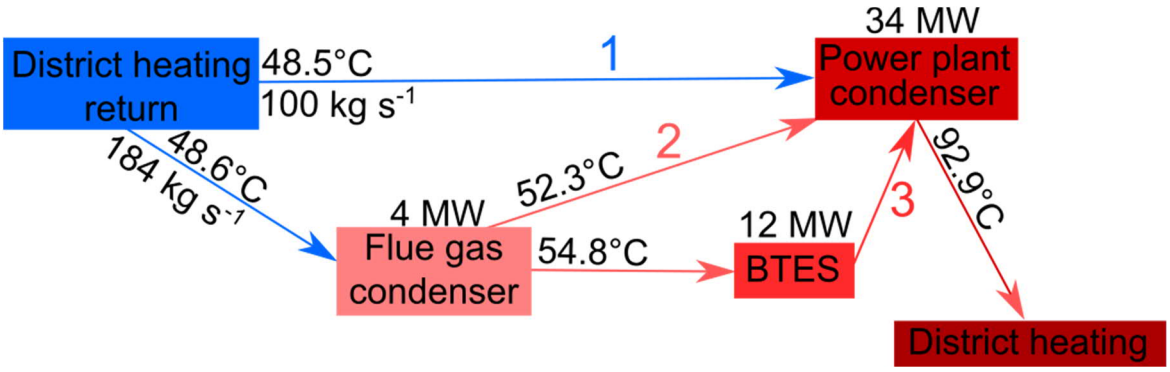

Figure 26. Flow chart of planned district heating network with pre-heaters and power plant condenser. If power plant and flue gas condenser satisfy heat demand, BTES is not needed. If not, extra thermal energy is taken from BTES. Mass flow rate for BTES is the total mass flow to the system, and it is divided among the parallel connections. Mass flows and temperatures are average values for the period.

Based on input data, the charging period is divided in 4,440 hours and the discharging period in 4,320 hours. However, most of the year power plant and flue gas condenser can satisfy heat demand; therefore, peak heat is demanded from BTES only 867 hours. During discharging, the district heating return and supply temperatures and pressures are known; therefore, enthalpy H_{supply} can be solved and the total mass flow to satisfy heating demand is calculated, as follows:

$$\dot{m}_{discharging}(t) = \frac{Q_{discharging}(t) + Q_{CHP} + Q_{FCG}}{H_{supply}(t) - H_{return}(t)}. \tag{3.27}$$

During the discharging period, maximum available mass flow rate in the district heating network is assumed to discharge the BTES system for 867 hours. In the rest of the discharging period, heat is not extracted from storage. Again, mass flow rate per borehole depends on the total number of parallel connections in the system:

$$\dot{m}(t) = \frac{\dot{m}_{discharging}(t)}{\left(\frac{n_{boreholes}}{n_{serial}}\right)}. \tag{3.28}$$

However, due to limitations of the pipe material, the mass flow rate may not exceed a value that causes a 3-bar pressure. Therefore, the pressure drop determines maximum allowable mass flow in the single U-tube pipe. That can be calculated by substituting Equation 3.15 into Equation 2.8:

$$\dot{m} = \sqrt{\frac{2\Delta p \rho_f}{f_r} \frac{2r_{pi}A_p^2}{l_b}}, \tag{3.29}$$

where the friction factor is calculated iteratively using the Colebrook-White equation (Bergman et al., 2011):

$$\frac{1}{\sqrt{f_r}} = -2\log\left(\frac{\varepsilon}{3.7D_h} + \frac{2.51}{Re\sqrt{f_r}}\right), \tag{3.30}$$

where pipe roughness ε is 0.3. Used enthalpy values are based on the IAEPWS I97 Excel steam tables macro provided by Holmgren (2006). Table 9 summarizes planned storage targets and Table 10 lists all the assumptions behind the calculations.

Table 9. Storage targets set for power and capacity.

Storage requirements	Peak demand extra power of 12 MW
	Storage expected capacity during discharging 4,460 MWh
	Waste heat production in power plant 110,000 MWh

Table 10. Model assumptions related to input data.

Assumptions	During charging period, maximum mass flow rate, which is required to collect all power plant's waste heat, is used to charge BTES
	During discharging period, maximum mass flow rate used to satisfy heat demand, is also circulated through BTES
	Pressure drop may not excess 3 bar (see PE-RT pressure limitation in Table 2)
	Storage is heated its operation temperature (heating period is neglected)
	Charging period 4,440 hours (starts at 19th of November)
	Discharging period 4,320 hours (starts at 19th of April)

3.3.2 Model parameters

Model parameters are prescribed values for the model environment. As the model neglects the heating period from natural underground temperature to the storage operation temperature, the initial domain temperature is chosen as 54.8 °C. This is the same temperature as the average fluid inlet temperature during the discharging period. However, the fluid inlet temperature follows along with the district heating return temperature after the flue gas condenser. During the discharging period, the BTES system is charged with fluid at 85 °C. Based on fluid inlet temperatures, the BTES yearly average temperature is assumed to be 69.9 °C. All prescribed temperatures are shown in Table 11.

Table 11. Model prescribed temperatures.

Parameter		**Unit**	**Value**
Fluid inlet temperature (charging)	T_{inlet}	°C	85
Fluid inlet temperature (discharging)	T_{inlet}	°C	Variable (avg. 54.8)
Bedrock initial temperature	T_{r0}	°C	54.8
Average temperature of the system	T_{avg}	°C	69.9

Table 12 lists pipe parameters used in the model. The typical borehole diameter in Finland is 0.115 meters (Juvonen and Lapinlampi, 2013). The single U-tube pipe is rated as SDR-11 (standard - diameter-to-pipe-wall –ratio) (see, e.g., The Nordic Plastic Pipe Association, 2011), and its radius is 0.025 m and its shaft spacing 0.059 m. Pipe material is assumed to be PE-RT, and therefore, pipe wall thermal conductivity k_p is 0.42 W m^{-1} K^{-1} (Reuss, 2015).

Table 12. Parameters for borehole and pipe used in the model.

Parameter		**Unit**	**Value**
Borehole radius	r_b	m	0.0575
Single U-tube pipe outer radius	r_{po}	m	0.0250
Single U-tube pipe inner radius	r_{pi}	m	0.0205
Single U-tube shaft spacing	s	m	0.0590
Thermal conductivity of pipe wall	k_p	W m^{-1} K^{-1}	0.42

The determined thermal properties of rocks were iterated to agree thermal properties at 69.9 °C. Cermak and Rybach (1982) and Whittington et al. (2009) have collected data on temperature dependence of rocks as units per K. Most of the iterations are based on Cermak and Rybach (1982); however, thermal diffusivity of granite is iterated based on Whittington et al. (2009), and the specific heat capacity of granite is then calculated using Equation 2.1. Iterated values used in the model are shown in Table 13.

Table 13. Thermal properties of the rock domain used in the model. (Sources: Cermak and Rybach [1], 1982, Whittington et al. [2], 2009).

Parameter		Unit	Change per K	Used value
Granite				
Thermal conductivity	k_r	W m^{-1} K^{-1}	-0.32 [1]	2.76
Density	ρ_r	kg m^{-3}	0	2610
Specific heat capacity	$c_{p,r}$	J kg^{-1} K^{-1}	1.03 [1][2]	722
Thermal diffusivity	α_r	m^2 s	$-1.46 \cdot 10^{-7}$ [2]	$1.46 \cdot 10^{-6}$
Hornblende gneiss				
Thermal conductivity	k_r	W m^{-1} K^{-1}	-0.001 [1]	2.01
Density	ρ_r	kg m^{-3}	0	2883
Specific heat capacity	$c_{p,r}$	J kg^{-1} K^{-1}	1.34 [1]	755
Thermal diffusivity	α_r	m^2 s	$-2.13 \cdot 10^{-9}$ [1]	$9.23 \cdot 10^{-7}$

As natural convection in a groundwater-filled borehole has no analytical solution and cannot be modelled realistically (Chiasson, 2016), bentonite-mixture is chose as the grout material in the model. Kim et al. (2017) describes wide variety of thermal properties of bentonite-mixtures. Thermal properties of grout material are based on sample number SC1-3 presented in their article. There are no studies related to temperature-dependent behaviour of grout material. For that reason, thermal properties of grout are based on room temperature as shown in Table 14.

Table 14. Thermal properties of the grout domain used in the model. (Source: Kim et al., 2017)

Parameter		Unit	Value
Thermal conductivity	k_g	W m^{-1} K^{-1}	1.88
Density	ρ_g	kg m^{-3}	2225
Specific heat capacity	$c_{p,g}$	J kg^{-1} K^{-1}	1071
Thermal diffusivity	α_g	m^2 s	$0.79 \cdot 10^{-7}$

The heat exchanger fluid used in the model is water and its thermal values are listed at Table 15. The thermal properties of water are based on the IAEPWS I97 Excel steam tables macro written by Holmgren (2006), and calculated at 69.9 °C.

Table 15. Thermal properties of fluid at 69.9 °C used in the model.

Parameter		Unit	Value
Thermal conductivity	k_g	W m^{-1} K^{-1}	0.66
Density	ρ_g	kg m^{-3}	977
Specific heat capacity	$c_{p,g}$	J kg^{-1} K^{-1}	4215
Thermal diffusivity	α_g	m^2 s	$1.60 \cdot 10^{-7}$
Dynamic viscosity	μ_f	Pa·s	$4.20 \cdot 10^{-4}$
Prandtl number	Pr		2.68

3.3.3 Developed model

According to Hirvonen et al. (2018) and Hirvonen and Siren (2018) the optimum number of serial connections in larger storages is three; therefore, three serial connections were chosen for the model. One block in the model represents seven-borehole unit connected in parallel. One unit represents the same section in the BTES field as shown in Figure 27.

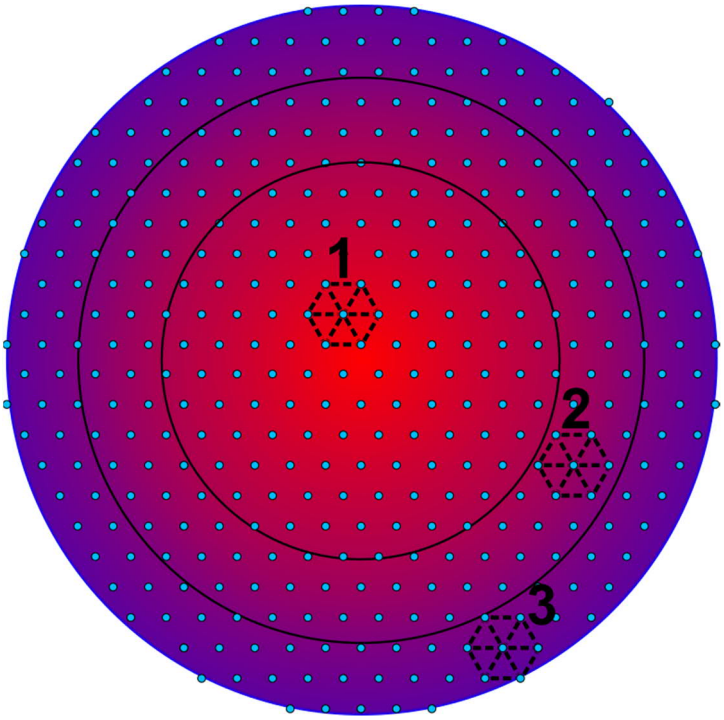

Figure 27. BTES divided into three sections, which represents the location of each model block. They represent one serial connection in BTES field

Each block has seven boreholes modelled in a hexagonal pattern. In total, there are three blocks; for that reason, the created model has 21 boreholes. Each block has periodic boundary conditions, which approximates an infinite BTES system. The first block in the storage centre have the boundary condition of the prescribed fluid inlet temperature T_{inlet} for charging period. The rest of the heat pipe element and underground domain are calculated numerically. However, each outlet

temperature of the blocks is calculated as an average value of seven-borehole unit connected in parallel. This average outlet temperature is copied and used as a boundary condition of fluid inlet temperature of adjacent blocks. During the discharging period, the flow direction is reversed and the third block, representing the storage outer edge, has the prescribed fluid inlet temperature T_{inlet} for discharging period.

The geometry and the mesh of the created model is depicted in Figure 28. The borehole geometry was created in a similar manner that pictured in Figure 23. The top volume of the model, which is limited by borehole length (l_h), has the first-order triangle elements. The smallest elements are described at the borehole wall and the size of the elements increases at a factor of 1.2. In total, there are ten horizontal layers into vertical direction. The base of the model is defined using first-order tetrahedral elements. Each block is divided into two different domains, where the upper block has thermal properties of granite and the lower block, of hornblende gneiss. Temperature probes shown in Figure 28 measure bedrock temperatures. Bedrock and borehole wall temperatures are the average values of the three blocks.

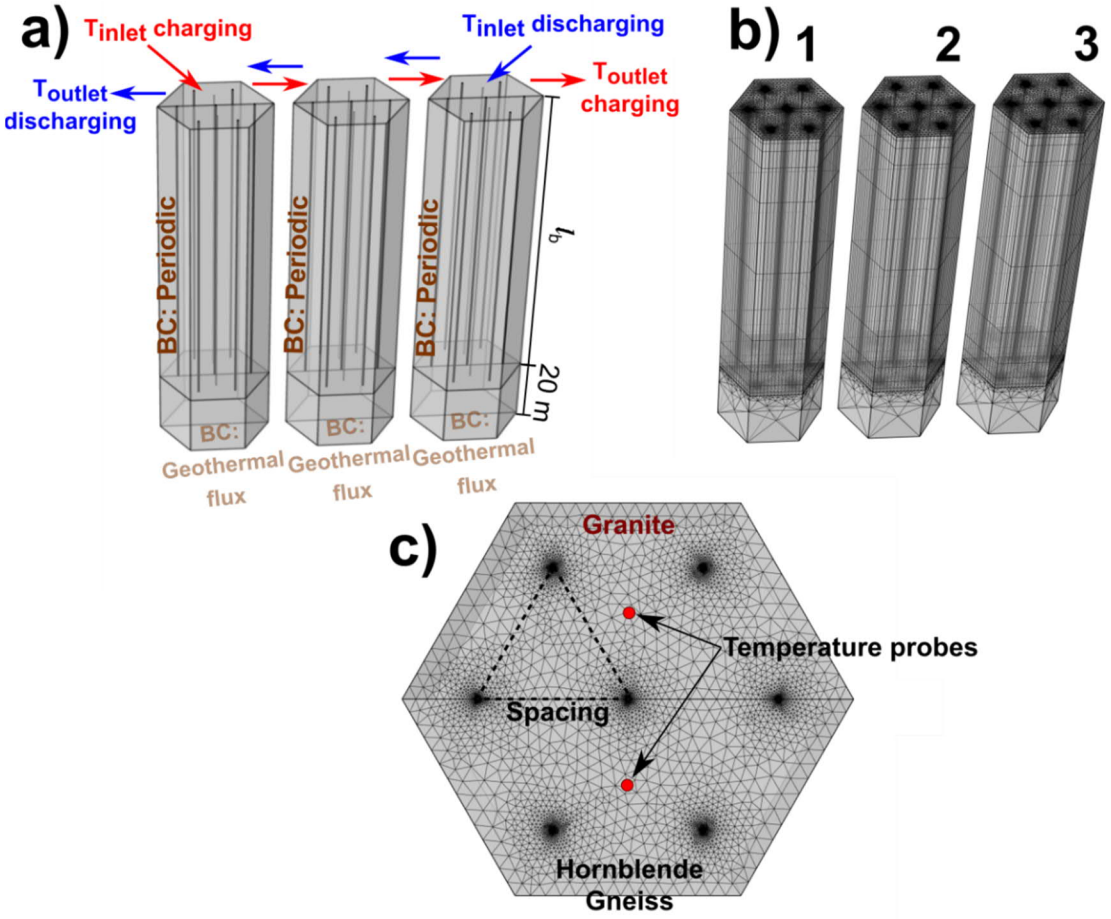

Figure 28. Geometry of the BTES model. a) Arrows show the flow direction during charging and discharging periods. b) Meshed model: block on the left represents the centre of the storage and block on the right represents the storage outer edge. c) Each block is divided into granite and hornblende gneiss blocks. The smallest elements are next to the borehole wall.

As modelling heat transfer in one-hour resolution is computationally expensive, solving the model requires geometrical simplifications. Therefore, model has some drawbacks, which include neglecting physical interaction between the blocks. However, fluid flow interacts between the blocks as each inlet temperature is prescribed by previous outlet temperature. Furthermore, the model does not consider heat that is lost into the surrounding bedrock or through the insulation layer on the top. All model assumptions are listed in Figure 29.

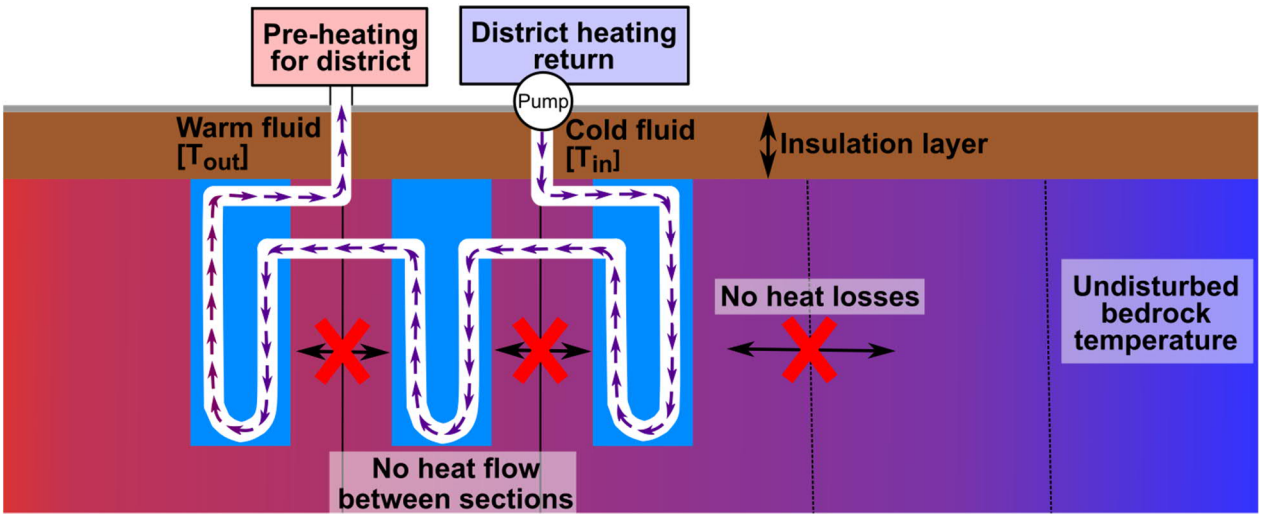

Figure 29. Model assumptions. Model does not consider heat lost in surrounding bedrock or through insulation layer. Additionally, there is no heat transfer interaction between the blocks.

In total, 21 cases were simulated using Dell Precision 5820 computer with 32 GB RAM and Intel® Xeon® W-2133 CPU (3.60 GHz) with six cores. The models were simulated assuming three different storage width to depth (D/L) –ratios. Each model with a given D/L –ratio was simulated with seven different borehole spacing values (see Table 16). However, the storage temperature change was initially unknown and assumed as 20 °C in each case. After the first round of simulations, number of boreholes was corrected according to the storage temperature found in the simulations. All the results are based on the second round of simulations.

Table 16. Modelled cases. Three different D/L -ratios of 0.5, 0.66 and 1.0 with seven different spacing values. Total of 21 cases.

Spacing [m]	Number of elements	Simulation time
2.0	265 547	4 h 00 min
2.5	289 789	4 h 23 min
3.0	310 695	4 h 57 min
3.5	326 970	5 h 6 min
4.0	340 600	5 h 14 min
4.5	355 237	5 h 44 min
5.0	368 180	5 h 57 min

3.3.4 Model output

As the outlet temperature is solved numerically, power profile of the model unit can be calculated during the charging $q_{charging}(t)$ and discharging $q_{discharging}(t)$ periods as:

$$q_{charging}(t) = \dot{m}(t) \cdot c_{p,f} \cdot \left(T_{inlet} - T_{outlet}(t)\right) \cdot n_{unit} \tag{3.32}$$

$$q_{discharging}(t) = \dot{m}(t) \cdot c_{p,f} \cdot \left(T_{inlet}(t) - T_{outlet}(t)\right) \cdot n_{unit} \cdot 0.65, \tag{3.32}$$

where $\dot{m}(t)$ is the mass flow rate at time t, $c_{p,f}$ is the specific heat capacity of fluid, T_{inlet} is fluid inlet temperature into storage during charging and discharging periods, T_{outlet} is fluid outlet temperature from storage at time t and n_{unit} is the number of boreholes in the model. As the created model neglects heat losses in the surrounding environment, it is assumed that 35 % of heat is lost during heat extraction. This assumption is based on 65 % heat recovery value found in Paskov (Rapantova et al., 2016) and Brædstrop (Sørensen and Schmidt, 2018). As discharging period is solved hourly, the sum of the each hour provides the discharging capacity of the model unit Q_{unit}. The first estimation of size of the BTES is performed by determining the number of model units (scale factor S) required to satisfy the heat demand capacity of the Salo's district heating network $Q_{district}$:

$$S = \frac{Q_{district}}{Q_{unit}}. \tag{3.33}$$

Therefore, total number of boreholes n required to satisfy the heat demand capacity of the district heating network is found by multiplying the number of boreholes in the model unit n_{unit} by scale factor S:

$$n = S \cdot n_{unit}. \tag{3.34}$$

The scaled power profile $q_s(t)$ can be calculated for discharging period as follows:

$$q_s(t) = q_{discharging}(t) \cdot S.$$

One borehole requires an area A_h defined by hexagon (see Figure 30). Therefore, one borehole requires an area defined by Equations 3.35 and 3.36.

$$s_h = 2 \cdot \left(\tan(30°) \cdot \frac{s_b}{2}\right) \tag{3.35}$$

$$A_h = \frac{3 \cdot \sqrt{3} \cdot s_h^2}{2}, \tag{3.36}$$

where s_h is the length of a side and s_b is the borehole spacing .

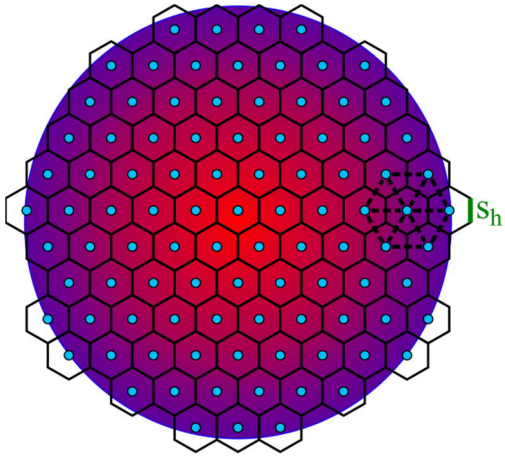

Figure 30. Storage with assumed cylindrical geometry and hexagonal borehole pattern.

As the optimal geometry of the storage is cylindrical, storage radius r_s can be calculated as follows:

$$r_s = \frac{\sqrt{A_h \cdot n}}{\pi} \tag{3.37}$$

Height of the storage L may be determined by using the width to depth (D/L) -ratio:

$$L = \frac{2r_s}{D/_L} \tag{3.38}$$

Volume of the storage V_s can be calculated as:

$$V_s = \pi \cdot r_s^2 \cdot L$$

According to Huusko (2019), the cost of a borehole with heat resistant pipe material is 25 € m^{-1}. Therefore, the price of the BTES field is:

$$P = n \cdot L \cdot 25 \text{ € m}^{-1} \tag{3.39}$$

The main results of the simulations compare how borehole spacing affects mass flow rate per borehole, discharging capacity, number of boreholes, storage temperature change, storage volume, radius and height, heating and discharging time, total borehole length and investment cost. Finally, horizontal temperature profiles are shown after the main discharging period (7786 h) to visualize how borehole spacing affects temperature distribution along the domain. The detailed simulation results are presented in Appendices A and B.

4 Results

This chapter defines bulk modelling environment with all assumptions and equations. Briefly explained flow charts with BTES system and models with BHEs were used to calculate and simulate results.

4.1 Code verification

The implementation of the heat equation is verified in Figure 31, which demonstrates that only minor differences exist between the solutions of COMSOL Multiphysics and MATLAB during heating of the 2D bedrock domain from 6 °C to 80 °C with a constant 85 °C heat source.

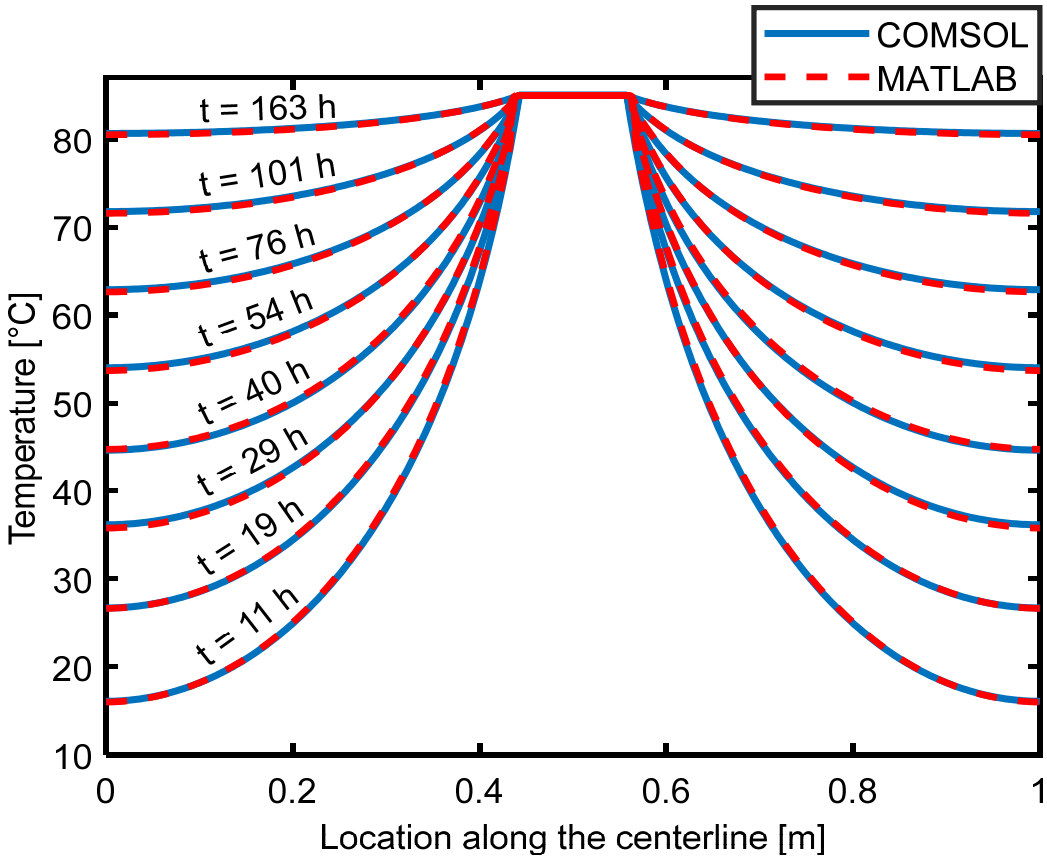

Figure 31. Verification of heat equation. Temperature distributions along the centreline of the domain in COMSOL and MATLAB at chosen time.

The solution of the temperature profile of the BHE is verified in Figure 32. The agreement between the analytical Excel based and numerical (COMSOL) solutions is nearly perfect. The solution includes two different cases, representing the charging period and discharging period.

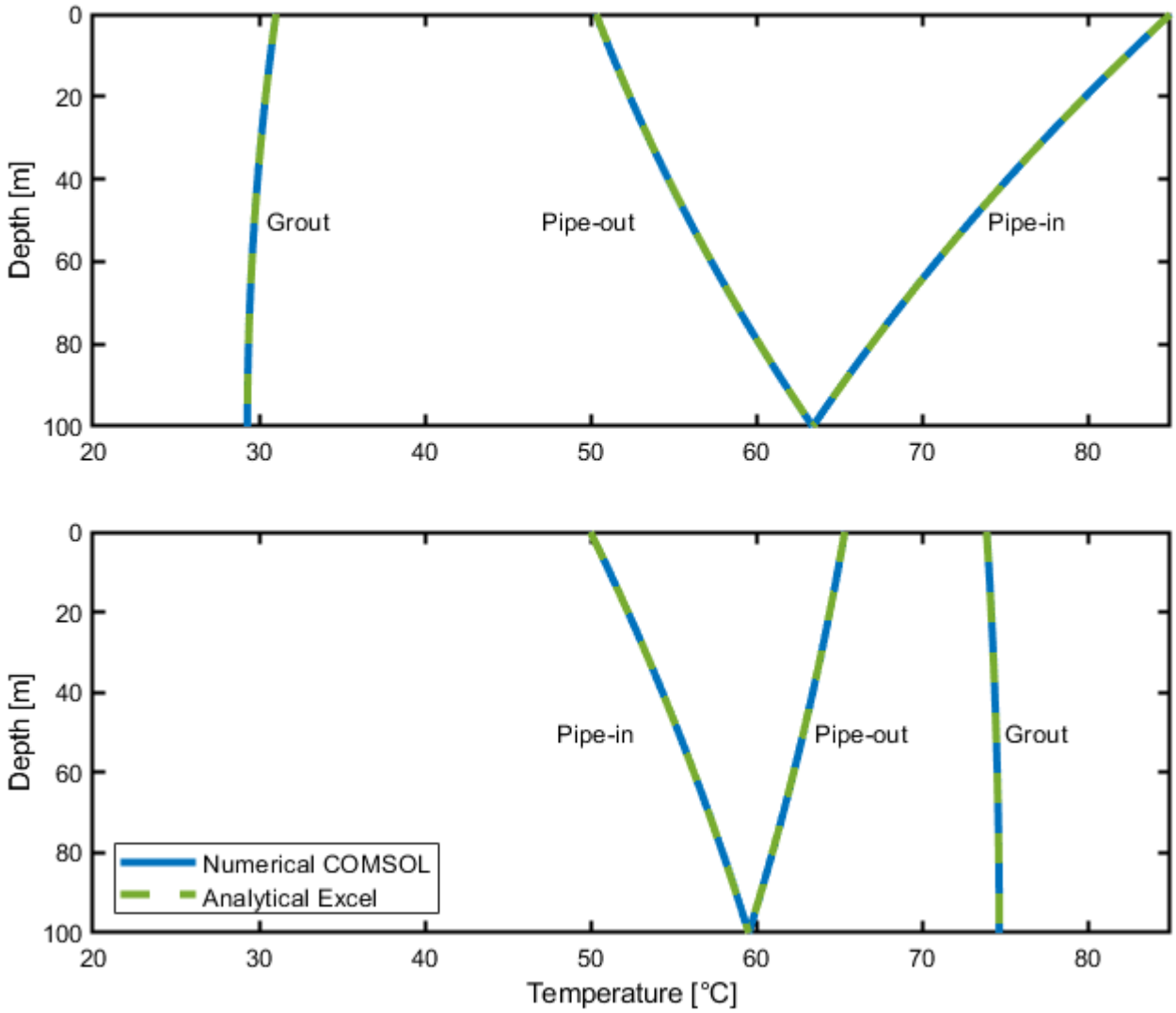

Figure 32. Numerical solution vs. analytical solution. Upper figure represents charging, when T_{inlet} = 85°C and T_b = 6 °C and lower figure represents discharging when T_{inlet} = 50°C and T_b = 85 °C.

4.2 Al-Khoury and Bonnier's method validation

The used method developed by Al-Khoury and Bonnier (2006) is validated in Figures 33 and 34. COMSOL simulation is compared with in-situ TRT results from the Espoo case (Figure 33) and Rovaniemi case (Figure 34), and the figures illustrate the differences between experimental and simulation results. As can be seen, numerical simulations solve fluid outlet temperature with acceptable accuracy. However, in the very beginning there are larger differences, which can be seen better in the power plot; particular, power seems to be overestimated during the first 10 hours. After that, the simulations agree well with the experimental tests. Furthermore, power flowing

through the surface between the borehole and bedrock is slightly less than the observed power released by fluid, as the BHE heats up during the observation period.

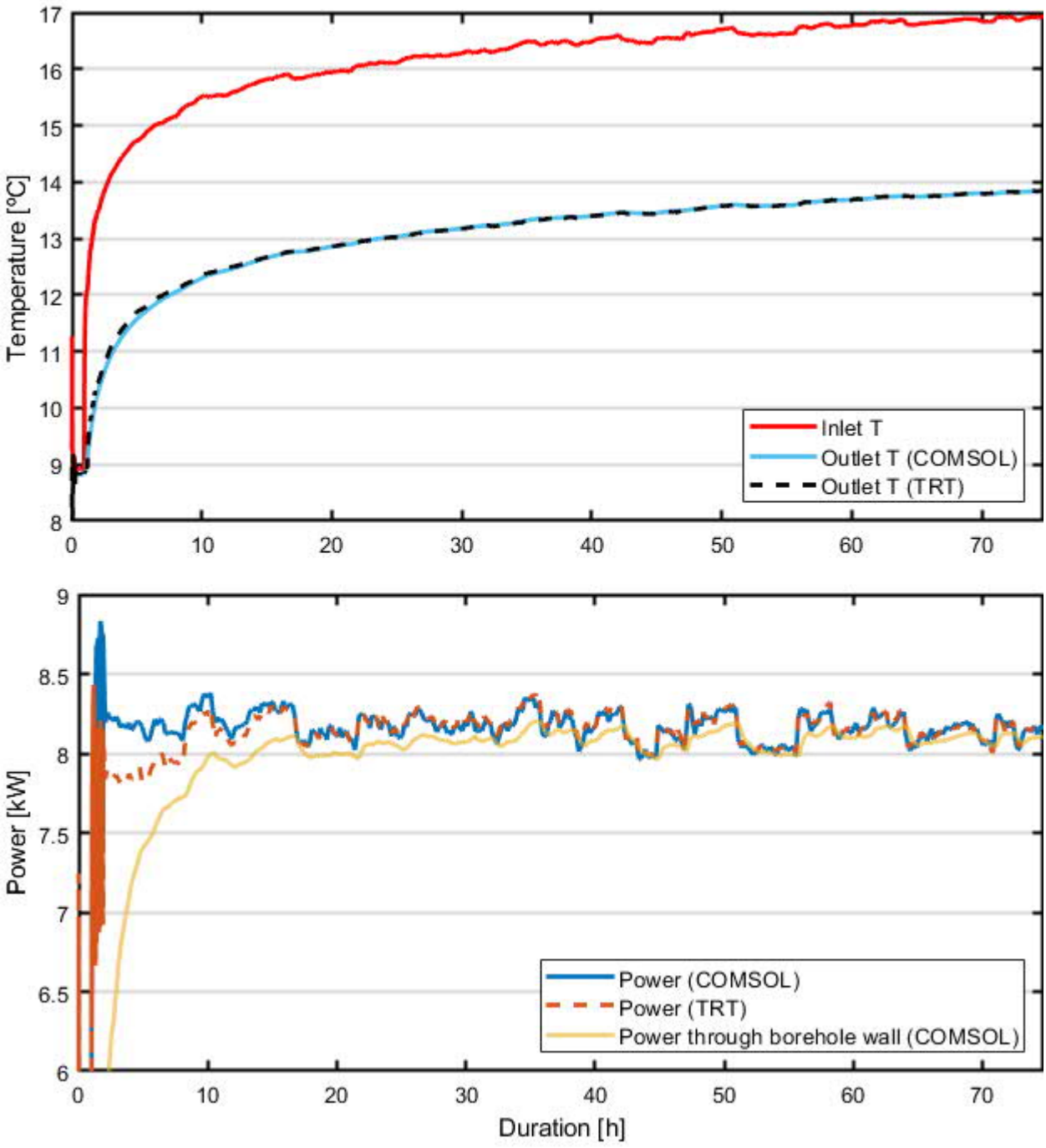

Figure 33. Espoo case validation. Upper figure: simulated (COMSOL) and observed (TRT) fluid outlet temperatures. Lower figure: simulated and observed power and integrated power flowing through borehole wall surface.

In the Rovaniemi case, fluid inlet and outlet temperatures are lower than in the Espoo case. Additionally, the temperature difference is slightly lower in Rovaniemi case; therefore, observed

power is slightly lower as well. However, there is slightly greater variation in power magnitude in the Rovaniemi case and it has slightly greater mismatch between simulation and experimental results.

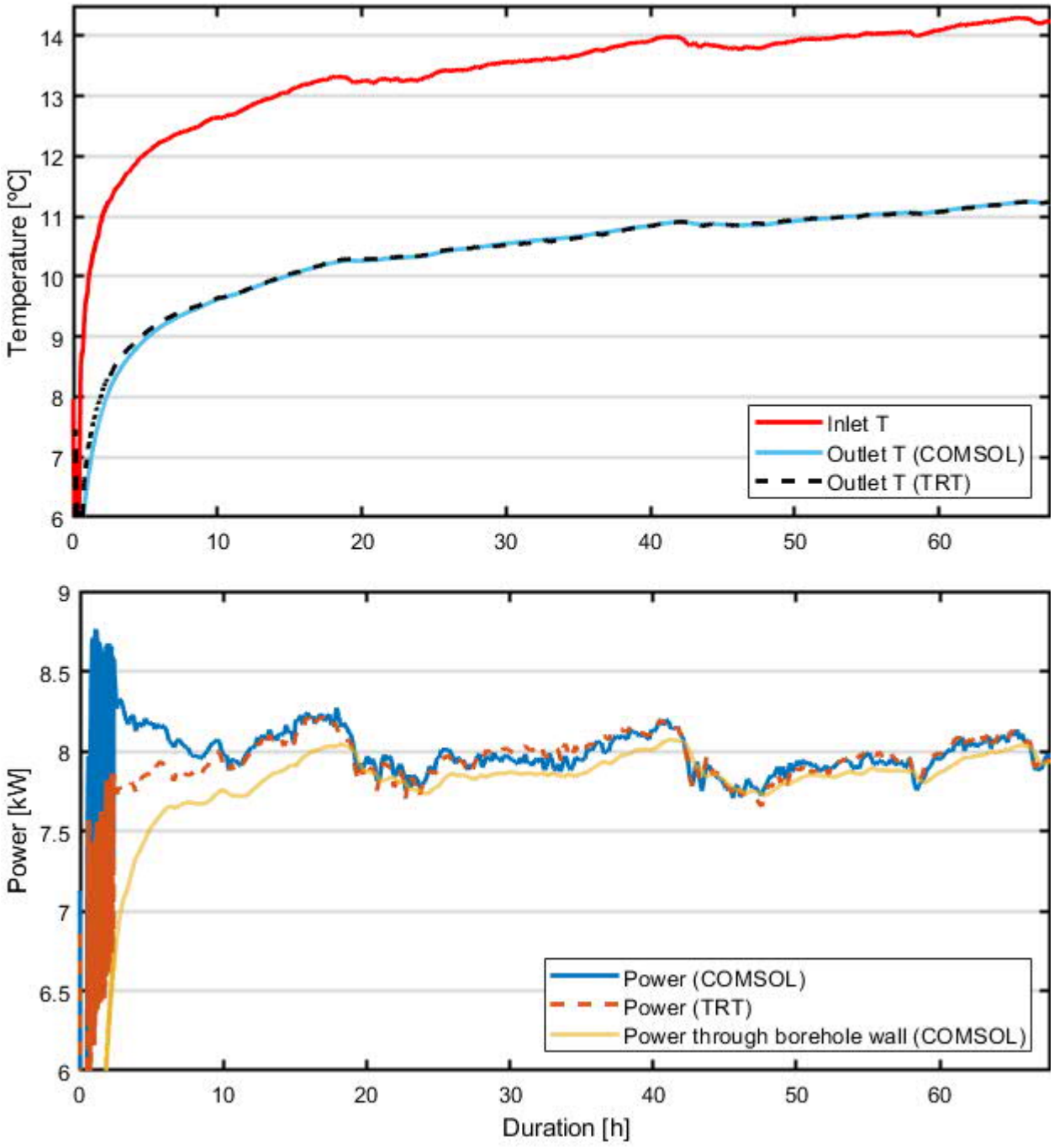

Figure 34. Rovaniemi case validation. Upper figure shows simulated and measured fluid outlet and average temperatures. Lower figure shows simulated and measured power and integrated power through borehole wall.

Figure 35 shows the error as the difference between experimental and simulation results. These figures demonstrate that the error is larger, for a longer time, in the Rovaniemi case. In spite of, the

Al-Khoury and Bonnier's method can evaluate outlet temperature and power with acceptable accuracy as the error is less than 10 % most of the time. The method can evaluate the Espoo case nearly perfectly, whereas the agreement is slightly weaker in the Rovaniemi case.

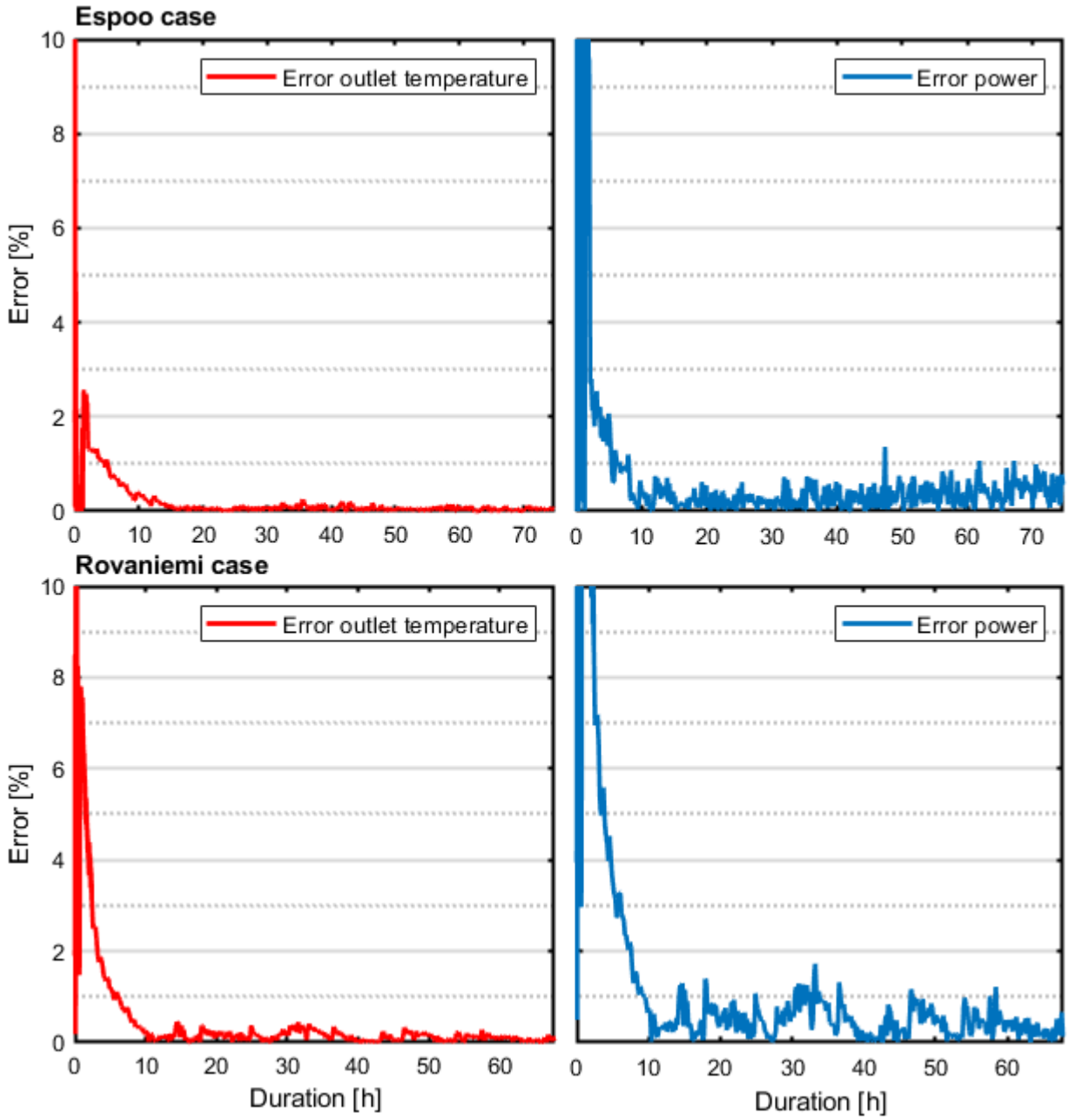

Figure 35. Figures on the left side demonstrate error in outlet temperature. Figures on the right side demonstrate error in power. Upper figures: Espoo case. Lower figures: Rovaniemi case.

4.3 Al-Khoury and Bonnier's method verification

Al-Khoury and Bonnier's method is verified by increasing mesh densities the model and calculate convergence rate Figures 36 and 37 visualize the effect of the number of elements on results. As

can be seen the number of vertical elements has only a minor effect on evaluation of fluid outlet temperature. However, the effect of vertical elements is significant in terms of evaluating power, that flows through the BHE's surface. A low number of vertical elements leads to underestimation of thermal energy flowing from the BHE to the bedrock.

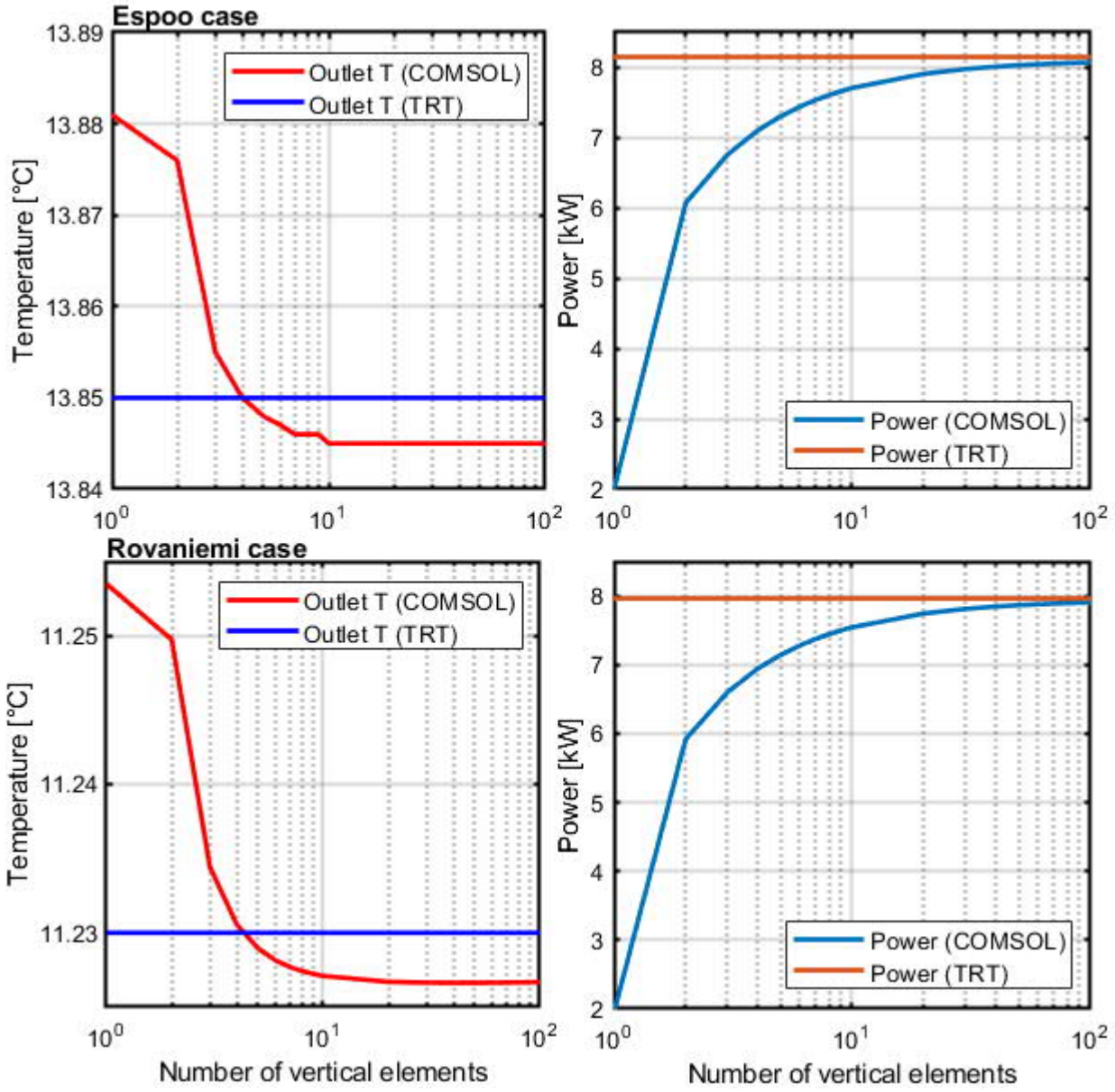

Figure 36. Figures on the left side demonstrate the effect of number of vertical elements on outlet temperature. Figures on the right side demonstrate the effect of number of vertical elements on power flowing through the BHE surface (number of horizontal elements constant at 2000 elements per layer: element growth rate 1.2). Upper figures: Espoo case. Lower figures: Rovaniemi case.

As shown in Figure 37, the number of horizontal elements per layer has a slightly larger effect on outlet temperature as compared to vertical elements. However, increasing the number of horizontal

elements decreases the power that flows through the BHE's surface. As can be seen from results, only number of vertical elements have significant effect on outlet temperature and power.

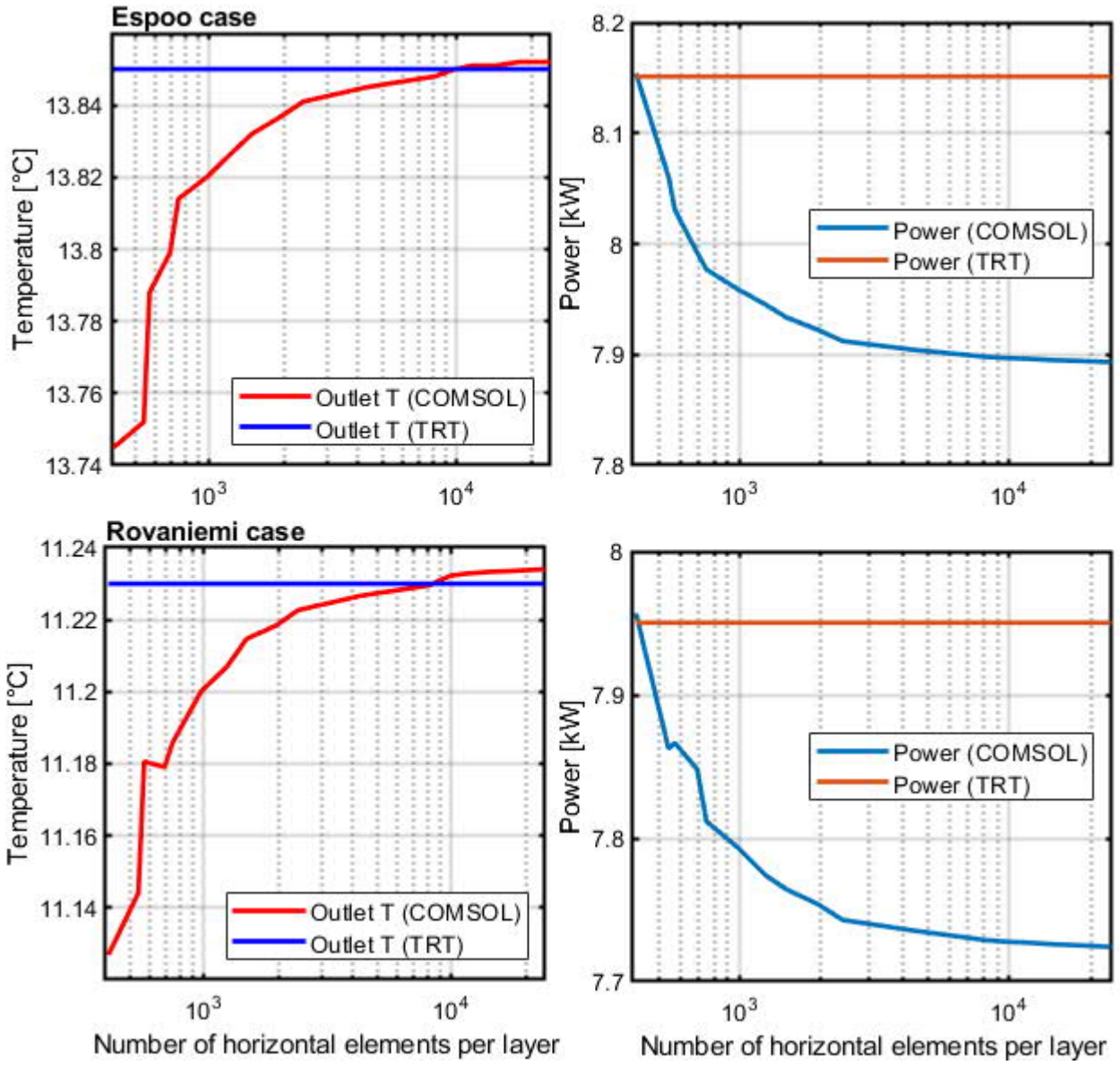

Figure 37. Figures on the left side demonstrate the effect of number of horizontal elements per layer on outlet temperature. Figures on the right side demonstrate error the effect of number of horizontal elements per layer on power flowing through the BHE surface (number of vertical elements constant 20 elements). Upper figures: Espoo case. Lower figures: Rovaniemi case.

Finally, Figure 38 demonstrates that the number of vertical elements has only a minor effect on temperature profile of BHE's and bedrock.

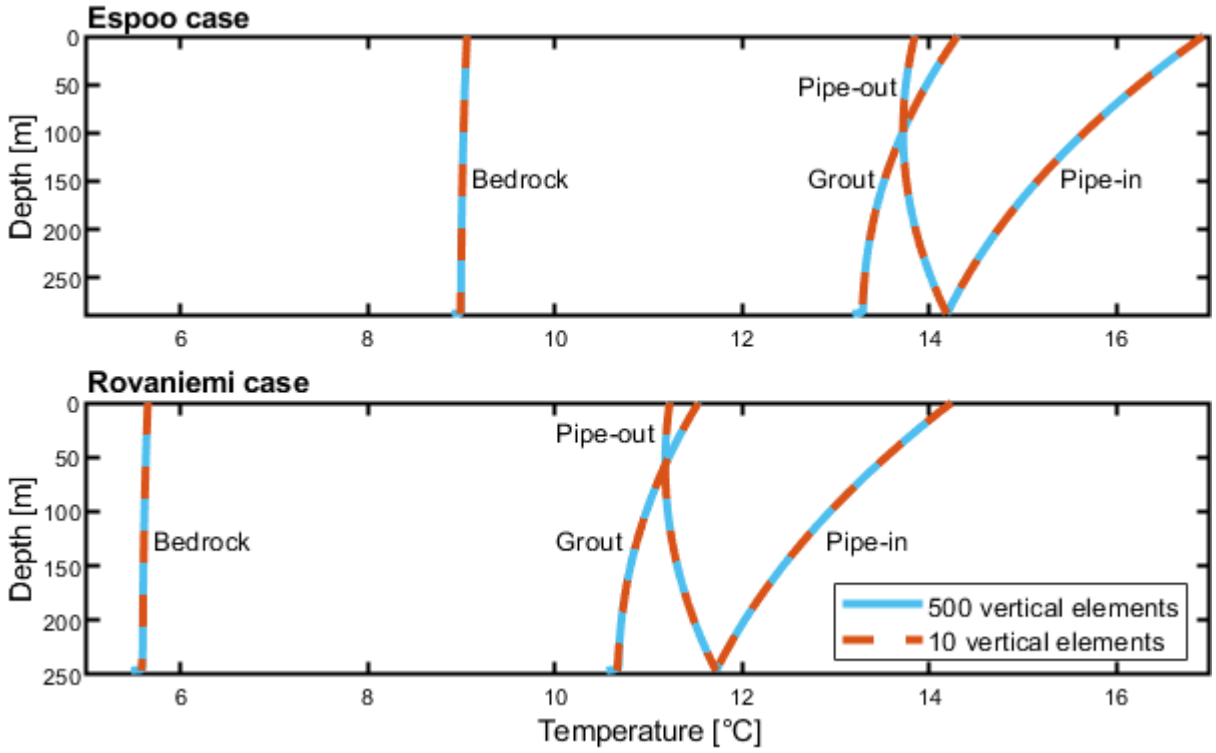

Figure 38. The effect of vertical elements on temperature profiles. Upper figure: Espoo case. Lower figure: Rovaniemi case.

4.4 BTES model: Applying Al-Khoury and Bonnier's BHE method to BTES

The BTES model utilizes the method developed by Al-Khoury and Bonnier (2006). In the method, BHE is modelled as a 1D heat pipe element, which is connected in 3D bedrock domain. The objective of the model is to find out how borehole spacing and D/L -ratio affects mass flow, capacity, size, performance and cost of the storage system.

In the BTES model, fluid mass flow rate is based on input data and approximated number of boreholes. Each borehole connected in series has the same mass flow rate. As Figures 39 and 40 illustrate, fluid mass flow rate is decreased as a function of number of boreholes, because total mass flow in the system remains the same. On the other hand, pipes are limited by their maximum mass flow, which is defined by maximum pressure drop (3 bar); therefore, the fluid mass flow rate cannot be increased if the spacing is greater than 4 m. For that reason, the maximum mass flow rate is reached when borehole spacing is 4 m.

As Figure 40 shows, the model unit's discharging capacity is at its maximum when borehole spacing is 4 m. A decreased D/L –ratio increases discharging capacity as the volume of the model unit is increased. However, discharging capacity is not increased anymore with spacing of 4.5 m

or greater due to limited heat transfer. On these reasons, required number of boreholes is minimized when spacing is 4 meters. On the other hand, the number of boreholes may be decreased by increasing the length of the boreholes. This also means that the D/L –ratio is decreased.

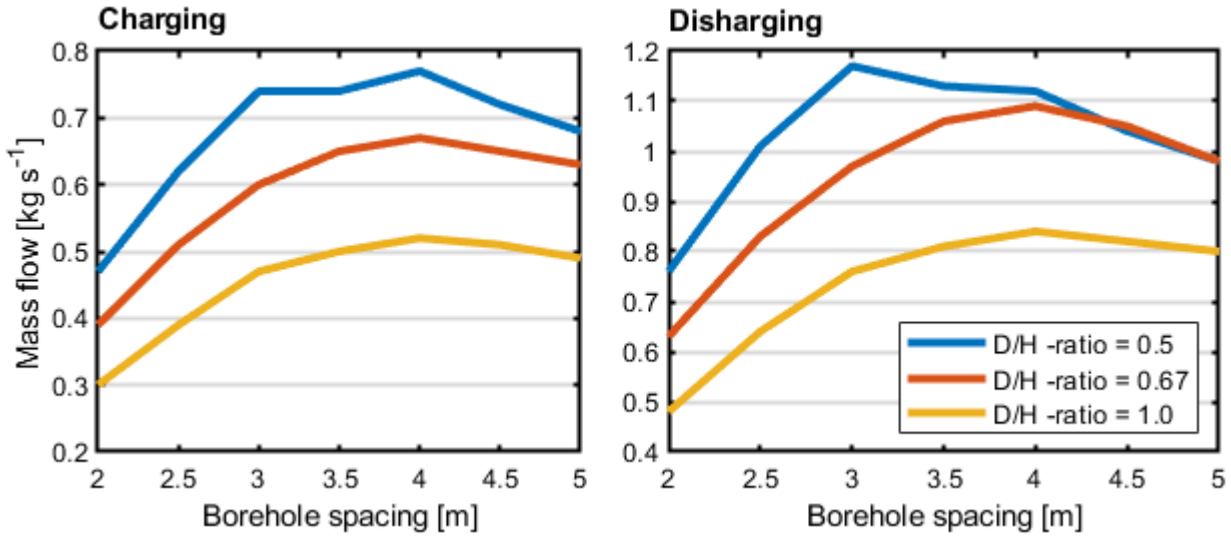

Figure 39. Average fluid mass flow rates per borehole in response to borehole spacing.

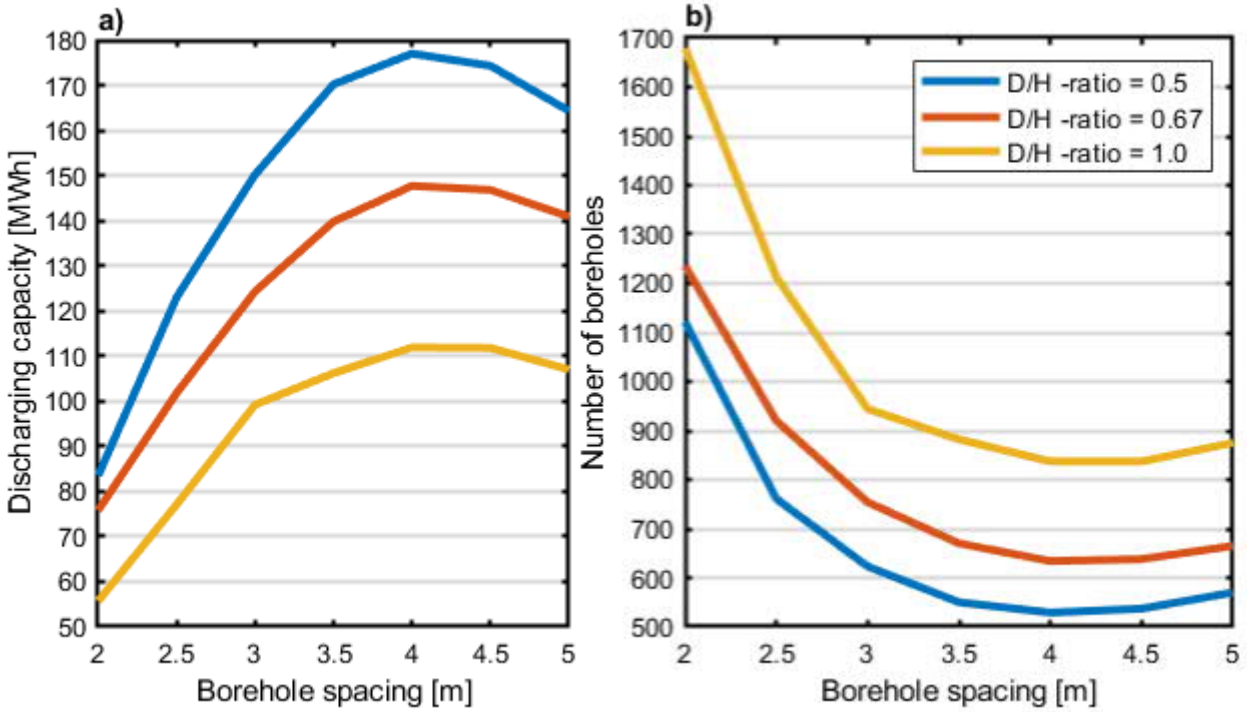

Figure 40. a) Discharging capacity of 21-borehole model unit in response to borehole spacing. b) Number of boreholes required to satisfy 4.46 GWh heat demand in response to borehole spacing.

Temperature change in the storage medium and borehole wall decreases almost linearly as borehole spacing increases. However, the length of the boreholes does not seem to have any significant

effect on how much the temperature drops during the discharging period, as can be seen in Figure 41. The temperature drops almost 25 °C when borehole spacing is 2 m, but only 3 °C with borehole spacing of 5 m. For this reason, the required storage volume increases as borehole spacing increases as shown in Figure 42. As the length of the boreholes does not affect temperature drop, D/L -ratio has minor effect on the required storage volume. Therefore, only borehole spacing defines the required volume.

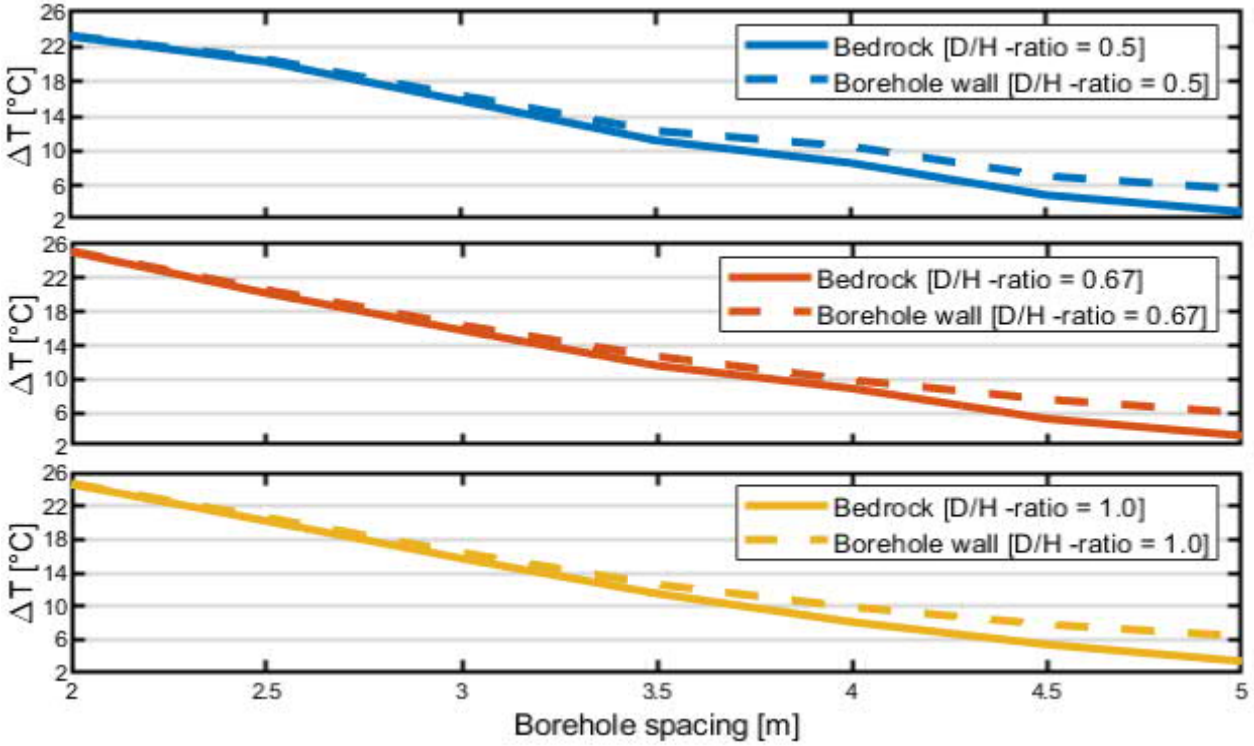

Figure 41. Storage medium (bedrock, measured from temperature probes) and borehole wall temperature change in response to borehole spacing. Temperature differences in discharging period (between hours 4440 and 8760).

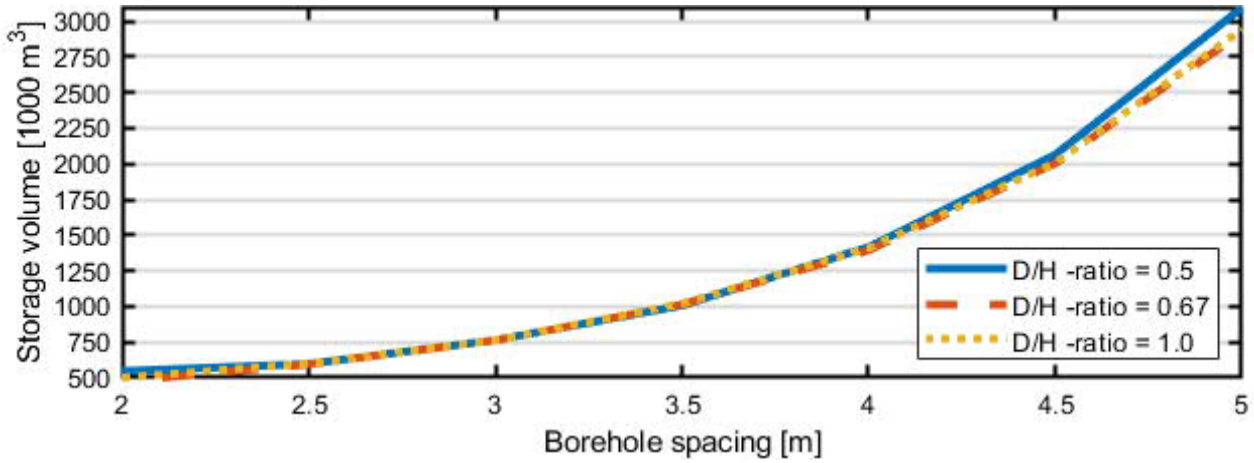

Figure 42. Required storage volume as a function of borehole spacing.

An increased D/L –ratio requires a larger storage radius but shorter borehole length as shown in Figure 43. On the other hand, a lower D/L –ratio requires less land area but longer boreholes. However, as borehole spacing is increased both storage radius and length are increased.

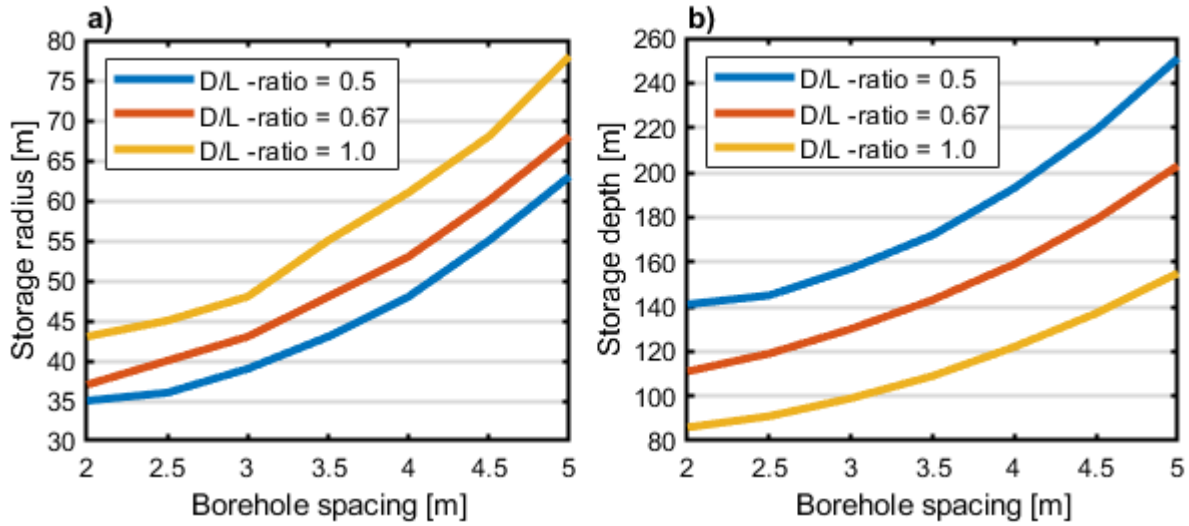

Figure 43. a) Storage radius as a function of borehole spacing. b) Storage height as a function of borehole spacing.

Furthermore, total borehole length defines the total investment cost as shown in Figure 44. Both total borehole length and investment cost are minimized when borehole spacing is 3.5 m. Suboptimal borehole spacing can increase storage price more than 1.5 million € because heat transfer is not optimized. However, D/L –ratio has no significant effect on total borehole length nor investment cost

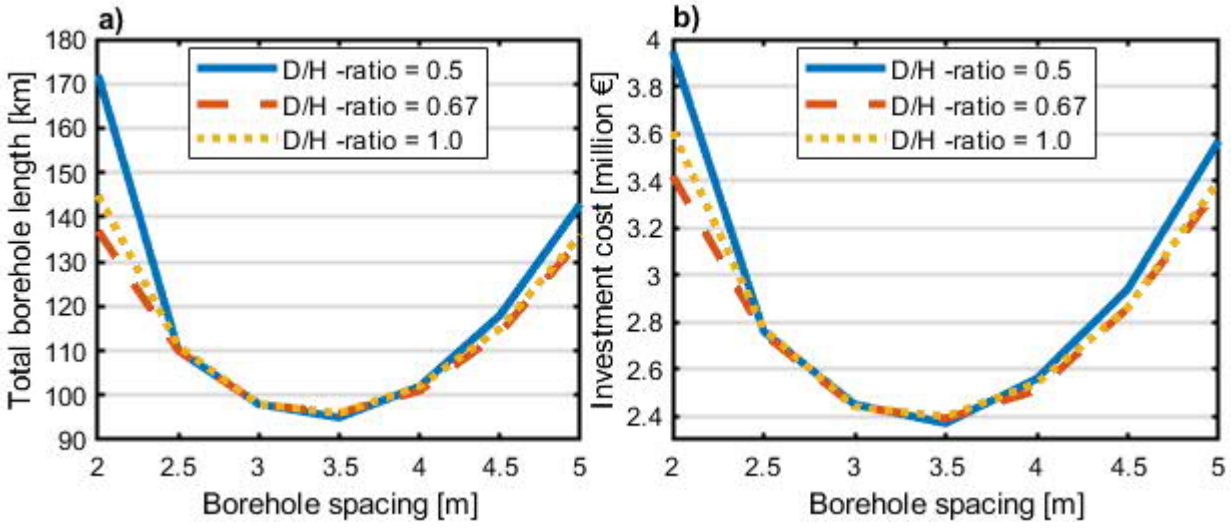

Figure 44. a) Total borehole length in response to borehole spacing. b) Investment cost in response to borehole spacing.

Figure 45 illustrates detailed results from the optimal case (spacing 3.5, D/L –ratio 1.0). As the results are recorded hourly intervals, the sum of each peak of discharged power represents the discharging capacity. The highest peak power can be extracted only during some hours, and then it drops to 100-200 kW. Due to the rapid drop in borehole wall temperature, less thermal energy is available for discharging. However, this causes a temperature difference between the storage medium and the borehole wall, causing heat flow towards the wall. Therefore, borehole wall heats again during periods of no heat extraction during discharging due to the temperature difference between borehole wall and surrounding rock. As the model unit has periodic boundary conditions, the storage can be scaled to full operation. The results reveal mismatch between estimated power and heat demand; however, the storage system may yield hours of 10 MW thermal energy at the beginning of each discharging period. Over longer periods, this storage system has the potential to yield 2–5 MW thermal energy.

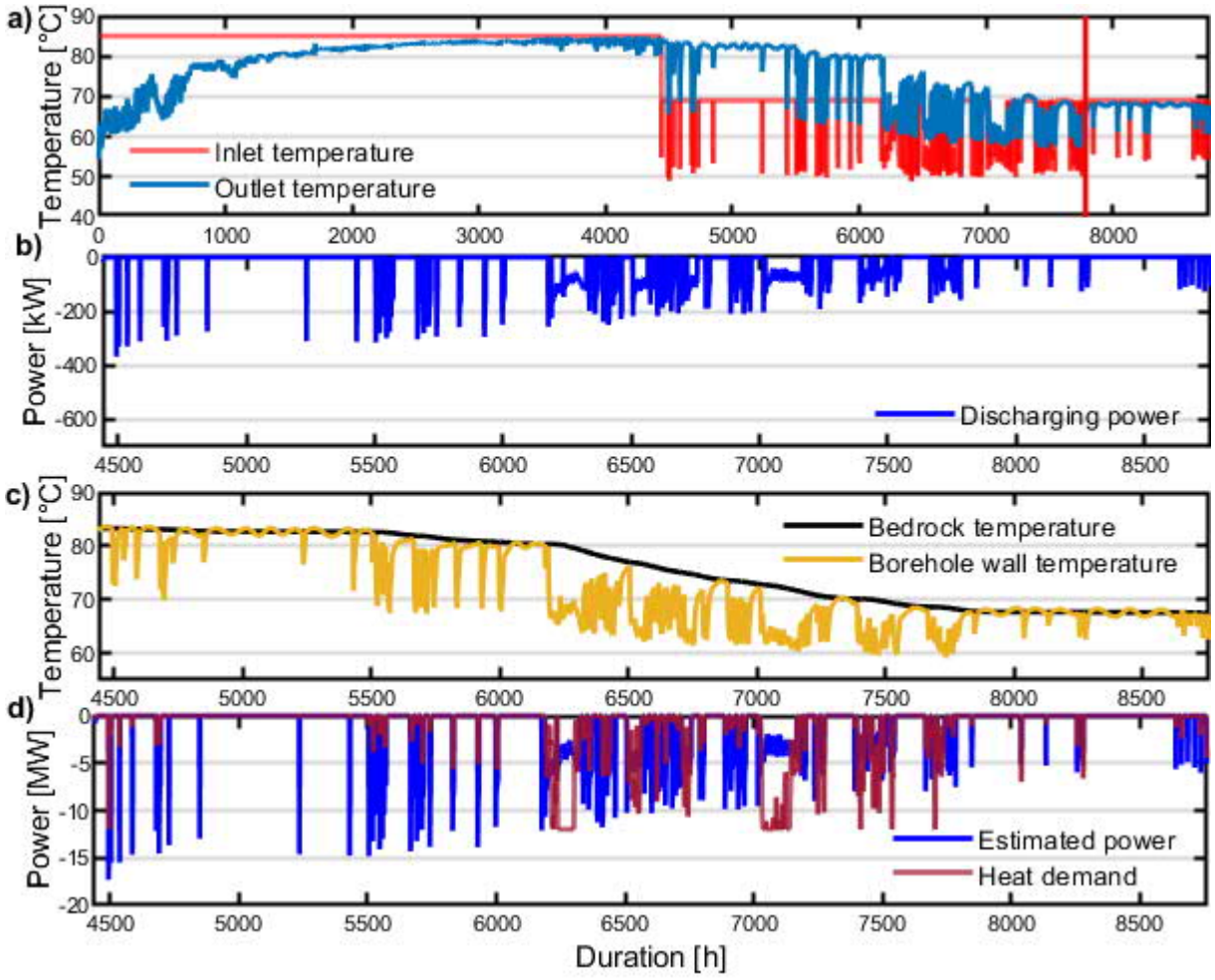

Figure 45. Case: borehole spacing 3.5m, D/L –ratio 1.0. a) Inlet and outlet temperatures during discharging. b) Discharging power of the model unit. Energy is extracted only during heat demand periods. c) Figure shows how extracted thermal energy cools down bedrock and borehole wall temperatures. d) Discharging power is scaled to full scale. Red line shows the point from which horizontal temperature profiles are plotted for Figure 46.

Figure 46 illustrates heating and cooling times required to achieve specified temperature change at the circumcentre point of the borehole pattern. During charging period, storage is heated continuously and, therefore heating time follows exponential growth. As the discharged energy is extracted in short time period, significant temperature changes are harder to achieve when boreholes are spaced sparsely. In such case, heat has no time to flow from the storage medium to BHE as Figure 46 illustrates.

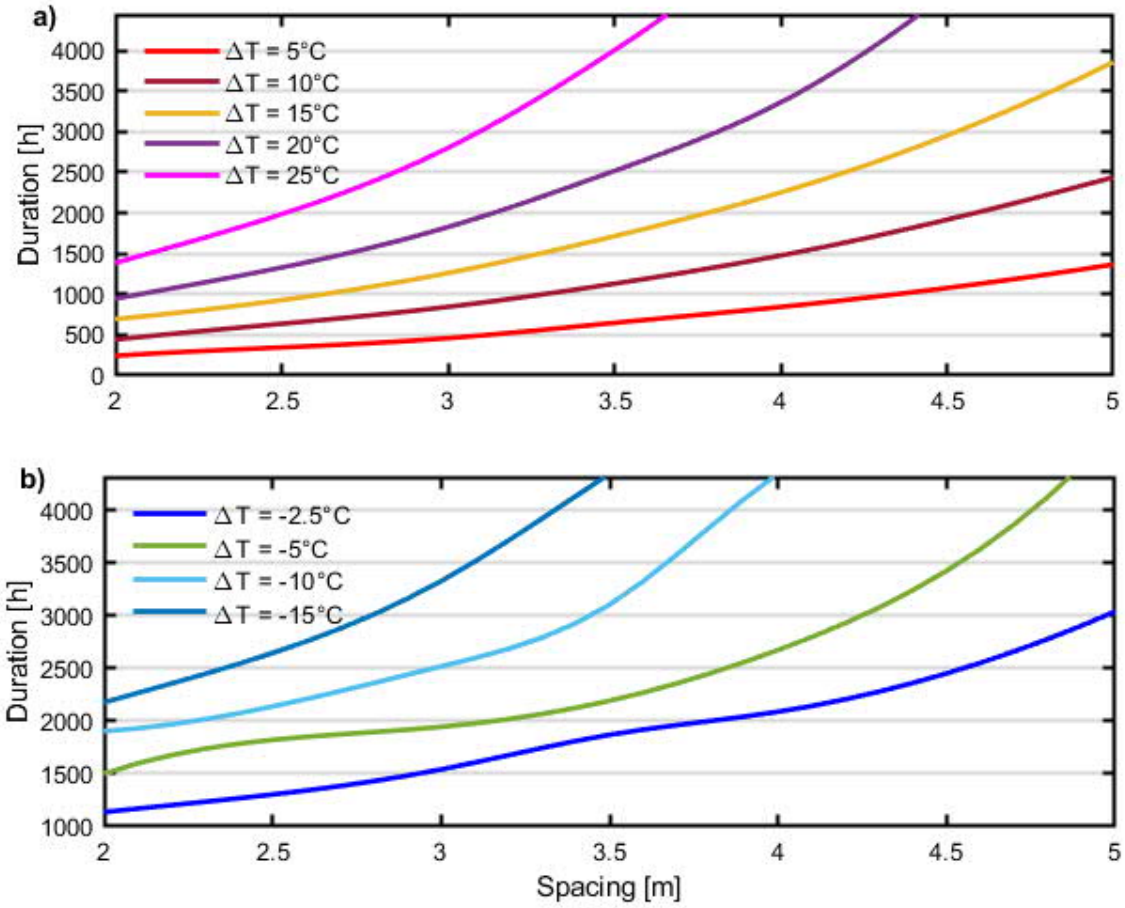

Figure 46. a) Heating time required for specified ΔT in response to borehole spacing during charging period. b) Cooling time required for specified ΔT in response to borehole spacing during discharging period. D/H –ratio is 1.0

Figure 48 visualizes the horizontal temperature profiles of each case with D/L-ratio 1.0 with different spacing from the midpoint of the borehole. As can be seen from the figure, the BHE effectively extracts thermal energy from a surrounding area with a diameter of approximately one metre. The upper part of the domain has the thermal properties of granite, which has higher thermal diffusivity than the lower part of the domain, which has the thermal properties of hornblende. Therefore, 2-3 °C differences exist inside of the model domain. Additionally, Figure 48 demonstrates that a domain with higher diffusivity can extract effectively thermal energy from a larger area.

Tabulated results are provided in Appendix A and detailed simulation results in Appendix B.

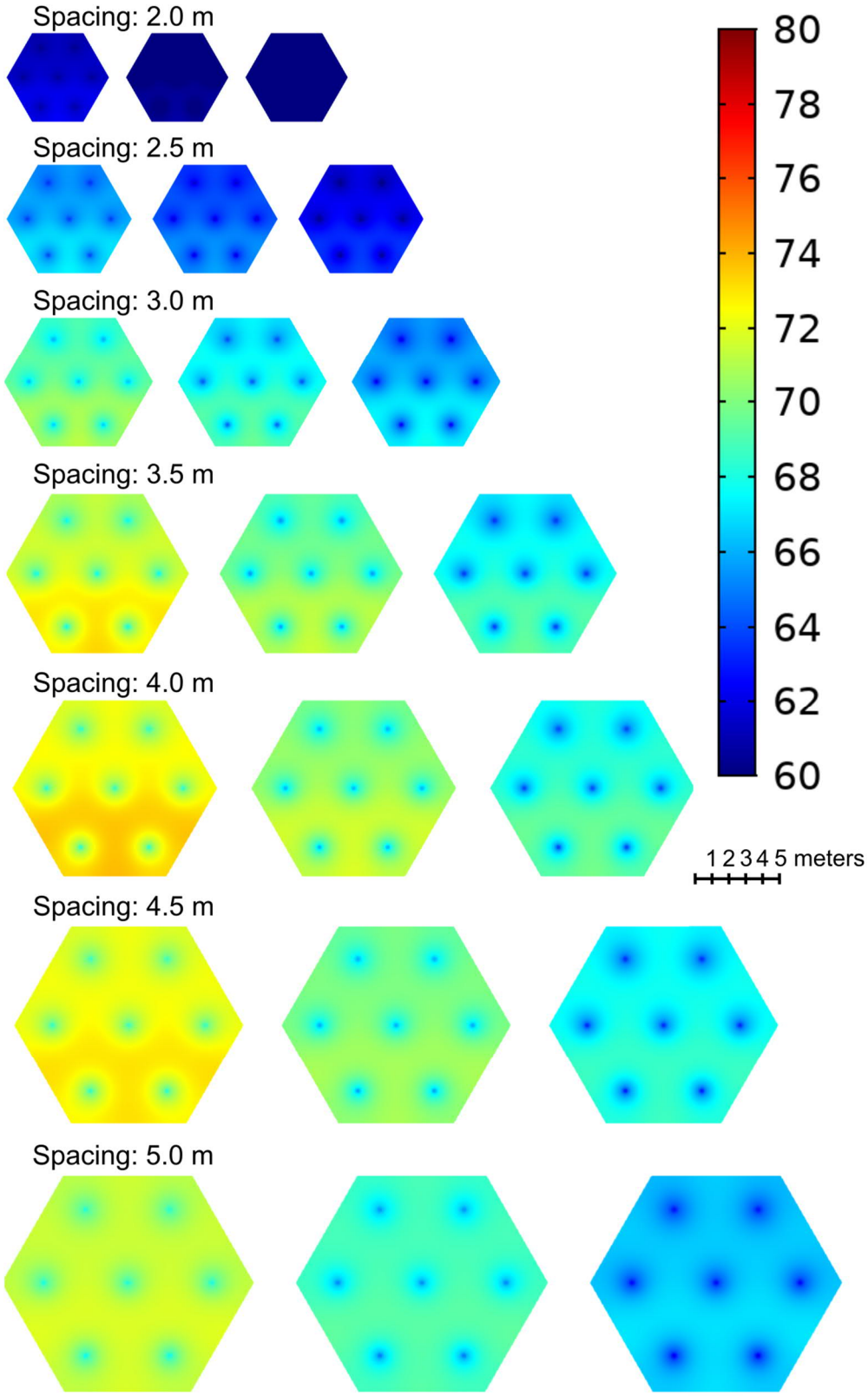

Figure 47. The horizontal temperature profiles of three sections of the storage (see storage sections from Figures 27 and 28), when D/L-ratio is 1.0. Temperature profiles on the left represents storage center and on the right outer section. The profiles are after the main discharging period at point of 7786h.

5 Discussion

COMSOL MultiPhysics is sufficient for BHE related problems, as the verifications confirm. Similar findings have been published by Ozudogru et al. (2014), Caballero Hernandez (2017) and Janiszewski et al. (2018a). Each study found that fluid flow and heat transfer in BHEs can be predicted with acceptable accuracy using COMSOL MultiPhysics. However, the accuracy of the method was determined to be slightly higher in this thesis than in the studies by Caballero Hernandez (2017) and Janiszewski et al. (2018a). The difference may be due to different approaches to creating the geometry of the borehole. This thesis considers the geometry of the borehole in 3D, while Caballero Hernandez (2017) and Janiszewski et al. (2018a) considered only the heat pipe element. In addition, the measurement accuracy of the thermal response tests performed by the Geological Survey of Finland is unknown and this is source of uncertainty in the findings.

The mesh sensitivity study revealed that the number of vertical elements has a crucial effect on thermal interaction between BHEs and the bedrock domain. The number of elements has only a minor effect on outlet temperature. However, Janiszewski (2018a) found greater effect of elements on outlet temperature. The reason may relate higher fluid temperature (55 °C) in Janiszewski's (2018a) mesh sensitivity analysis; therefore, the effect of mesh on outlet temperature may be temperature dependent.

Many BTES simulations are based on analytical solutions of DST models due to their efficient solutions. Only a few numerical BTES simulations can be found (e.g., Catolico et al., 2016; Tordrup et al., 2017., Korhonen et al., 2018;). Tordrup et al. (2017) and Korhonen et al. (2018) have simulated BTES in full scale. Only Catolico et al. (2016) have used the symmetry of the storage by modelling only $¼^{th}$ of the storage size and relying on periodic boundary conditions. This thesis used the same boundary conditions; however, the geometry was simplified even further including only small units from each section in order to minimize computational cost. The drawback of the efficient modelling is decreased accuracy. This model cannot evaluate heat losses; therefore, temperature and extracted thermal energy may be overestimated. In order to get more a realistic estimation of the discharging phase, 35 % of the extracted thermal energy is assumed to be heat losses. This approach may cause error.

Although each BTES system has varying thermal properties and they cannot be compared straightforwardly, the BTES system in Brædstrup has similarities with the model unit created in this thesis as their storage medium volumetric capacity is similar (1.9 MJ m^{-3} K^{-1}). However, the thermal diffusivity of the storage medium is almost twice lower in Brædstrup ($0.75 \cdot 10^{-6}$ m^2s^{-1}) as in Korvenmäki ($1.31 \cdot 10^{-6}$ m^2s^{-1}). The system in Brædstrup has reached a maximum power of 600

kW, discharging capacity of 227 MWh with a total borehole length of 2.1 km (Schmidt and Sørensen, 2018; Sørensen and Schmidt, 2018), while models in this thesis reached a maximum power of 560 kW and discharging capacity of 177 MWh with a total borehole length of 3.6 km. Another comparable case is in Chifeng, China, where 468 boreholes, each with a length of 80 m (total borehole length of 34 km), have been modelled to yield 2.2 GWh energy (Xu et al., 2018), while this thesis estimates at least 550 boreholes of 172 m each (total borehole length of 98 km) are required in order to achieve 4.46 GWh. In this estimation, twice the amount of energy requires three times greater total borehole length, although thermal diffusivity of the storage medium in Chifeng is $0.52 \cdot 10^{-6}\ m^2s^{-1}$. The numbers shown in this thesis seems to be realistically achievable; however, this method might overestimate required total borehole length and therefore required investment. However, higher thermal diffusivity values in Korvenmäki would predict less heat exchanging surface area required for the same amount of the extracted energy.

One reason for overestimation might be heat pumps, which are connected to the BTES systems in Brædstrup and Chigeng (Schmidt and Sørensen, 2018; Sørensen and Schmidt, 2018; Xu et al., 2018). Heat pumps may be used to decrease fluid inlet temperature; therefore, heat transfer between BHE and storage medium may be enhanced by increasing the temperature difference between the fluid and storage medium (Welsch et al., 2016; Malmberg, 2017; Xu et al., 2018). However, increased storage temperature may lead to significant heat losses as the temperature difference between storage medium and natural ground temperature increases (Skarphagen et al., 2019). For example, BTES systems in Brædstrup use a storage temperature of 50 °C to keep heat losses at minimum (Sørensen et al., 2012). Therefore, heating the storage up to 85 °C may be suboptimal in terms of heat losses. Figure 49 suggests how a BTES set up used in this thesis may be enhanced.

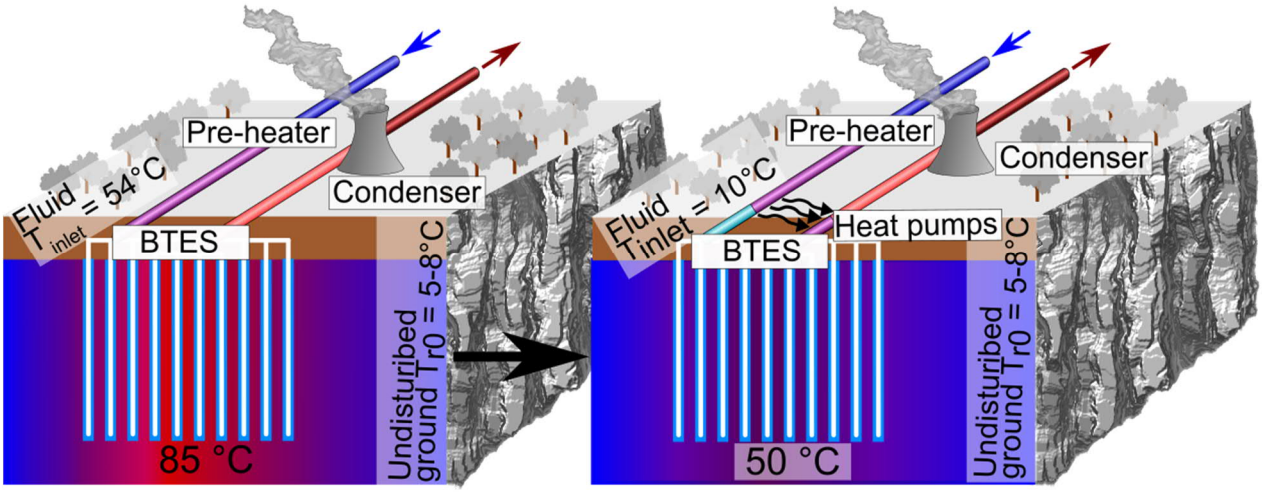

Figure 48. Left-hand side: BTES and district heating set up used in this thesis. Right-hand side: Suggested BTES and district heating set up with heat pumps and lowered storage temperature to enhance storage performance and decrease heat losses. According to Kukkonen (1989) natural ground temperature is between 5-8 °C in Finland.

The model does not accurately match power with real heat demand, as Figure 46 visualizes. Therefore, the model overestimates the capacity of BTES, as power is occasionally overproduced. For that reason, an iterative solution for the discharging period must be developed in order to achieve a more accurate estimate of investment cost.

Previous studies have not focused on the effect of borehole spacing on detail. The key finding of this study is the effect of borehole spacing on storage performance and investment cost. Bergman et al. (2011) define that time required for changing temperature at distance ξ depends on temperature differences, heat flux, thermal conductivity, diffusivity and boundary conditions in semi-infinite solid. Therefore, the factors determining correct borehole spacing are the thermal properties of the storage medium, the amount of injected and extracted energy, heat losses, fluid inlet temperatures in the discharging and charging periods, storage minimum and maximum temperatures and time within which thermal energy must be injected or extracted. As injected heat is desired to extract in given time period, the thermal properties and temperature differences defines the radius ξ where heat may be extracted effectively during this period. However, too densely spaced boreholes may extract heat too fast. Therefore, drilling extra boreholes may be required to satisfy the capacity. On the other hand, too sparsely spaced boreholes cannot extract heat effectively from the system. If the spacing of a HT-BTES system is designed considering all these factors, the investment cost may be reduced significantly for the same capacity. However, in order to achieve optimal BTES, the borehole field must be spaced densely. According to Skarphagen et al. (2019) horizontal deviation of a borehole can be 26 m with 150 m deep boreholes. Therefore, densely spaced borehole field requires more expensive drilling methods in order to drill straight boreholes. As the cost difference between designs with optimal and suboptimal spacing is 1.5 million €, more expensive drilling methods may be cost effective.

This thesis did not find significant savings related to deeper boreholes. However, deeper boreholes cause suboptimal storage shapes as the most optimal storage shape has the same dimensions for diameter and depth (Janiszewski et al., 2018b; Skarphagen et al., 2019). The extra cost caused by unfavourable storage shape was not considered in this thesis. Although MD-BTES has a disfavoured storage shape, it benefits from achieving higher temperatures, as the temperature gradient is 16 °C km^{-1} in Helsinki region (Leary et al. 2017). Therefore, deeper HT-BTES may operate closer to natural bedrock temperature and reduce heat losses (Bär et al., 2015). However, less thermal energy can be injected due to lower temperature difference between fluid and storage. Therefore, the cost-effectiveness of the MD-BTES solution requires further investigation.

6 Conclusion

Typically, the design of a BTES system is based on analytical methods. However, those methods do not consider temperature differences between fluid and bedrock or varying power levels. Numerical solutions provide more accurate insights into fluid flow and heat transfer in the storage system and the method is validated and verified in this thesis. However, the drawback of numerical solutions is increased computational cost. For that reason, the model developed in this thesis is balanced between efficiency and accuracy. Simplified geometry is efficient but creates inaccuracies due to the inability to evaluate heat losses. The model has not yet validated against experimental results yet; therefore, the optimisation requires further study.

The objectives of the thesis were to find whether the BTES system is sufficient for peak load purposes and the effects of borehole spacing and storage width to depth –ratio on the storage performance and cost. Borehole spacing is one of the key parameters in designing cost-effective BTES system. The results show that borehole spacing affects strongly to storage temperature change during discharging period and temperature change is affected by time-dependent behaviour of heat flow. Storage temperature change affects all the other parameters as required storage volume, number of boreholes and total borehole length in the system. On the other hand, the number of boreholes connected in parallel determines mass flow rate of the single U-tube pipe. Therefore, it is recommended that further investigations consider the thermal properties of the storage medium, the amount of injected and extracted energy, heat losses, fluid inlet temperatures in discharging and charging periods, storage minimum and maximum temperatures and time within which thermal energy is demanded to be injected or extracted in order to design effective storage. As the storage geometry affects heat losses, the created model cannot evaluate the optimal storage width to depth –ratio accurately.

In this master's thesis, BTES system is found to have potential to yield 2-5 MW thermal energy for peak load purposes continuously. At the beginning of each discharging period, the storage system has the potential to yield 10 MW some hours. The investment cost of the system for the optimal design is estimated to be 2.4 million €, when borehole spacing is 3.5 m and depth 172 m. Based on literature survey, cylindrical storage shape and hexagonal borehole pattern are found to be the most optimal. However, this thesis didn't consider the storage long-term performance or heat losses accurately, which may lead to different outcome. Therefore, the long-term performance and heat losses should be taken in consideration in further studies. Additionally, time-dependent behaviour of the heat transfer and its effect on the cost-effectiveness of BTES requires further studies in order to assist BTES system become potential clean investment in the district heating system.

References

Åberg, B., Johansson, S., 1988. Vattenströmning till och från borrhålsvärmelager (Water flow to and from borehole heat stores). Stockholm, Sweden.

Aho, R., 2015. Kallioperän rakenteiden kehitys Salon alueella Etelä-Suomessa. Master's thesis. Unversity of Turku.

Al-Khoury, R., Bonnier, P.G., 2006. Efficient finite element formulation for geothermal heating systems. Part II: Transient. Int. J. Numer. Methods Eng. 67, 725–745. https://doi.org/10.1002/nme.1662

Al-Khoury, R., Bonnier, P.G., Brinkgreve, R.B.J., 2005. Efficient finite element formulation for geothermal heating systems. Part I: steady state. Int. J. Numer. Methods Eng. 63, 988–1013. https://doi.org/10.1002/nme.1313

Alva, G., Lin, Y., Fang, G., 2018. An overview of thermal energy storage systems. Energy 144, 341–378. https://doi.org/10.1016/j.energy.2017.12.037

Arola, T., 2015. Groundwater as an energy resource in Finland. Doctoral dissertation. University of Helsinki.

Arola, T., Hakala, P., Vallin, S., 2019. Optimizing geothermal energy storage in harsh conditions.

Bach, P.-F., 2012. An Energy System with Seasonal Storage.

Bakema, G., Snijders, A.L., Nordell, B., 1995. Underground thermal energy storage - State of art 1994. https://doi.org/90-802769-1-x

Banks, D., 2012. An introduction to thermogeology: Ground source heating and cooling, 2nd ed. John Wiley & Sons, West Sussex, UK. https://doi.org/10.1002/9781118447512

Banks, D., Robins, N., 2002. An introduction to groundwater in crystalline bedrock. https://doi.org/82-7386-100-1

Bär, K., Rühaak, W., Welsch, B., Schulte, D., Homuth, S., Sass, I., 2015. Seasonal High Temperature Heat Storage with Medium Deep Borehole Heat Exchangers. Energy Procedia 76, 351–360. https://doi.org/10.1016/j.egypro.2015.07.841

Bauer, D., Drück, H., Lang, S., Marx, R., Plaz, T., 2016. Weiterentwicklung innovativer Technologien zur solaren Nahwärme und saisonale Wärmespeicherung Akronym, Wintersun. Stuttgart, Germany.

Bergman, T.L., Incropera, F.P., DeWitt, D.P., Lavine, A.S., 2011. Fundamentals of Heat and Mass Transfer, 7th ed, Water. John Wiley & Sons. https://doi.org/10.1016/j.applthermaleng.2011.03.022

Bonte, M., Stuyfzand, P.J., Hulsmann, A., van Beelen, P., 2011. Underground thermal energy storage: Environmental risks and policy developments in the Netherlands and European Union. Ecol. Soc. 16. https://doi.org/10.5751/ES-03762-160122

Brielmann, H., Griebler, C., Schmidt, S.I., Michel, R., Lueders, T., 2009. Effects of thermal energy discharge on shallow groundwater ecosystems. FEMS Microbiol. Ecol. 68, 273–286. https://doi.org/10.1111/j.1574-6941.2009.00674.x

Caballero Hernandez, E., 2017. In situ experimentation and numerical model validation of thermal flow in shallow crystalline rock, Otaniemi case. Master's thesis. Aalto University.

Catolico, N., Ge, S., McCartney, J.S., 2016. Numerical Modeling of a Soil-Borehole Thermal Energy Storage System. Vadose Zo. J. 15, 1–17. https://doi.org/10.2136/vzj2015.05.0078

Cermak, V., Rybach, L., 1982. Thermal properties: thermal conductivity and specific heat of minerals and rocks, in: Angeneister, G. (Ed.), Landolt-Bornstein Zahlenwerte and Funktionen Aus Naturwissenschaften Und Technik, Neue Serie, Physichalische Eigenschaften Der Gesteine. Springer-Verlag, Berlin, Heidelberg, New York, pp. 305–343.

Chiasson, A.D., 2016. Borehole heat exchangers, in: Geothermal Heat Pump and Heat Engine Systems: Theory and Practice. John Wiley & Sons, Ltd, West Sussex, UK, pp. 138–180. https://doi.org/10.1002/9781118961957

Child, M., Breyer, C., 2016. The Role of Energy Storage Solutions in a 100% Renewable Finnish Energy System, in: Energy Procedia, Volume 99. pp. 25–34. https://doi.org/10.1016/j.egypro.2016.10.094

Cho, W.J., Kwon, S., Choi, J.W., 2009. The thermal conductivity for granite with various water contents. Eng. Geol. 107, 167–171. https://doi.org/10.1016/j.enggeo.2009.05.012

Claesson, J., Hellström, G., 2011. Multipole method to calculate borehole thermal resistances in a borehole heat exchanger. HVAC R Res. 17, 895–911. https://doi.org/10.1080/10789669.2011.609927

Clauser, C., Huenges, E., 1995. Thermal Conductivity of Rocks and Minerals, in: Ahrens, T.J. (Ed.), Rock Physics & Phase Relations: A Handbook of Physical Constants, Volume 3. American Geophysical Union, Washington, DC, ISA, pp. 105–126. https://doi.org/10.1029/RF003p0105

Cui, Y., Zhu, J., Twaha, S., Riffat, S., 2018. A comprehensive review on 2D and 3D models of vertical ground heat exchangers. Renew. Sustain. Energy Rev. https://doi.org/10.1016/j.rser.2018.05.063

Diersch, H.J.G., Bauer, D., Heidemann, W., Rühaak, W., Schätzl, P., 2011. Finite element modeling of borehole heat exchanger systems. Part 1. Fundamentals. Comput. Geosci. 37, 1122–1135. https://doi.org/10.1016/j.cageo.2010.08.003

Diersch, H.J.G., Bauer, D., Heidemann, W., Rühaak, W., Schätzl, P., 2010. FEFLOW Finite

Element Subsurface Flow & Transport Simulation System, White Papers Vol 5. Berlin, Germany.

Energiateollisuus, 2018. District heating in Finland 2017. Helsinki.

Energiateollisuus, 2014. Teho ja vesivirta kaukolämmön maksuperusteina.

Eppelbaum, L., Kutasov, I., Pilchin, A., 2014. Thermal properties of rocks and density of fluids, in: Applied Geothermics. Lecture Notes in Earth System Sciences. Springer-Verlag, Berlin, Heidelberg, pp. 99–149. https://doi.org/10.1007/978-3-642-34023-9_2

Eskilson, P., 1987. Thermal Analyses of Heat Extraction Boreholes. Doctoral dissertation. Lund University. https://doi.org/91-7900-298-6

Eskilson, P., Claesson, J., 1988. Simulation model for thermally interacting heat extraction boreholes. Numer. Heat Transf. 13, 149–165. https://doi.org/10.1080/10407788808913609

Fisch, M.N., Guigas, M., Dalenbäck, J.O., 1998. A review of large-scale solar heating systems in Europe. Sol. Energy 63, 355–366. https://doi.org/10.1016/S0038-092X(98)00103-0

Gadd, H., Werner, S., 2015. Thermal energy storage systems for district heating and cooling, in: Cabeza, L.F. (Ed.), Advances in Thermal Energy Storage Systems: Methods and Applications. Woodhead Publishing Series in Energy, pp. 467–478. https://doi.org/10.1533/9781782420965.4.467

Gao, L., Zhao, J., Tang, Z., 2015. A Review on Borehole Seasonal Solar Thermal Energy Storage. Energy Procedia 70, 209–218. https://doi.org/10.1016/j.egypro.2015.02.117

Gehlin, S., 2016. Borehole thermal energy storage, in: Rees, S.J. (Ed.), Advances in Ground-Source Heat Pump Systems. Elsevier, Heidelberg London, pp. 295–327. https://doi.org/10.1016/B978-0-08-100311-4.00011-X

Gill, R., 2010. Igneous rocks and processes: a practical guide, 1st ed. Wiley-Blackwell.

Guo, F., Yang, X., Xu, L., Torrens, I., Hensen, J., 2017. A central solar industrial waste heat heating system with large scale borehole thermal storagge. Procedia Eng. 205, 1584–1591. https://doi.org/10.1016/j.proeng.2017.10.274

Gustafsson, A.M., Gehlin, S., 2008. Influence of natural convection in water-filled boreholes for GCHP, in: ASHRAE Transactions, 114. pp. 416–423.

Hellström, G., 1989. Heat Storage in the Duct Ground Heat Storage Model, Manual for Computer Code. Doctoral dissertation. Univesity of Lund.

Hirth, L., 2013. The market value of variable renewables. The effect of solar wind power variability on their relative price. Energy Econ. https://doi.org/10.1016/j.eneco.2013.02.004

Hirvonen, J., Sirén, K., 2018. A novel fully electrified solar heating system with a high renewable fraction - Optimal designs for a high latitude community. Renew. Energy 127, 298–309.

https://doi.org/10.1016/j.renene.2018.04.028

Hirvonen, J., ur Rehman, H., Sirén, K., 2018. Techno-economic optimization and analysis of a high latitude solar district heating system with seasonal storage, considering different community sizes. Sol. Energy 162, 472–488. https://doi.org/10.1016/j.solener.2018.01.052

Holmgren, M., 2006. X Steam version 2.5. IAPWS Steam Tables.

Huusko, A., 2019. The price of borehole. [email]. 26.4.2019. Geological Survey of Finland.

IEA ECES, 1998. Annual Report 1997 Annex 12.

Janiszewski, M., Caballero Hernández, E., Siren, T., Uotinen, L., Kukkonen, I., Rinne, M., 2018a. In situ experiment and numerical model validation of a borehole heat exchanger in shallow hard crystalline rock. Energies 11, 963–984. https://doi.org/10.3390/en11040963

Janiszewski, M., Kopaly, A., Honkonen, M., Kukkonen, I., Uotinen, L., Siren, T., Rinne, M., 2016. Feasibility of underground seasonal storage of solar heat in Finland, in: Ranjith, R.G., Zhao, J. (Eds.), International Conference on Geo-Mechanics, Geo-Energy and Geo-Resources: Conference Proceedings [236]. Monash University, Melbourne, Australia, pp. 959–965.

Janiszewski, M., Siren, T., Uotinen, L.K.T., Oosterbaan, H., Rinne, M., 2018b. Effective modelling of borehole solar thermal energy storage systems in high latitudes. Geomech. Eng. 16, 503–512. https://doi.org/10.12989/gae.2018.16.5.503

Javed, S., Spitler, J., 2017. Accuracy of borehole thermal resistance calculation methods for grouted single U-tube ground heat exchangers. Appl. Energy 187, 790–806. https://doi.org/10.1016/j.apenergy.2016.11.079

Juvonen, J., Lapinlampi, T., 2013. Energiakaivo: maalämmön hyödyntäminen pientaloissa, Ympäristöopas 2013. Helsinki.

Kim, Daehoon, Kim, G., Kim, Donghui, Baek, H., 2017. Experimental and numerical investigation of thermal properties of cement-based grouts used for vertical ground heat exchanger. Renew. Energy 112, 260–267. https://doi.org/10.1016/j.renene.2017.05.045

Korhonen, K., Leppäharju, N., Hakala, P., Arola, T., 2018. Simulated temperature evolution of large BTES – case study from Finland, in: International Ground-Source Heat Pump Association Research Conference. Proceedings of the IGSHPA Research Track 2018, Stockholm, Sweden, pp. 1–9. https://doi.org/10.22488/okstate.18.000033

Kotzé, J.P., von Backström, T.W., Erens, P.J., 2013. High Temperature Thermal Energy Storage Utilizing Metallic Phase Change Materials and Metallic Heat Transfer Fluids. J. Sol. Energy Eng. 135, 035001-(1-6). https://doi.org/10.1115/1.4023485

Kukkonen, I., 1989. Terrestrial heat flow in Finland, the central Fennoscandian shield. Espoo. https://doi.org/YST-68

Kukkonen, I., Lindberg, A., 1998. Thermal properties of rocks at the investigation sites: measured and calculated thermal conductivity, specific heat capacities and thermal diffusivity.

Lahtonen, R., Korja, A., Nironen, M., 2005. Paleoproterozoic tectonic evolution, in: Lehtinen, M., Nurmi, P.A., Rämö, O.T. (Eds.), Precambrian Geology of Finland - Key to the Evolution of the Fennoscandian Shield. Elsevier, Amsterdam, pp. 481–532.

Lanahan, M., Tabares-Velasco, P.C., 2017. Seasonal thermal-energy storage: A critical review on BTES systems, modeling, and system design for higher system efficiency. Energies 10, 743–767. https://doi.org/10.3390/en10060743

Lanini, S., Delaleux, F., Py, X., Olivès, R., Nguyen, D., 2014. Improvement of borehole thermal energy storage design based on experimental and modelling results. Energy Build. 77, 393–400. https://doi.org/10.1016/j.enbuild.2014.03.056

Lehijärvi, M., 1955. Suomen Geologinen Kartta: 2021 - Salo. Helsinki.

Lehtinen, M., Nurmi, P., Rämö, T., 1998. Suomen kallioperä: 3000 vuosimiljoonaa. Suomen Geologinen Seura ry., Helsinki.

Liebel, V., Reuss, M., 2006. PE-X borehole heat exchanger for high temperature UTES applications, in: EcoStock: Tenth International Conference on Thermal Energy Storage. Richard Stockton College of New Jersey, Pomona, NJ.

Lieskoski, M., 2019. Dow-factory material PE-RT (calculations). [email]. Geopipe GP Oy.

Lounavoima, 2019. Tietoa Laitoksesta [WWW Document]. URL https://www.lounavoima.fi/laitos/ (accessed 5.26.19).

Mäkelä, V.-M., Tuunanen, J., 2015. Suomalainen kaukolämmitys. Mikkelin ammattikorkeakoulu (University of Applied Sciences), Mikkeli, Finland.

Malmberg, M., 2017. Transient modeling of a high temperature borehole thermal energy storage coupled with a combined heat and power plant. Master's thesis. KTH Royal Institute of Technology. https://doi.org/EGI 2017: 0106 MSC

Manonelles, J.J., 2014. Large-scale underground thermal energy storage - using industrial waste heat to supply district heating. Master's thesis. Universitat de Lleida.

Marcotte, D., Pasquier, P., 2009. The effect of borehole inclination on fluid and ground temperature for GLHE systems. Geothermics 38, 392–398. https://doi.org/10.1016/j.geothermics.2009.06.001

Nordell, B., 2000. Large-scale thermal energy storage, in: Proceedings of Winter Cities, Energy and Environment. Luleå, Sweden. https://doi.org/10.1088/2040-8978/13/5/055203

Nordell, B., 1994. Borehole heat store design optimization. Doctoral dissertation. Luleå University of Technology. https://doi.org/ISSN: 0348-8373

Nordell, B., Scorpo, A.L., Andersson, O., Rydell, L., Carlsson, B., 2015. Long Term Evaluation of Operation and Design of the Emmaboda BTES: Operation and Experiences 2010-2015. Luleå, Sweden. https://doi.org/978-91-7583-530-3

Nussbicker, J., Heidemann, W., Mueller-Steinhagen, H., 2006. Monitoring results and operational experiences for a central solar district heating system with Borehole Thermal Energy Store in Neckarsulm (Germany), in: EcoStock: Tenth International Conference on Thermal Energy Storage. Richard Stockton College of New Jersey, Pomona, NJ.

Nussbicker, J., Heidemann, W., Müller-Steinhagen, H., 2007. 10 Jahre solar unterstützte Nahwärmeversorgung in Neckarsulm-Amorbach, in: OTTI Anwnederforum Oberflächennahe Geothermie, 26.-27.04.2007. Freising, Germany.

Oberkampf, W.L., Roy, C.J., 2011. Verification and validation in scientific computing, Verification and Validation in Scientific Computing. https://doi.org/10.1017/CBO9780511760396

Ozudogru, T.Y., Olgun, C.G., Senol, A., 2014. 3D numerical modeling of vertical geothermal heat exchangers. Geothermics 51, 312–324. https://doi.org/10.1016/j.geothermics.2014.02.005

Park, S.H., Jang, Y.S., Kim, E.J., 2018. Using duct storage (DST) model for irregular arrangements of borehole heat exchangers. Energy 142, 851–861. https://doi.org/10.1016/j.energy.2017.10.092

Petukhov, B.S., 1970. Heat Transfer and Friction in Turbulent Pipe Flow with Variable Physical Properties. Adv. Heat Transf. 6, 503–564. https://doi.org/10.1016/S0065-2717(08)70153-9

Philippe, M., Marchio, D., Hagspiel, S., Riederer, P., Partenay, V., 2009. Analysis of 30 underground thermal energy storage systems for building heating and cooling and district heating, in: Conference Proceedings, Effstock. Stockholm, Sweden.

Picard, D., Helsen, L., 2014. A new hybrid model for borefield heat exchanger performance evaluation, in: Proceedings of the 10th International Modelica Conference, March 10-12, 2014, Lund, Sweden. pp. 857–866. https://doi.org/10.3384/ecp14096857

Pirajno, F., 2009. Hydrothermal Processes and Wall Rock Alteration, in: Pirajno, F. (Ed.), Hydrothermal Processes and Mineral Systems. Springer Netherlands, pp. 73–164. https://doi.org/10.1007/978-1-4020-8613-7_2

Poelchau, H.S., Baker, D.R., Hantschel, T.H., Horsfield, B., Wygrala, B., 1997. Basin Simulation and the Design of the Conceptual Basin Model, in: Welte, D.H., Horsfield, B., Baker, D.R. (Eds.), Petroleum and Basin Evolution. Springer, Berlin, Heidelberg, pp. 3–70.

Rapantova, N., Pospisil, P., Koziorek, J., Vojcinak, P., Grycz, D., Rozehnal, Z., 2016. Optimisation of experimental operation of borehole thermal energy storage. Appl. Energy 181, 464–476. https://doi.org/10.1016/j.apenergy.2016.08.091

Reuss, M., 2015. The use of borehole thermal energy storage (BTES) systems, in: Cabeza, L.F.

(Ed.), Advances in Thermal Energy Storage Systems: Methods and Applications. Woodhead Publishing Series in Energy, pp. 117–147. https://doi.org/10.1533/9781782420965.1.117

Riedel, T., 2019. Temperature-associated change in groundwater quality. J. Hydrol. https://doi.org/https://doi.org/10.1016/j.jhydrol.2019.02.059

Ringkjøb, H.K., Haugan, P.M., Solbrekke, I.M., 2018. A review of modelling tools for energy and electricity systems with large shares of variable renewables. Renew. Sustain. Energy Rev. https://doi.org/10.1016/j.rser.2018.08.002

Ritola, J., 1988. Lämmön varastointi kallioon porareikäputkistolla. Helsinki.

Rossi Espagnet, A., 2016. Techno-economic assessment of thermal energy storage integration into low temperature district heating networks. Master's thesis. KTH Royal Institute of Technology.

Saeid, S., Al-Khoury, R., Barends, F., 2013. An efficient computational model for deep low-enthalpy geothermal systems. Comput. Geosci. 51, 400–409. https://doi.org/10.1016/j.cageo.2012.08.019

Saito, T., Hamamoto, S., Ueki, T., Ohkubo, S., Moldrup, P., Kawamoto, K., Komatsu, T., 2016. Temperature change affected groundwater quality in a confined marine aquifer during long-term heating and cooling. Water Res. 94, 120–127. https://doi.org/10.1016/j.watres.2016.01.043

Santhoshkumar, T.G., Abraham, B.M., Sridharan, A., Jose, B.T., 2016. Role of bentonite in improving the efficiency of cement grouting in coarse sand. Geotech. Eng. 47, 136–143.

Sargent, R.G., 2013. Verification and validation of simulation models. J. Simul. https://doi.org/10.1057/jos.2012.20

Schärli, U., Rybach, L., 2001. Determination of specific heat capacity on rock fragments. Geothermics 30, 93–110. https://doi.org/10.1016/S0375-6505(00)00035-3

Schmidt, T., Sørensen, P.A., 2018. Monitoring results from large scale heat storages for District Heating in Denmark, in: 14th International Conference on Energy Storage 25-28 April 2018. EnerSTOCK2018, Adana, Turkey.

Schön, J.H., 2015. Physical properties of rocks, Volume 65, 2nd ed, Developments in Petroleum Science. Elsevier. https://doi.org/10.1016/B978-0-08-100404-3.00008-1

Shah, S.K., Aye, L., Rismanchi, B., 2018. Seasonal thermal energy storage system for cold climate zones: A review of recent developments. Renew. Sustain. Energy Rev. https://doi.org/10.1016/j.rser.2018.08.025

Sibbitt, B., Carriere, J., Kokko, J., Djebbar, R., Thornton, J., McClenahan, D., Wong, B., 2011. Measured and Simulated Performance of a High Solar Fraction District Heating System with Seasonal Storage, in: Proceedings of the ISES Solar World Congress. Kessel, Germany (Vol.

10), pp. 1–12. https://doi.org/10.18086/swc.2011.21.06

Sibbitt, B., McClenahan, D., 2015. Seasonal borehole thermal energy storage – guidelines for design & construction.

Sibbitt, B., McClenahan, D., Djebbar, R., Thornton, J., Wong, B., Carriere, J., Kokko, J., 2012. The performance of a high solar fraction seasonal storage district heating system - Five years of operation, in: Energy Procedia, Volume 30. pp. 856–865. https://doi.org/10.1016/j.egypro.2012.11.097

Skarphagen, H., Banks, D., Frengstad, B.S., Gether, H., 2019. Design Considerations for Borehole Thermal Energy Storage (BTES): A Review with Emphasis on Convective Heat Transfer. Geofluids 26. https://doi.org/https://doi.org/10.1155/2019/4961781

Sørensen, P.A., Larsen, J., Thøgersen, L., Andersen, J.D., Østergaard, C., Schmidt, T., 2012. Boreholes in Brædstrup.

Sørensen, P.A., Schmidt, T., 2018. Design and construction of large scale heat storages for district heating in Denmark, in: 14th International Conference on Energy Storage 25-28 April 20182. EnerSTOCK2018, Adana, Turkey.

The Nordic Plastic Pipe Association, 2011. Tryckrörssystem av polyeten (PE).

Tordrup, K.W., Poulsen, S.E., Bjørn, H., 2017. An improved method for upscaling borehole thermal energy storage using inverse finite element modelling. Renew. Energy 105, 13–21. https://doi.org/10.1016/j.renene.2016.12.011

Tveit, T.M., Savola, T., Gebremedhin, A., Fogelholm, C.J., 2009. Multi-period MINLP model for optimising operation and structural changes to CHP plants in district heating networks with long-term thermal storage. Energy Convers. Manag. 50, 639–647. https://doi.org/10.1016/j.enconman.2008.10.010

Vosteen, H.D., Schellschmidt, R., 2003. Influence of temperature on thermal conductivity, thermal capacity and thermal diffusivity for different types of rock. Phys. Chem. Earth 28, 499–509. https://doi.org/10.1016/S1474-7065(03)00069-X

Vuorinen, V., 2018. Matlab code: Heat2D - A simple 2D code using finite difference methods for solving the heat equation in 2D Cartesian grid. Space: 2nd order central difference, Time: 4th order Runge-Kutta method.

Waples, D.W., Waples, J.S., 2004. A review and evaluation of specific heat capacities of rocks, minerals, and subsurface fluids. Part 1: minerals and nonporous rocks. Nat. Resour. Res. 13, 97–122.

Welsch, B., 2019. Technical, Environmental and Economic Assessment of Medium Deep Borehole Thermal Energy Storage Systems. Doctoral dissertation. Technische Universität Darmstadt.

Welsch, B., Göllner-Völker, L., Schulte, D.O., Bär, K., Sass, I., Schebek, L., 2018. Environmental

and economic assessment of borehole thermal energy storage in district heating systems. Appl. Energy 216, 73–90. https://doi.org/10.1016/j.apenergy.2018.02.011

Welsch, B., Rühaak, W., Schulte, D.O., Bär, K., Sass, I., 2016. Characteristics of medium deep borehole thermal energy storage. Int. J. Energy Res. https://doi.org/10.1002/er.3570

Whittington, A.G., Hofmeister, A.M., Nabelek, P.I., 2009. Temperature-dependent thermal diffusivity of the Earth's crust and implications for magmatism. Nature 458, 319–321. https://doi.org/10.1038/nature07818

Xu, J., Wang, R.Z., Li, Y., 2014. A review of available technologies for seasonal thermal energy storage. Sol. Energy 103, 610–638. https://doi.org/10.1016/j.solener.2013.06.006

Xu, L., Torrens, J.I., Guo, F., Yang, X., Hensen, J.L.M., 2018. Application of large underground seasonal thermal energy storage in district heating system: A model-based energy performance assessment of a pilot system in Chifeng, China. Appl. Therm. Eng. https://doi.org/10.1016/j.applthermaleng.2018.03.047

Zhang, Z., Zhang, W., Zhai, Z.J., Chen, Q.Y., 2007. Evaluation of various turbulence models in predicting airflow and turbulence in enclosed environments by CFD: Part 2—comparison with experimental data from literature. HVAC R Res. 13, 871–886. https://doi.org/10.1080/10789669.2007.10391460

Appendices

A. Tabulated results

Table 17. D/L –ratio 1.0. Fluid average mass flow rates in different cases.

Spacing	Average mass flow (charging)	Average mass flow (discharging)
m	**kg s^{-1}**	**kg s^{-1}**
2.0	0.30	0.48
2.5	0.39	0.64
3.0	0.47	0.76
3.5	0.50	0.81
4.0	0.52	0.84
4.5	0.51	0.82
5.0	0.49	0.80

Table 18. D/L –ratio 0.67. Fluid average mass flow rates in different cases.

Spacing	Average mass flow (charging)	Average mass flow (discharging)
m	**kg s^{-1}**	**kg s^{-1}**
2.0	0.39	0.63
2.5	0.51	0.83
3.0	0.60	0.97
3.5	0.65	1.06
4.0	0.67	1.09
4.5	0.65	1.05
5.0	0.63	0.98

Table 19. D/L –ratio 0.5. Fluid average mass flow rates in different cases.

Spacing	Average mass flow (charging)	Average mass flow (discharging)
m	**kg s^{-1}**	**kg s^{-1}**
2.0	0.47	0.76
2.5	0.62	1.01
3.0	0.74	1.17
3.5	0.74	1.13
4.0	0.77	1.12
4.5	0.72	1.04
5.0	0.68	0.98

Table 20. Storage width to depth -ratio = 1.0

Spacing	Pattern discharging capacity	Scale factor [4.46 GWh]	No. of boreholes	Radius	Depth	Volume	Storage ΔT	Borehole wall ΔT
m	MWh			m	m	1000 m^3	ºC	ºC
2.0	55.7	80	1680	43	86	501	24.6	24.7
2.5	77.1	58	1213	45	91	601	20.2	20.6
3.0	99.2	36	944	48	99	763	15.7	16.4
3.5	106.2	42	882	55	109	1020	11.5	12.6
4.0	111.9	40	837	61	122	1410	8.1	9.9
4.5	111.8	40	837	68	137	2008	5.4	7.8
5.0	107.0	63	875	78	155	2942	3.4	6.4

Table 21. Storage width to depth -ratio = 0.67

Spacing	Pattern discharging capacity	Scale factor [4.46 GWh]	No. of boreholes	Radius	Depth	Volume	Storage ΔT	Borehole wall ΔT
m	MWh			m	m	1000 m^3	ºC	ºC
2.0	75.8	59	1236	37	111	474	25.1	25.2
2.5	101.8	44	920	40	119	595	20.2	20.6
3.0	124.3	36	754	43	130	762	15.8	16.4
3.5	139.8	32	670	48	143	1014	11.6	12.7
4.0	147.7	30	634	53	159	1394	8.9	9.9
4.5	146.8	30	638	60	179	2003	5.3	7.6
5.0	140.9	32	665	68	203	2920	3.3	6.0

Table 22. Storage width to depth -ratio = 0.5

Spacing	Pattern discharging capacity	Scale factor [4.46 GWh]	No. of boreholes	Radius	Depth	Volume	Storage ΔT	Borehole wall ΔT
m	MWh			m	m	1000 m^3	ºC	ºC
2.0	83.5	53	1122	35	141	547	23.2	23.3
2.5	123.0	36	761	36	145	597	20.3	20.6
3.0	150.2	30	623	39	157	764	15.8	16.4
3.5	170.2	26	550	43	172	1007	11.2	12.3
4.0	177.0	25	529	48	193	1417	8.6	10.5
4.5	174.3	26	537	55	219	2064	4.9	7.1
5.0	164.3	27	570	63	251	3094	3.0	5.6

Table 23. Storage width to depth -ratio = 1.0

Spacing	Total borehole length	Investment cost	Capacity cost
m	km	million €	€ MWh^{-1}
2.0	145	3.61	811
2.5	111	2.77	622
3.0	98	2.44	549
3.5	96	2.40	539
4.0	102	2.54	570
4.5	115	2.86	642
5.0	136	3.40	762

Table 24. Storage width to depth -ratio = 0.67

Spacing	Total borehole length	Investment cost	Capacity cost
m	km	million €	€ MWh^{-1}
2.0	137	3.42	767
2.5	110	2.75	616
3.0	98	2.44	548
3.5	96	2.39	536
4.0	101	2.51	564
4.5	114	2.86	640
5.0	135	3.37	756

Table 25. Storage width to depth -ratio = 0.5

Spacing	Total borehole length	Investment cost	Capacity cost
m	km	million €	€ MWh^{-1}
2.0	172	3.95	885
2.5	110	2.76	618
3.0	98	2.45	550
3.5	95	2.37	532
4.0	102	2.56	573
4.5	118	2.94	660
5.0	143	3.57	801

B. Simulation results

Explanation of figures:

a) Fluid inlet and outlet temperatures during charging and discharging (0-8760 h)
b) Charging power (kW) of model unit during charging period (0-4440 h)
c) Storage medium (bedrock) and borehole wall temperatures during charging period (0-4440 h)
d) Discharging power (kW) of model unit during discharging period (4440-8760 h) including 35 % of heat losses
e) Storage medium (bedrock) and borehole wall temperatures during discharging period (4440-8760 h)
f) Storage discharging power (MW) scaled using scale factor (S) (estimated power) in order to satisfy heat demand capacity of 4.46 GWh. Heat demand represents actual heat demand in district heating network of Salo.

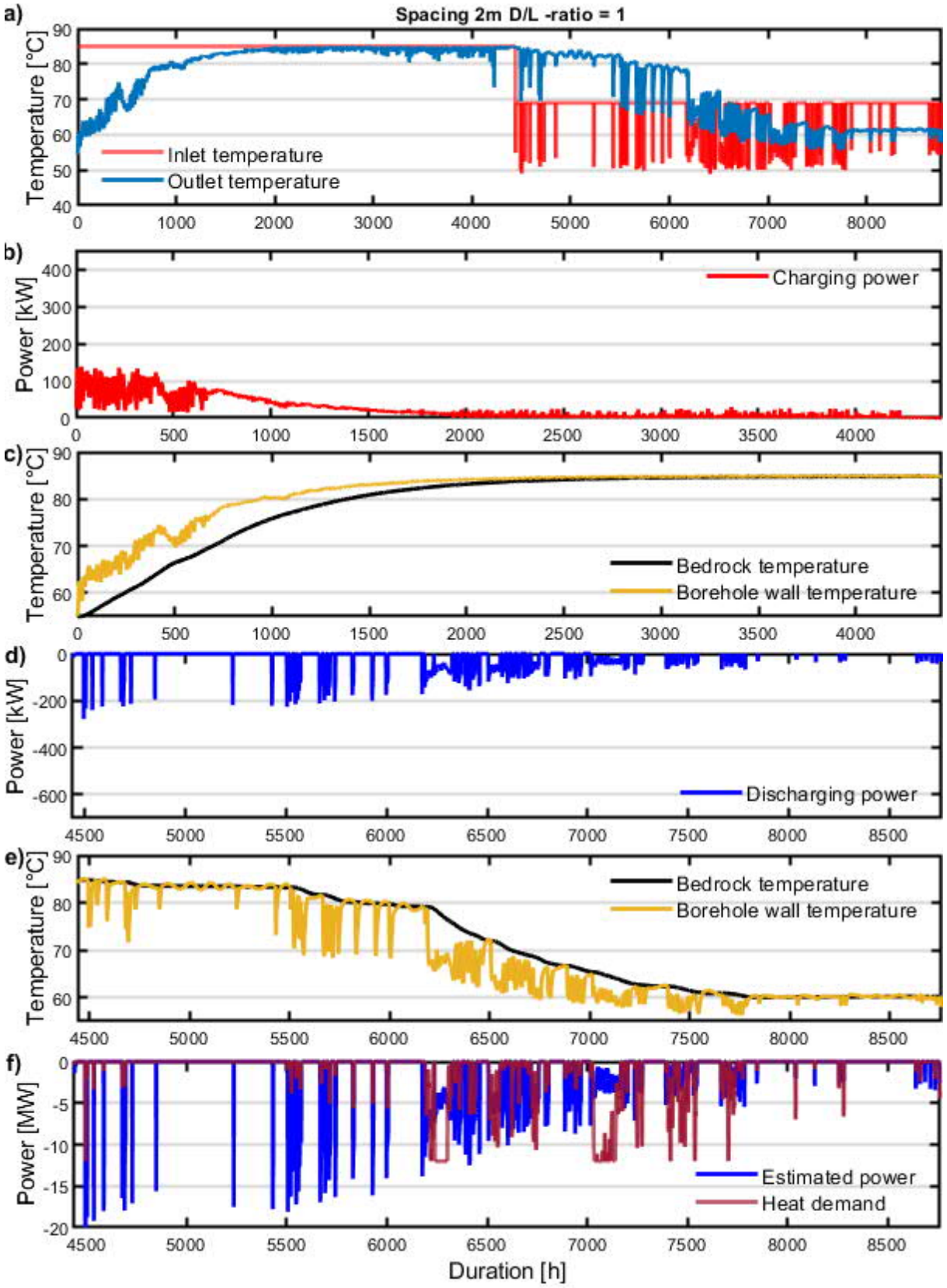
a)
Spacing 2m D/L -ratio = 1
Temperature [°C]
Inlet temperature
Outlet temperature
b)
Power [kW]
Charging power
c)
Temperature [°C]
Bedrock temperature
Borehole wall temperature
d)
Power [kW]
Discharging power
e)
Temperature [°C]
Bedrock temperature
Borehole wall temperature
f)
Power [MW]
Estimated power
Heat demand
Duration [h]

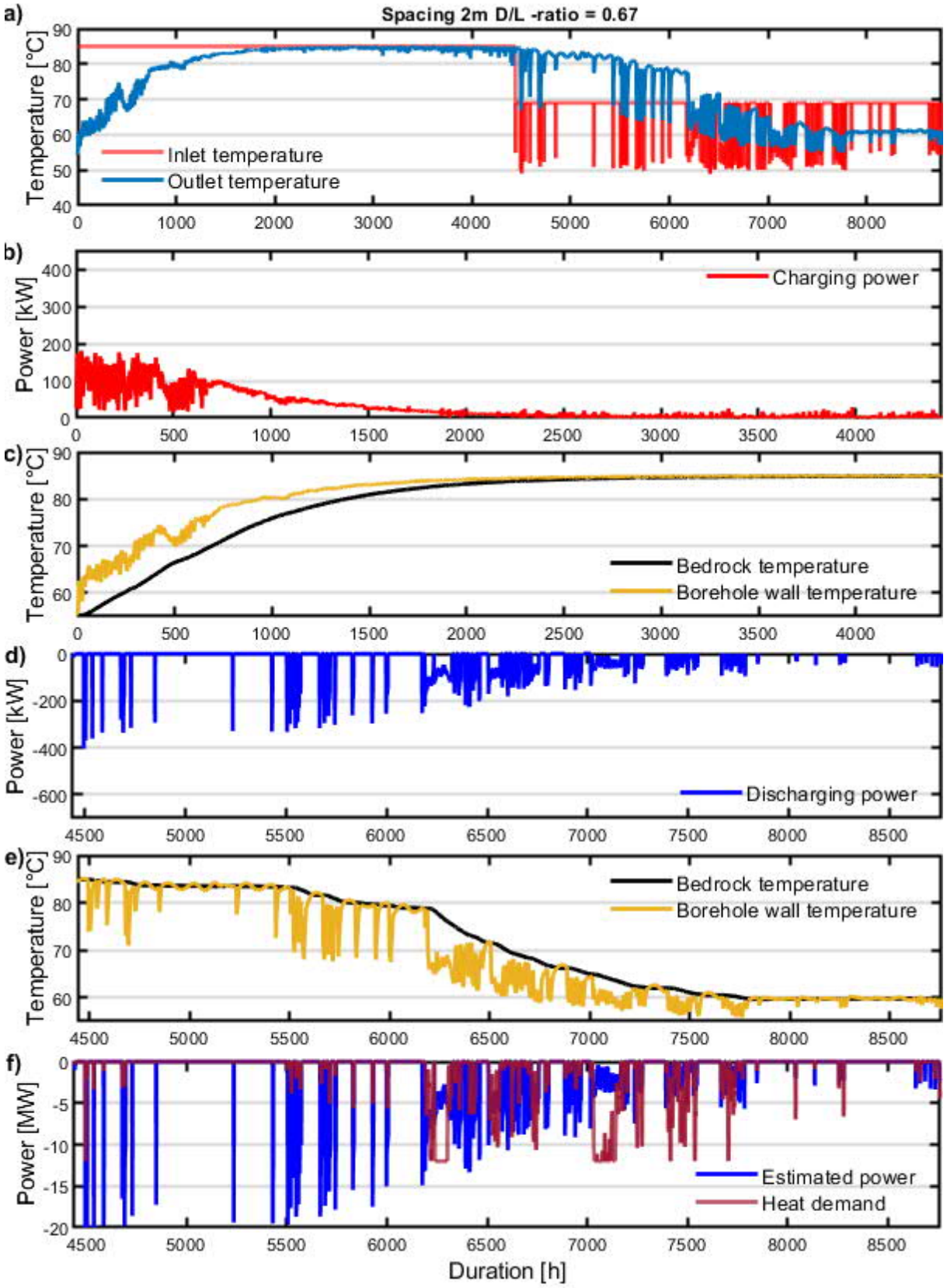
a)
Spacing 2m D/L -ratio = 0.67
Temperature [°C]
Inlet temperature
Outlet temperature
b)
Power [kW]
Charging power
c)
Temperature [°C]
Bedrock temperature
Borehole wall temperature
d)
Power [kW]
Discharging power
e)
Temperature [°C]
Bedrock temperature
Borehole wall temperature
f)
Power [MW]
Estimated power
Heat demand
Duration [h]

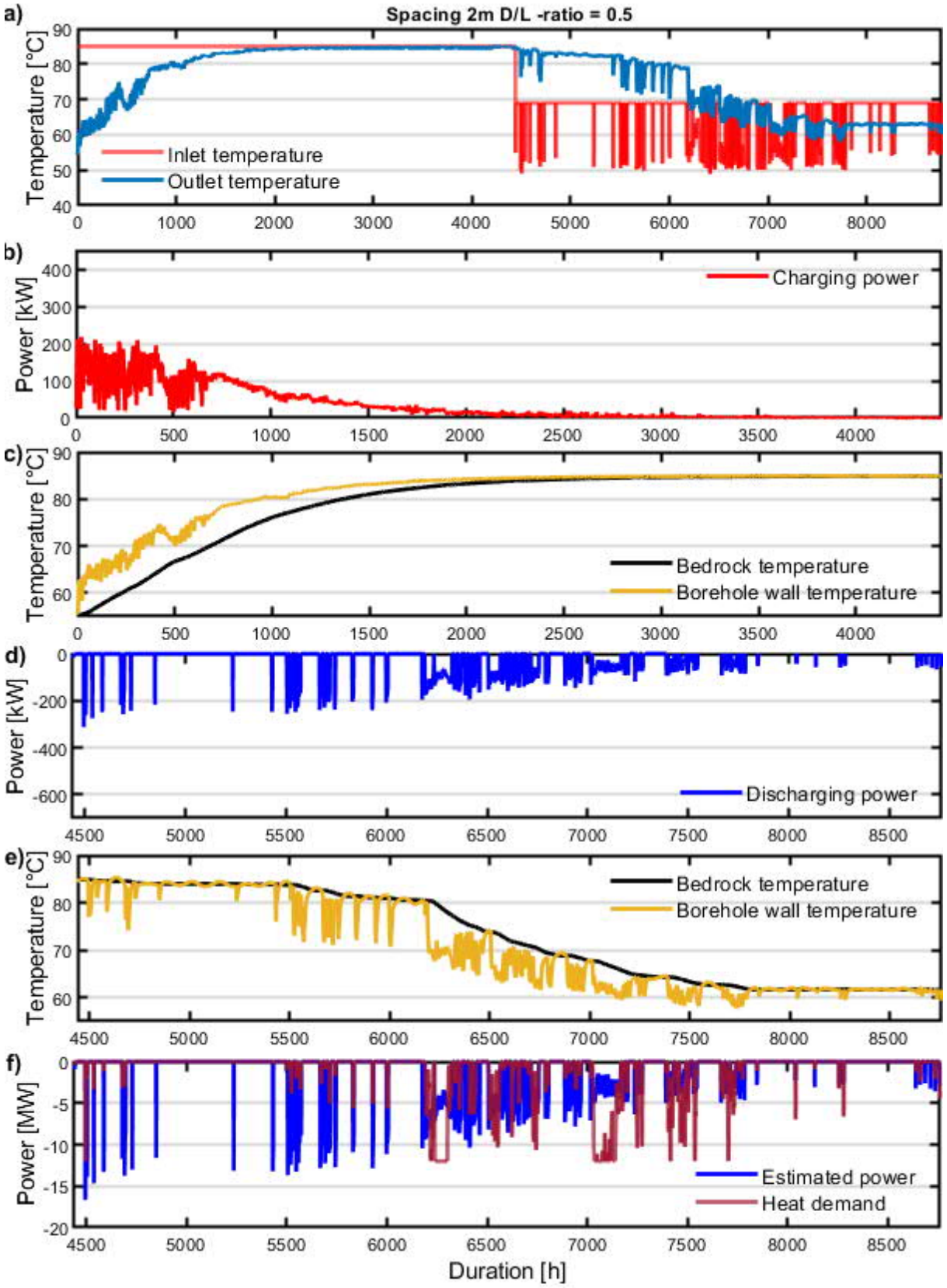
a)
Spacing 2m D/L -ratio = 0.5
Temperature [°C]
Inlet temperature
Outlet temperature
b)
Power [kW]
Charging power
c)
Temperature [°C]
Bedrock temperature
Borehole wall temperature
d)
Power [kW]
Discharging power
e)
Temperature [°C]
Bedrock temperature
Borehole wall temperature
f)
Power [MW]
Estimated power
Heat demand
Duration [h]

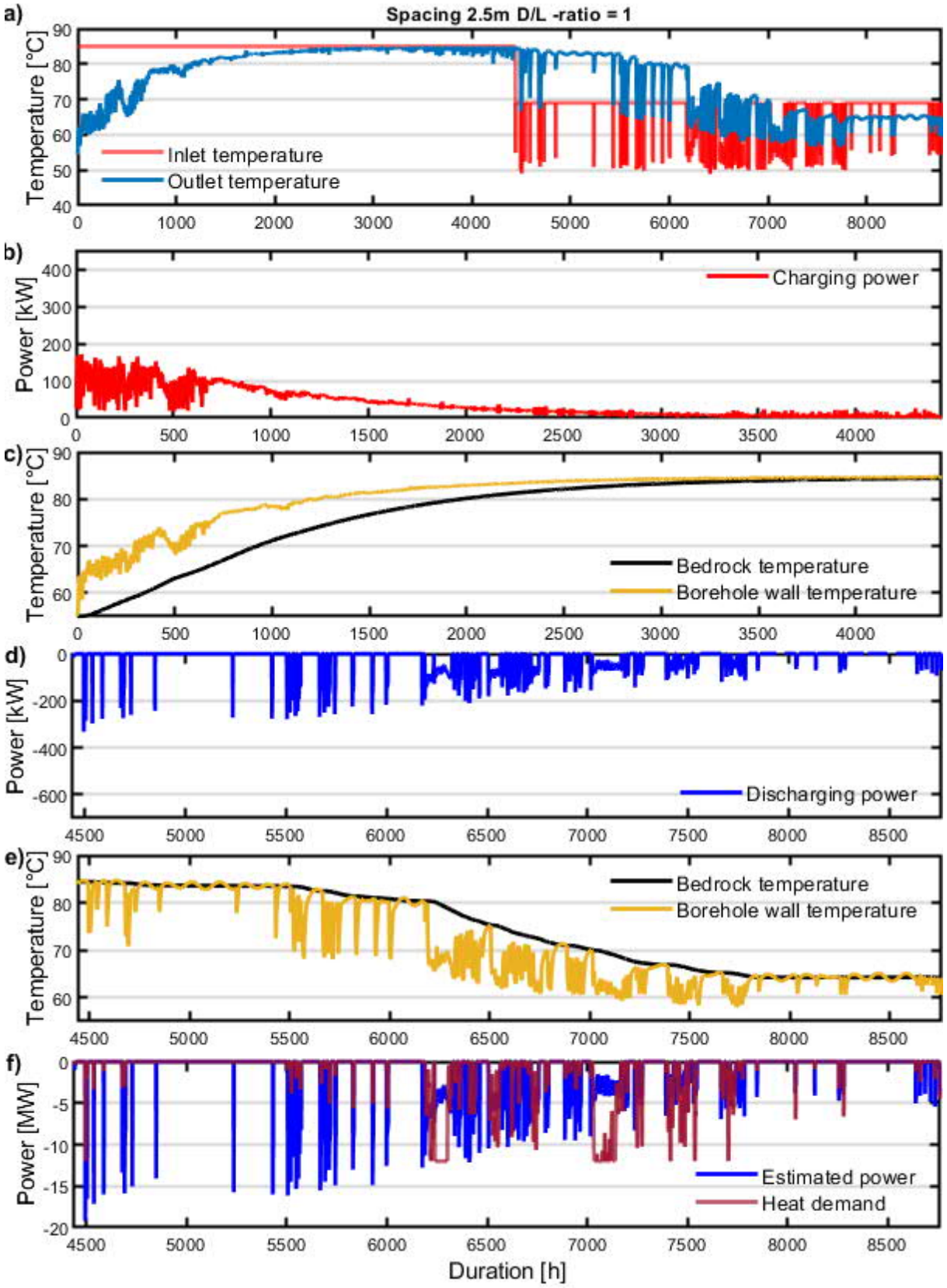
a)
Spacing 2.5m D/L -ratio = 1
Temperature [°C]
Inlet temperature
Outlet temperature
b)
Power [kW]
Charging power
c)
Temperature [°C]
Bedrock temperature
Borehole wall temperature
d)
Power [kW]
Discharging power
e)
Temperature [°C]
Bedrock temperature
Borehole wall temperature
f)
Power [MW]
Estimated power
Heat demand
Duration [h]

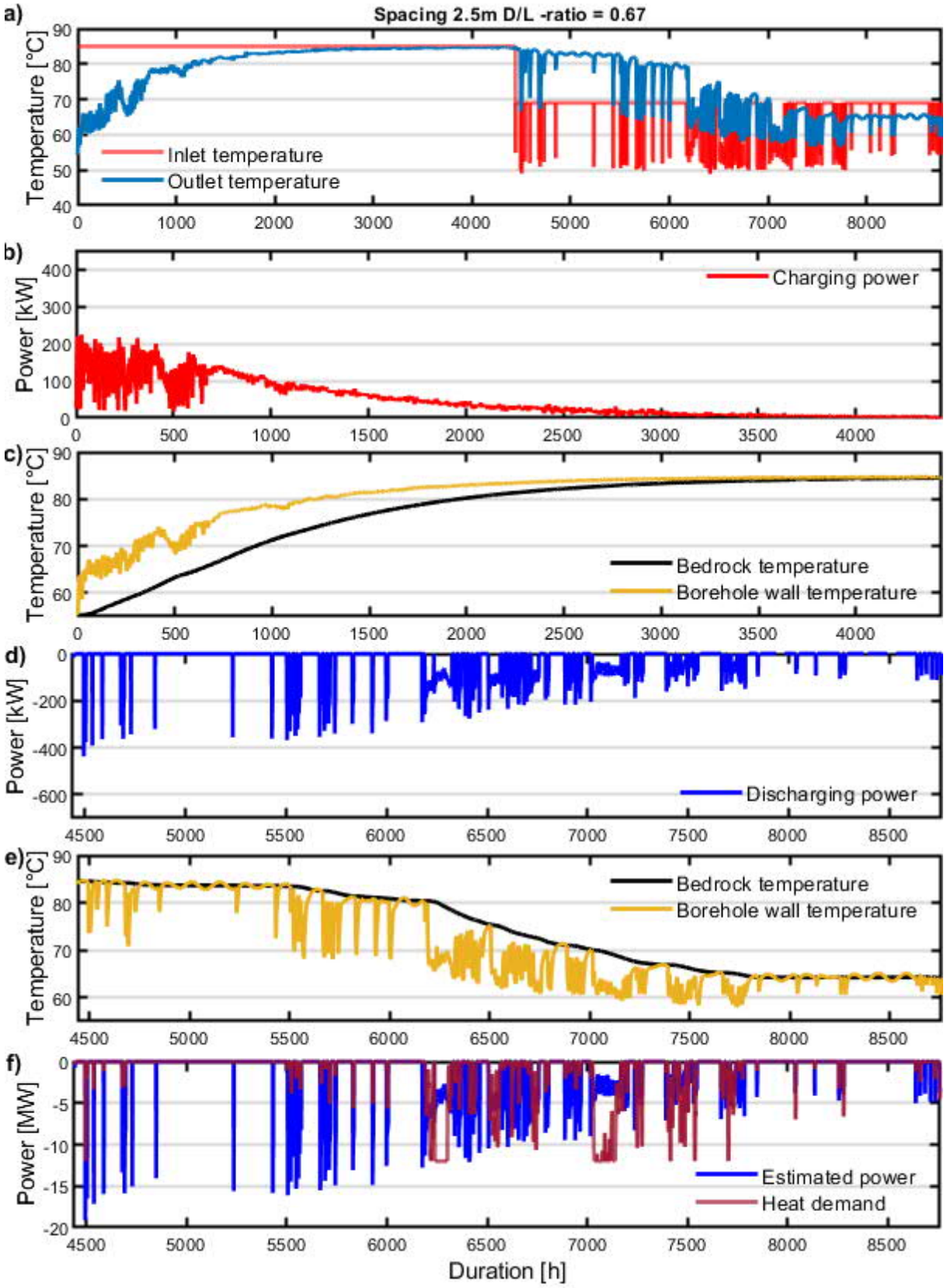
a)
Spacing 2.5m D/L -ratio = 0.67
Temperature [°C]
Inlet temperature
Outlet temperature
b)
Power [kW]
Charging power
c)
Temperature [°C]
Bedrock temperature
Borehole wall temperature
d)
Power [kW]
Discharging power
e)
Temperature [°C]
Bedrock temperature
Borehole wall temperature
f)
Power [MW]
Estimated power
Heat demand
Duration [h]

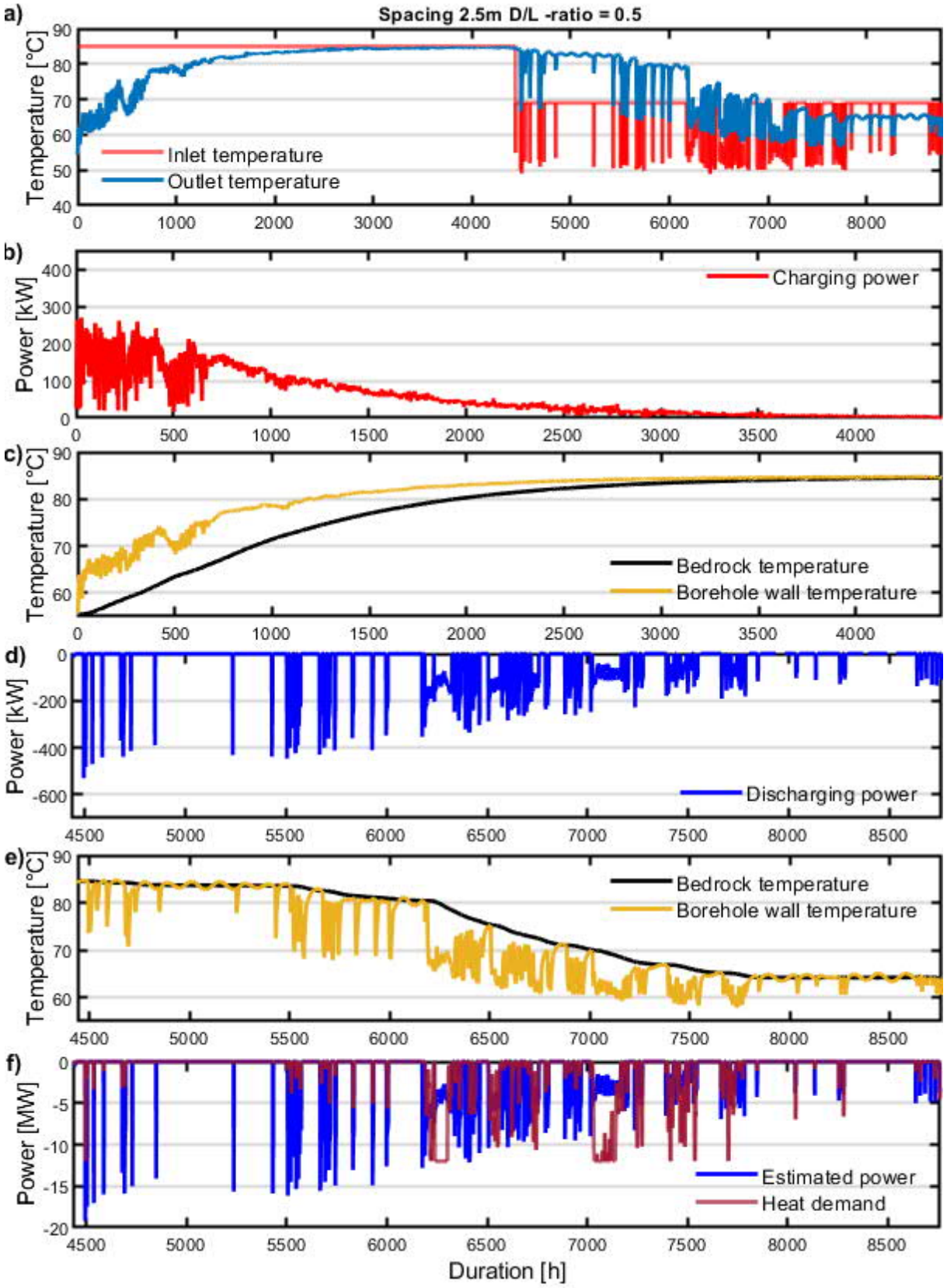
a)
Spacing 2.5m D/L -ratio = 0.5
Temperature [°C]
Inlet temperature
Outlet temperature
b)
Power [kW]
Charging power
c)
Temperature [°C]
Bedrock temperature
Borehole wall temperature
d)
Power [kW]
Discharging power
e)
Temperature [°C]
Bedrock temperature
Borehole wall temperature
f)
Power [MW]
Estimated power
Heat demand
Duration [h]

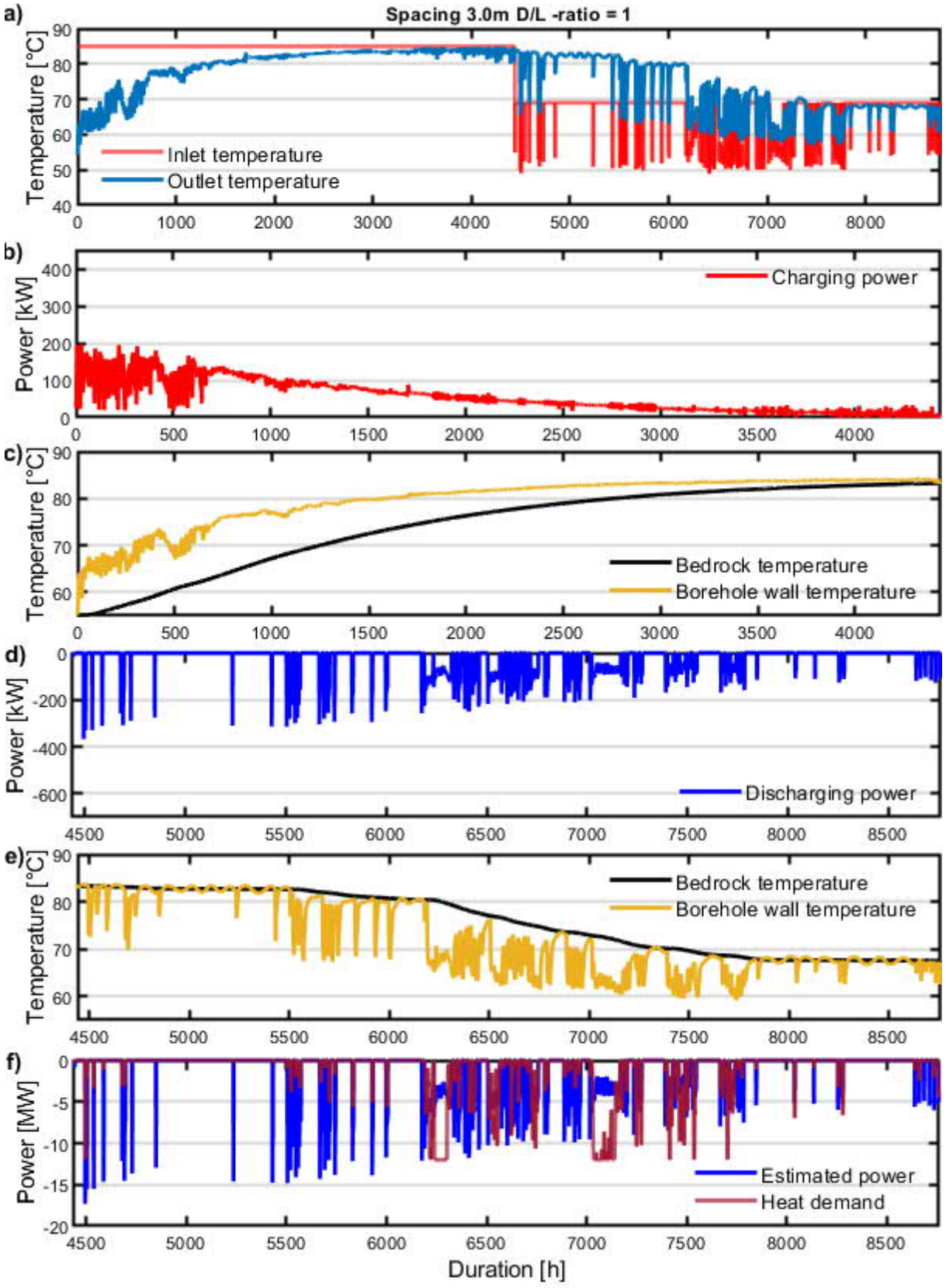
a)
Spacing 3.0m D/L -ratio = 1
Temperature [°C]
Inlet temperature
Outlet temperature
b)
Power [kW]
Charging power
c)
Temperature [°C]
Bedrock temperature
Borehole wall temperature
d)
Power [kW]
Discharging power
e)
Temperature [°C]
Bedrock temperature
Borehole wall temperature
f)
Power [MW]
Estimated power
Heat demand
Duration [h]

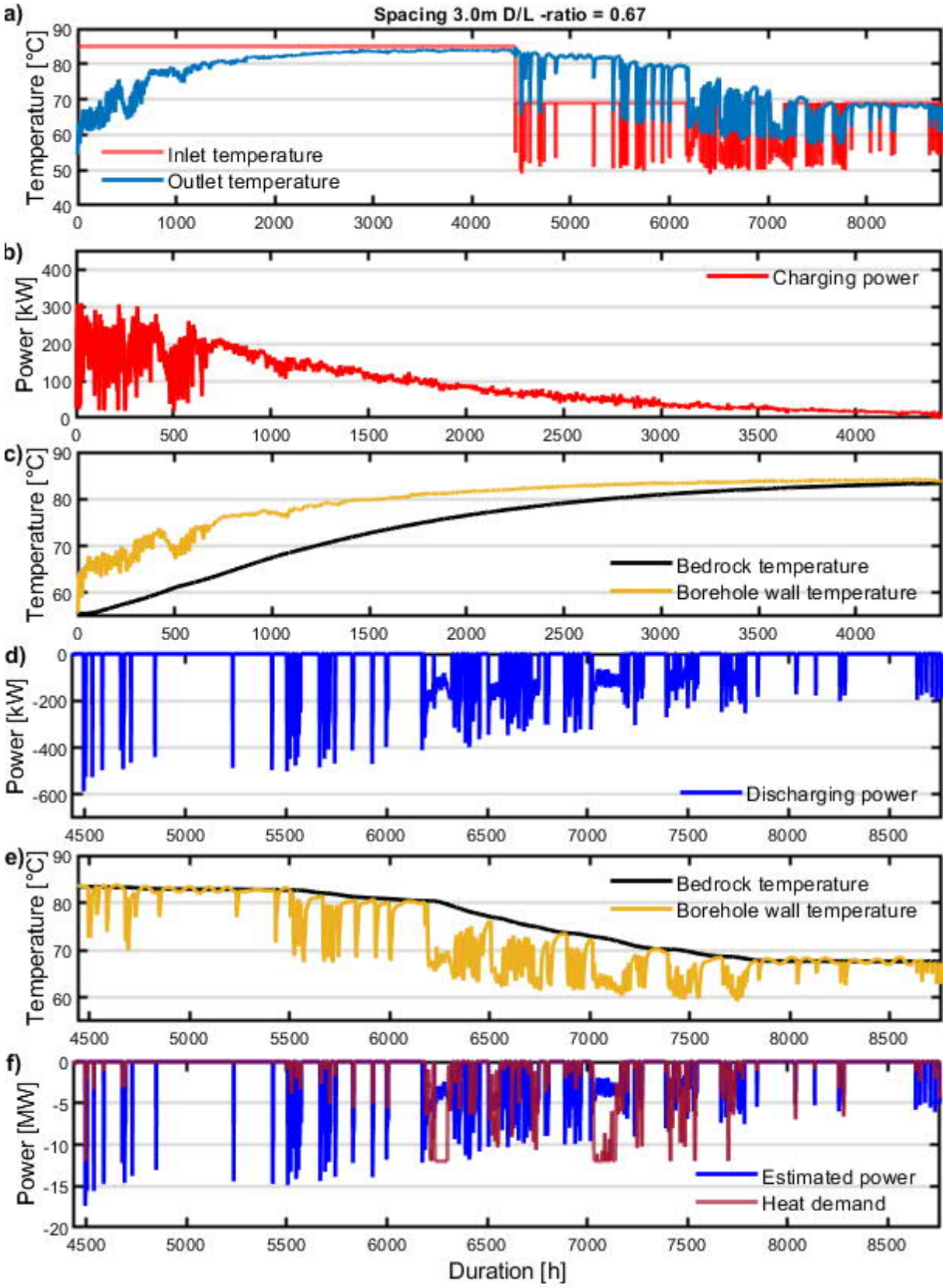
a)
Spacing 3.0m D/L -ratio = 0.67
Temperature [°C]
Inlet temperature
Outlet temperature
b)
Power [kW]
Charging power
c)
Temperature [°C]
Bedrock temperature
Borehole wall temperature
d)
Power [kW]
Discharging power
e)
Temperature [°C]
Bedrock temperature
Borehole wall temperature
f)
Power [MW]
Estimated power
Heat demand
Duration [h]

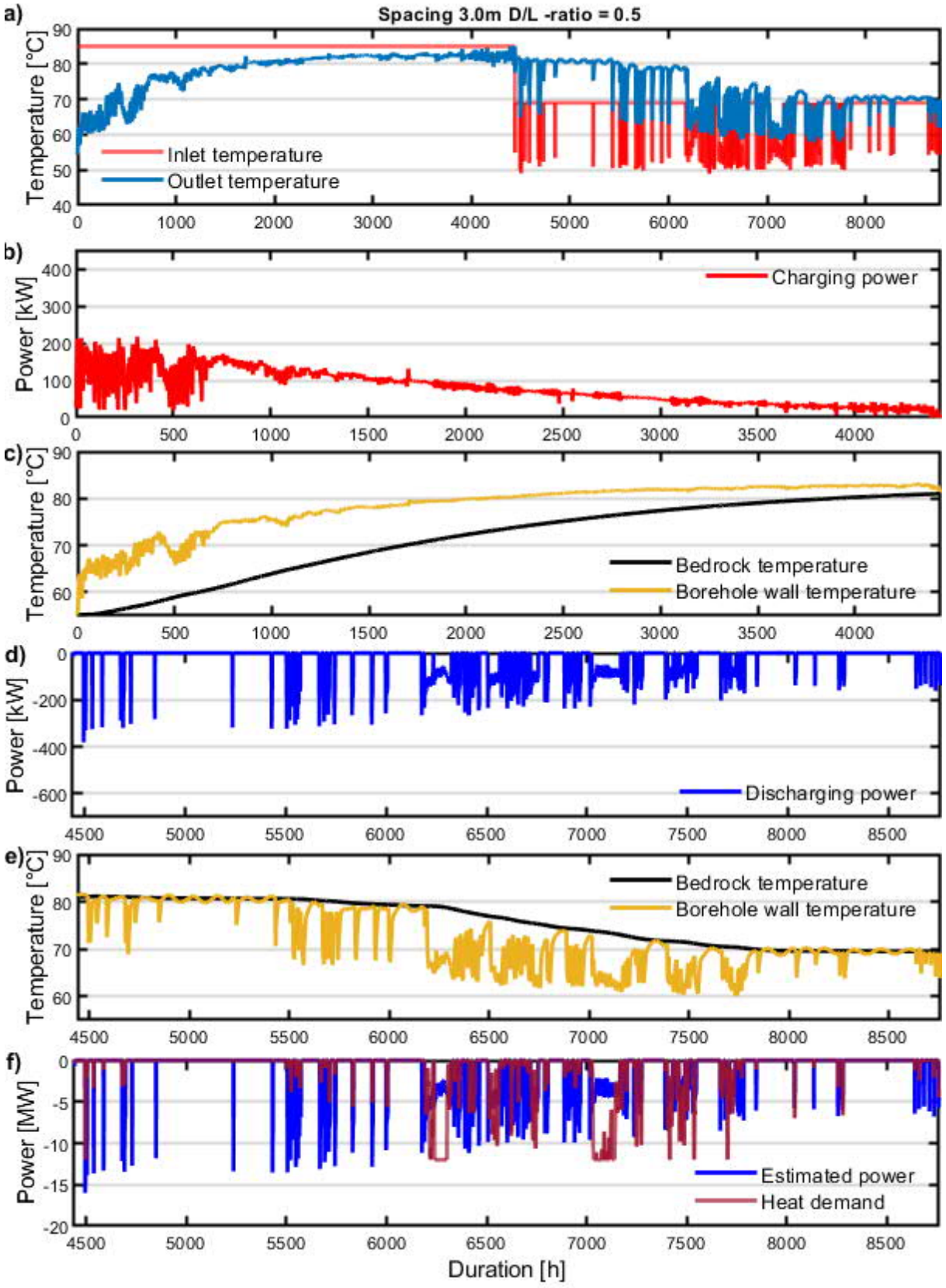
a)
Spacing 3.0m D/L -ratio = 0.5
Temperature [°C]
Inlet temperature
Outlet temperature
b)
Power [kW]
Charging power
c)
Temperature [°C]
Bedrock temperature
Borehole wall temperature
d)
Power [kW]
Discharging power
e)
Temperature [°C]
Bedrock temperature
Borehole wall temperature
f)
Power [MW]
Estimated power
Heat demand
Duration [h]

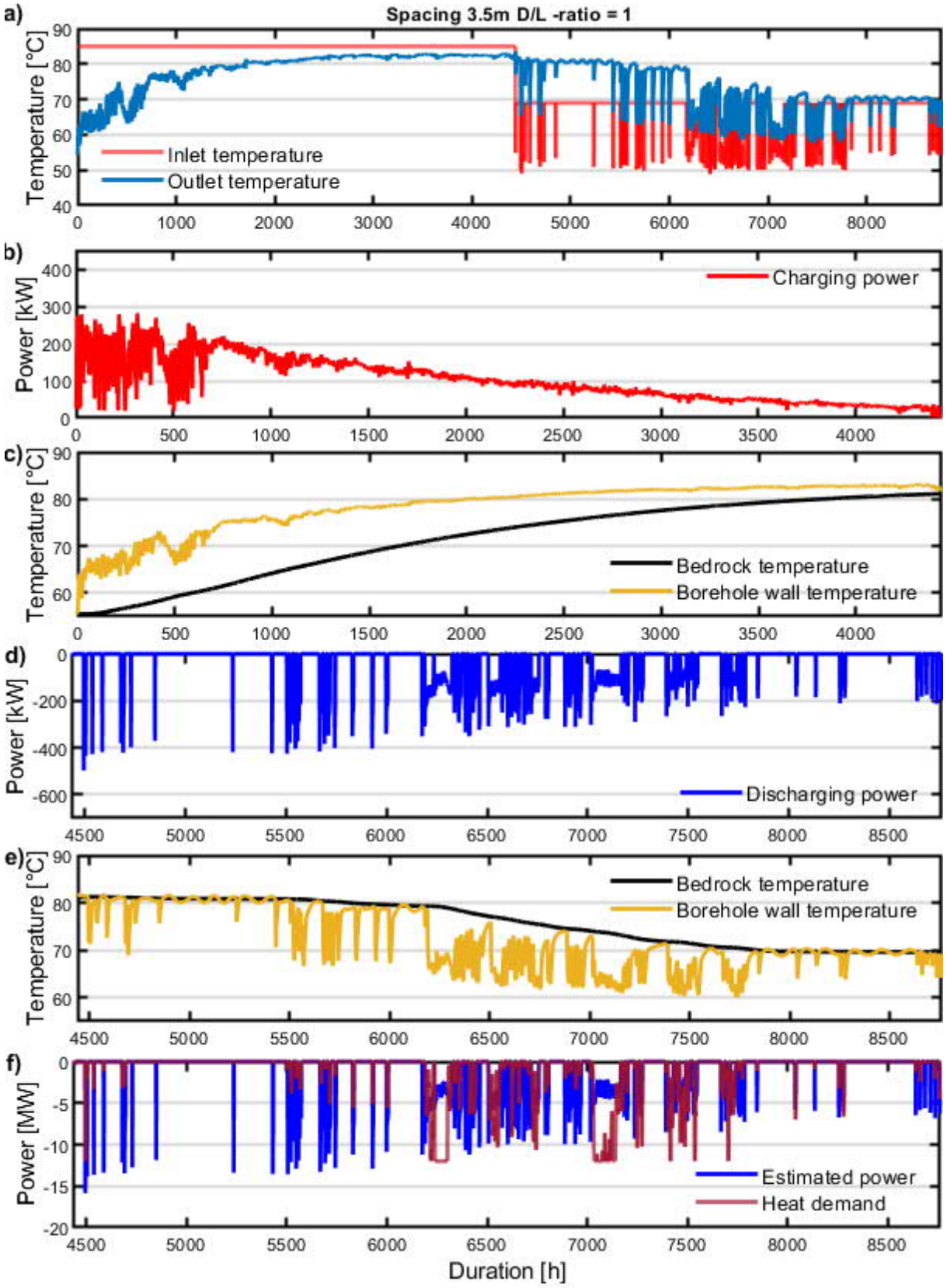
a)
Spacing 3.5m D/L -ratio = 1
Temperature [°C]
Inlet temperature
Outlet temperature
b)
Power [kW]
Charging power
c)
Temperature [°C]
Bedrock temperature
Borehole wall temperature
d)
Power [kW]
Discharging power
e)
Temperature [°C]
Bedrock temperature
Borehole wall temperature
f)
Power [MW]
Estimated power
Heat demand
Duration [h]

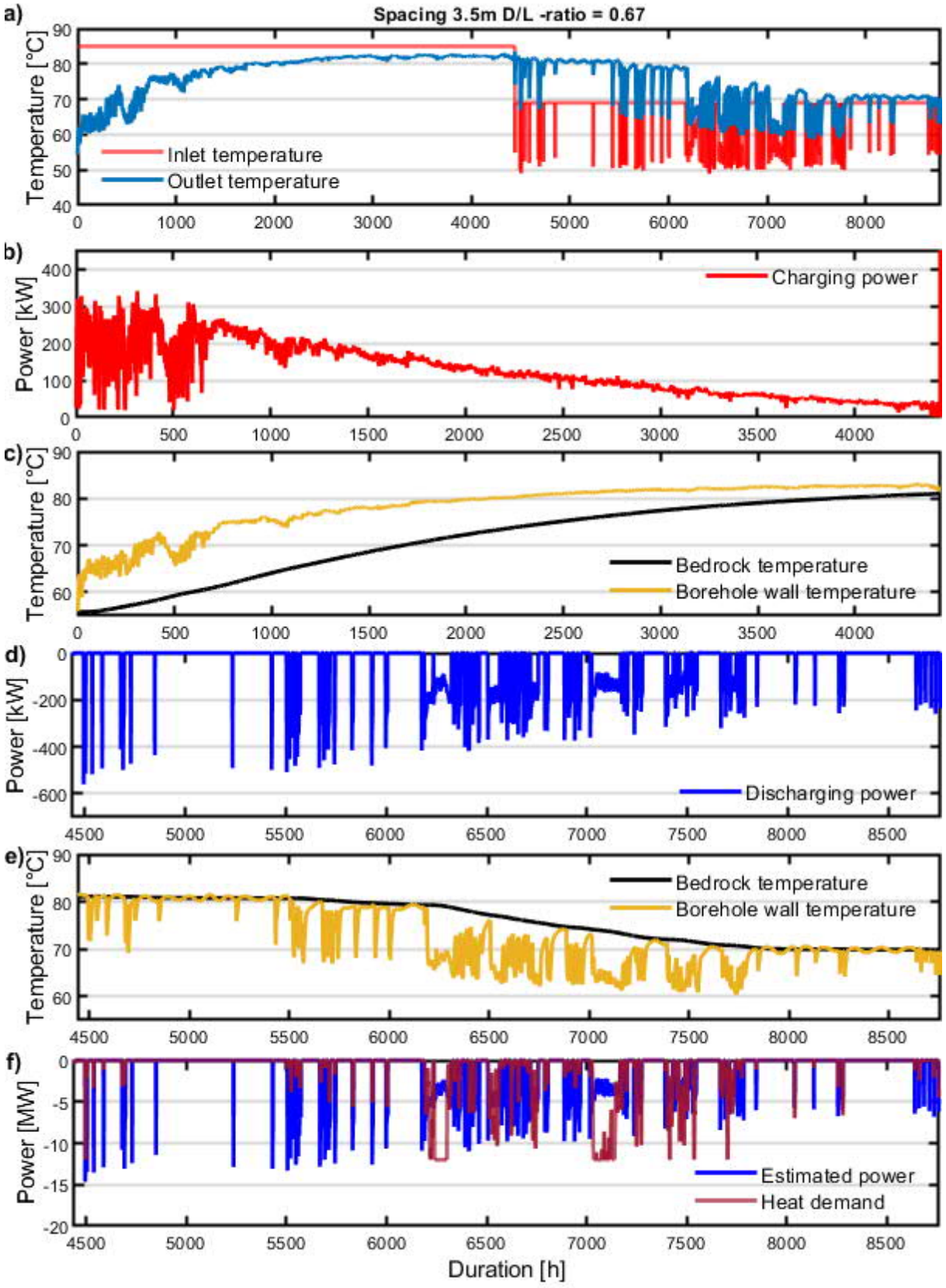
a)
Spacing 3.5m D/L -ratio = 0.67
Temperature [°C]
Inlet temperature
Outlet temperature
b)
Power [kW]
Charging power
c)
Temperature [°C]
Bedrock temperature
Borehole wall temperature
d)
Power [kW]
Discharging power
e)
Temperature [°C]
Bedrock temperature
Borehole wall temperature
f)
Power [MW]
Estimated power
Heat demand
Duration [h]

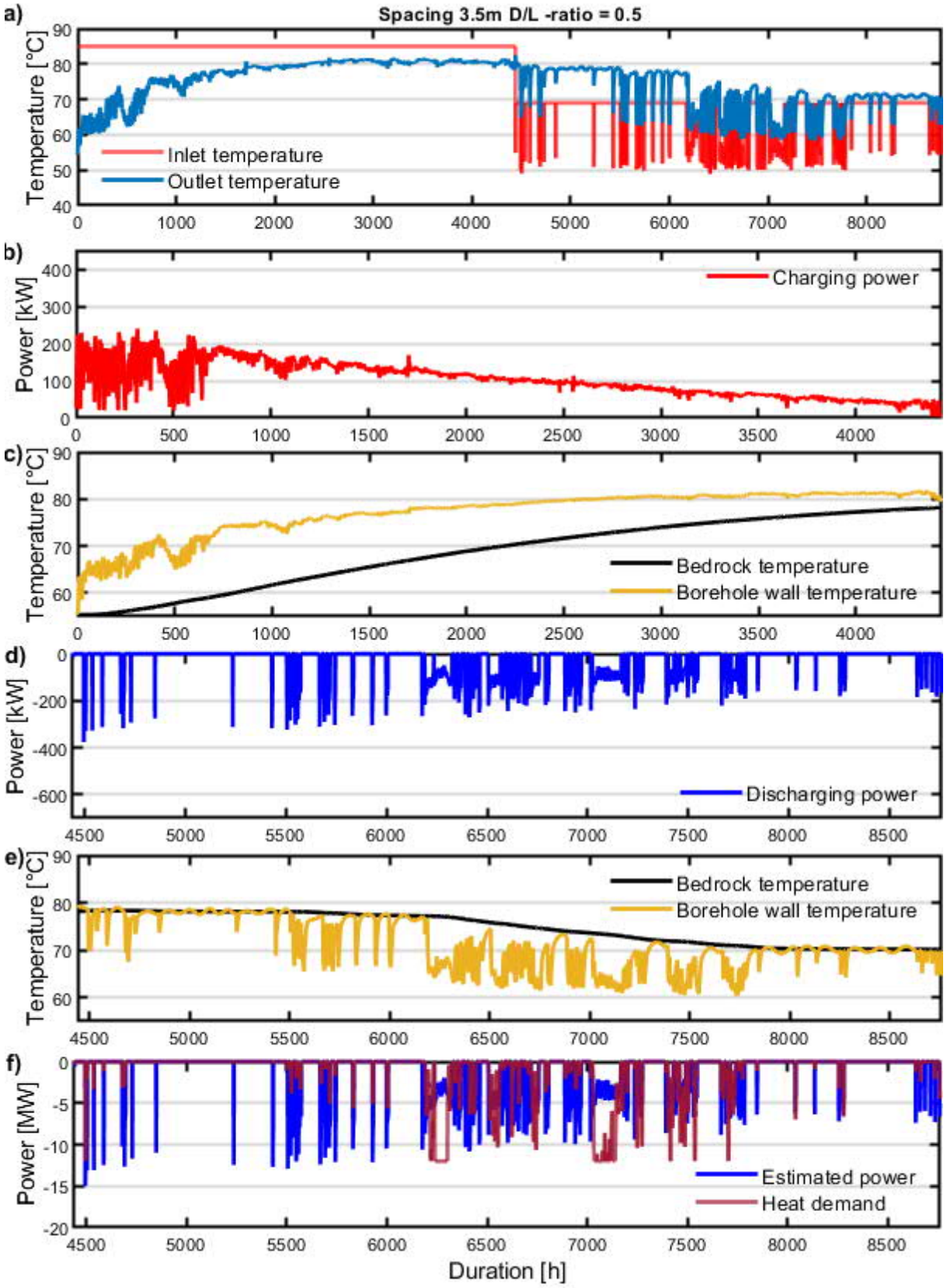
a)
Spacing 3.5m D/L -ratio = 0.5
Temperature [°C]
Inlet temperature
Outlet temperature
b)
Power [kW]
Charging power
c)
Temperature [°C]
Bedrock temperature
Borehole wall temperature
d)
Power [kW]
Discharging power
e)
Temperature [°C]
Bedrock temperature
Borehole wall temperature
f)
Power [MW]
Estimated power
Heat demand
Duration [h]

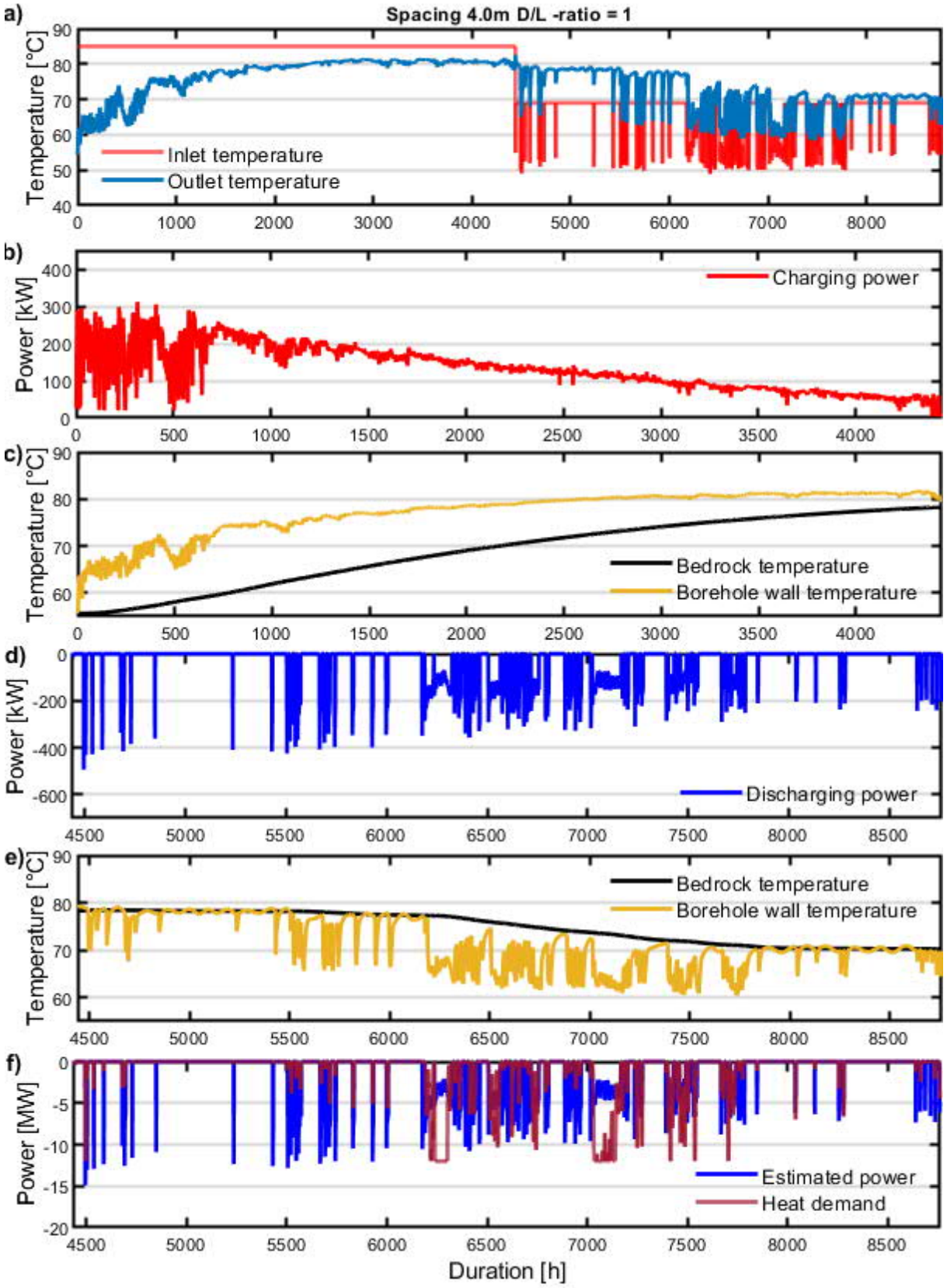
a)
Spacing 4.0m D/L -ratio = 1
Temperature [°C]
Inlet temperature
Outlet temperature
b)
Power [kW]
Charging power
c)
Temperature [°C]
Bedrock temperature
Borehole wall temperature
d)
Power [kW]
Discharging power
e)
Temperature [°C]
Bedrock temperature
Borehole wall temperature
f)
Power [MW]
Estimated power
Heat demand
Duration [h]

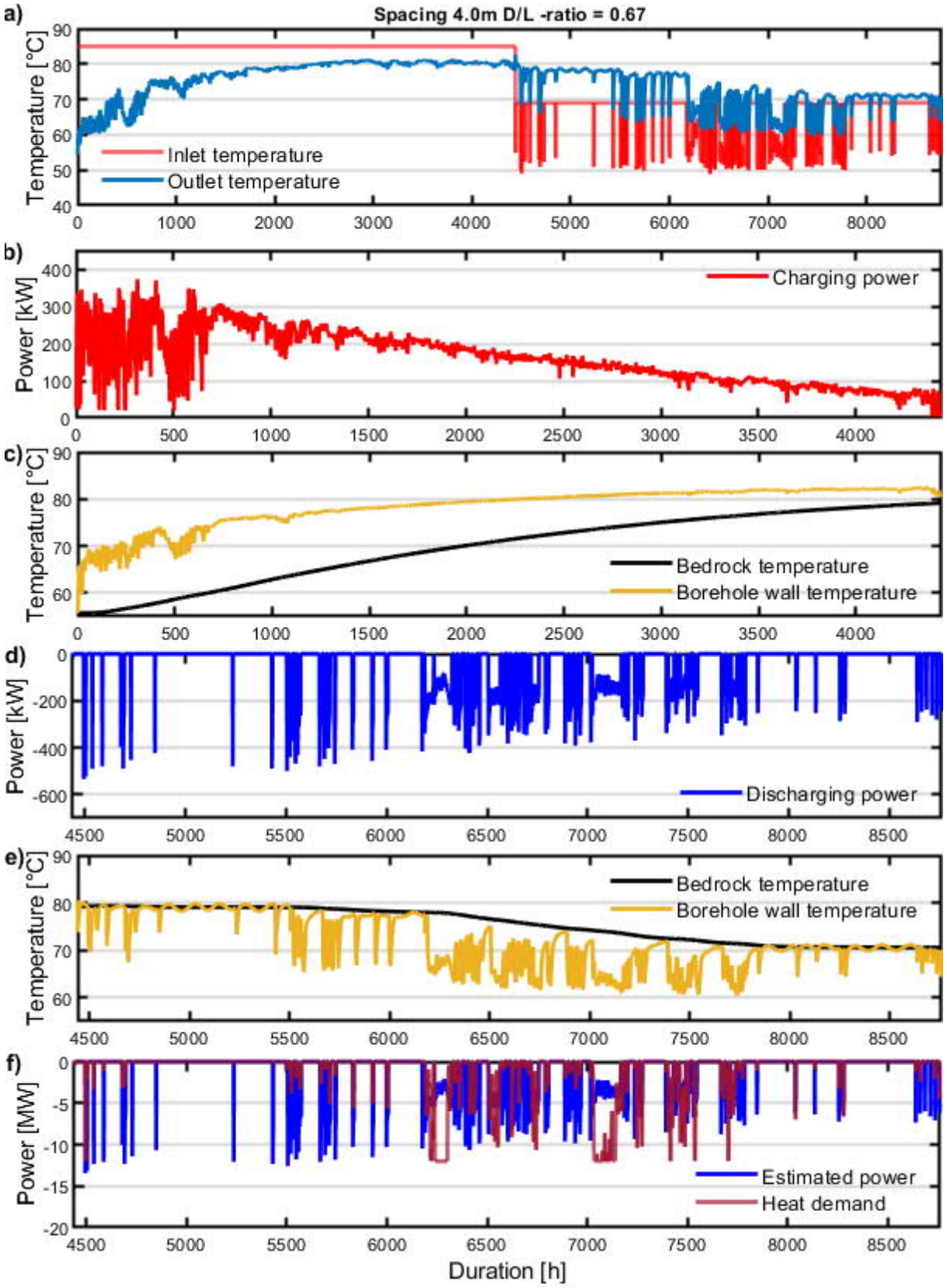
a)
Spacing 4.0m D/L -ratio = 0.67
Temperature [°C]
Inlet temperature
Outlet temperature
b)
Power [kW]
Charging power
c)
Temperature [°C]
Bedrock temperature
Borehole wall temperature
d)
Power [kW]
Discharging power
e)
Temperature [°C]
Bedrock temperature
Borehole wall temperature
f)
Power [MW]
Estimated power
Heat demand
Duration [h]

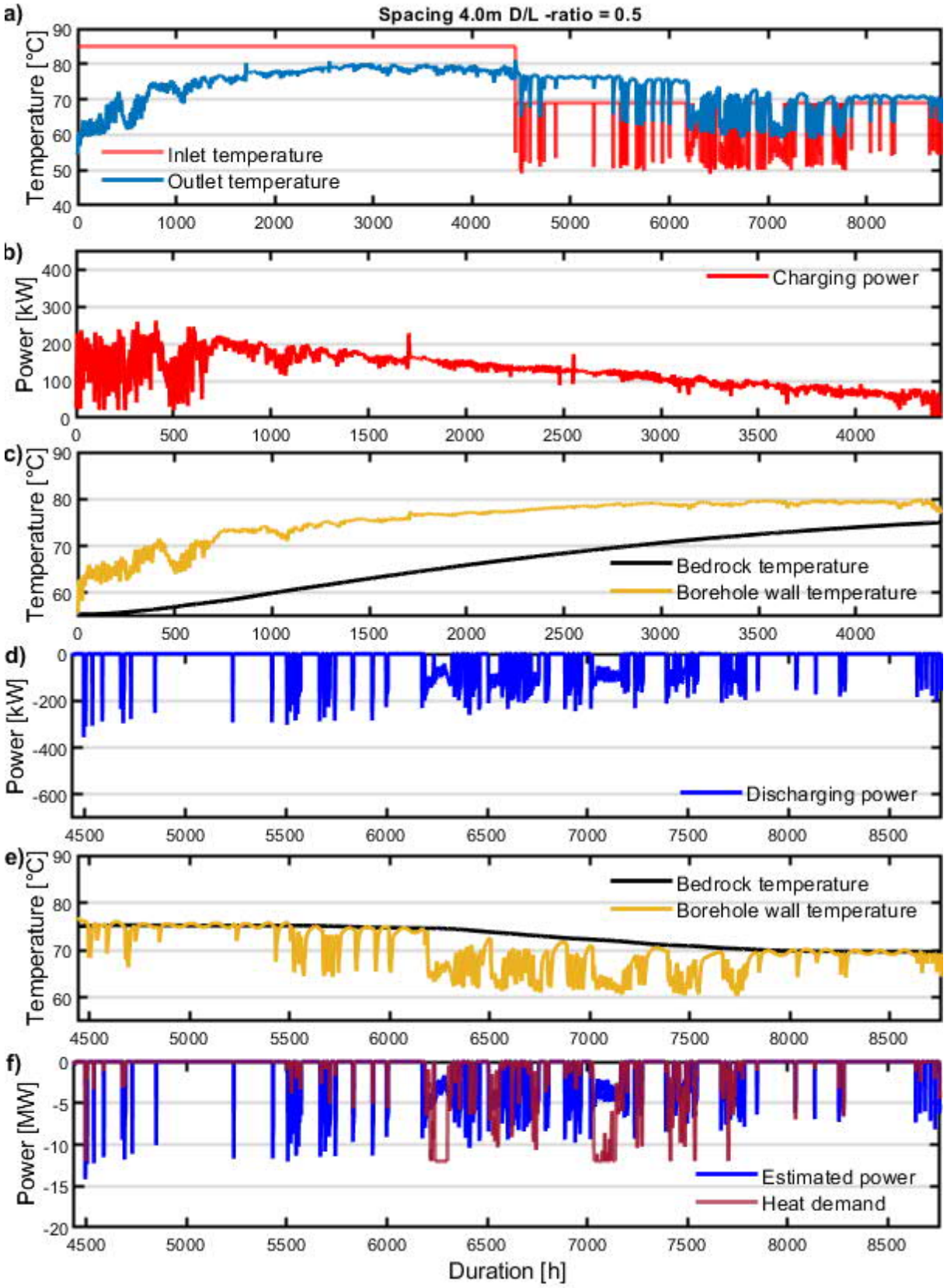
a)
Spacing 4.0m D/L -ratio = 0.5
Temperature [°C]
Inlet temperature
Outlet temperature
b)
Power [kW]
Charging power
c)
Temperature [°C]
Bedrock temperature
Borehole wall temperature
d)
Power [kW]
Discharging power
e)
Temperature [°C]
Bedrock temperature
Borehole wall temperature
f)
Power [MW]
Estimated power
Heat demand
Duration [h]

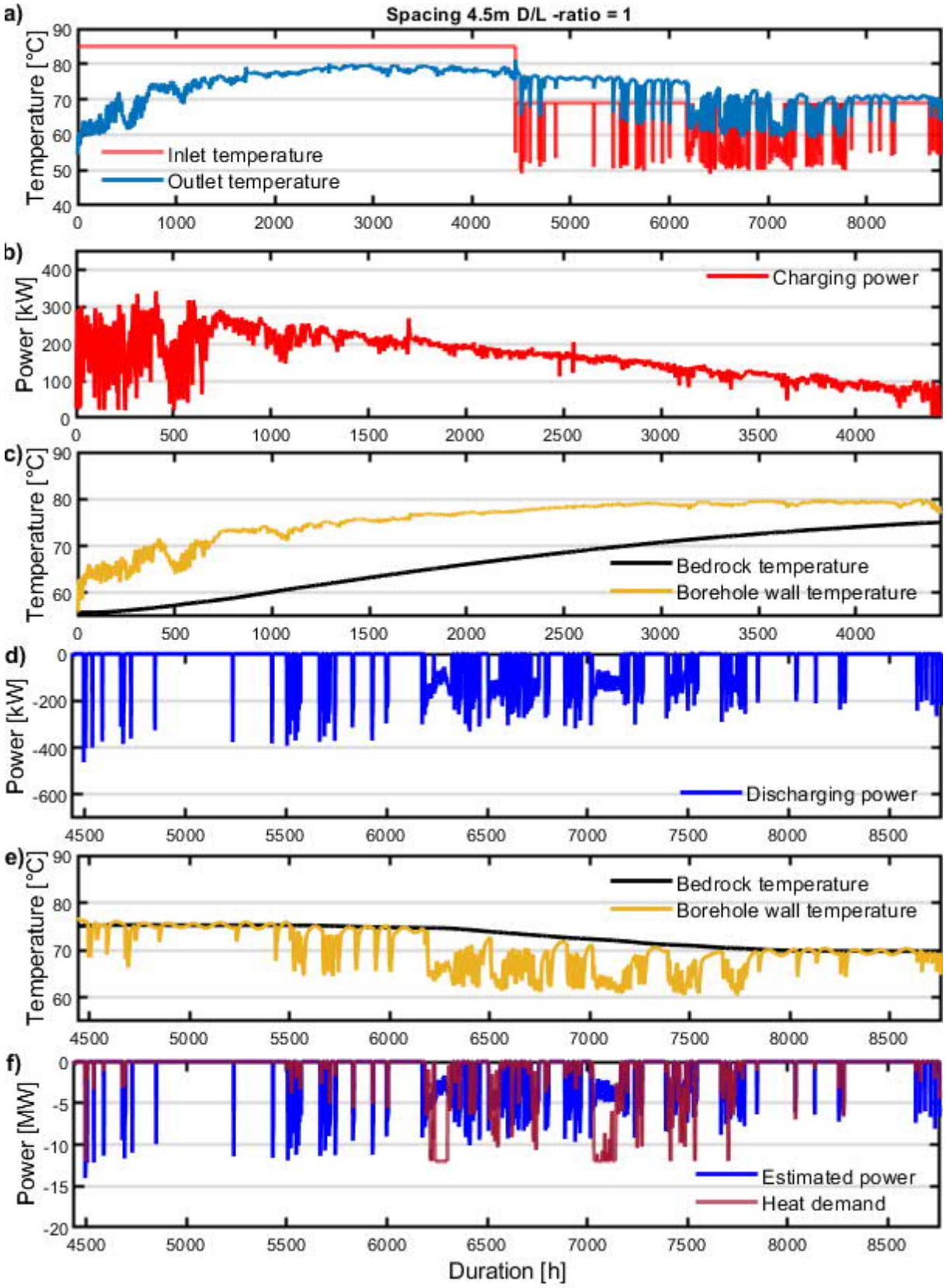
a)
Spacing 4.5m D/L -ratio = 1
Temperature [°C]
Inlet temperature
Outlet temperature
b)
Power [kW]
Charging power
c)
Temperature [°C]
Bedrock temperature
Borehole wall temperature
d)
Power [kW]
Discharging power
e)
Temperature [°C]
Bedrock temperature
Borehole wall temperature
f)
Power [MW]
Estimated power
Heat demand
Duration [h]

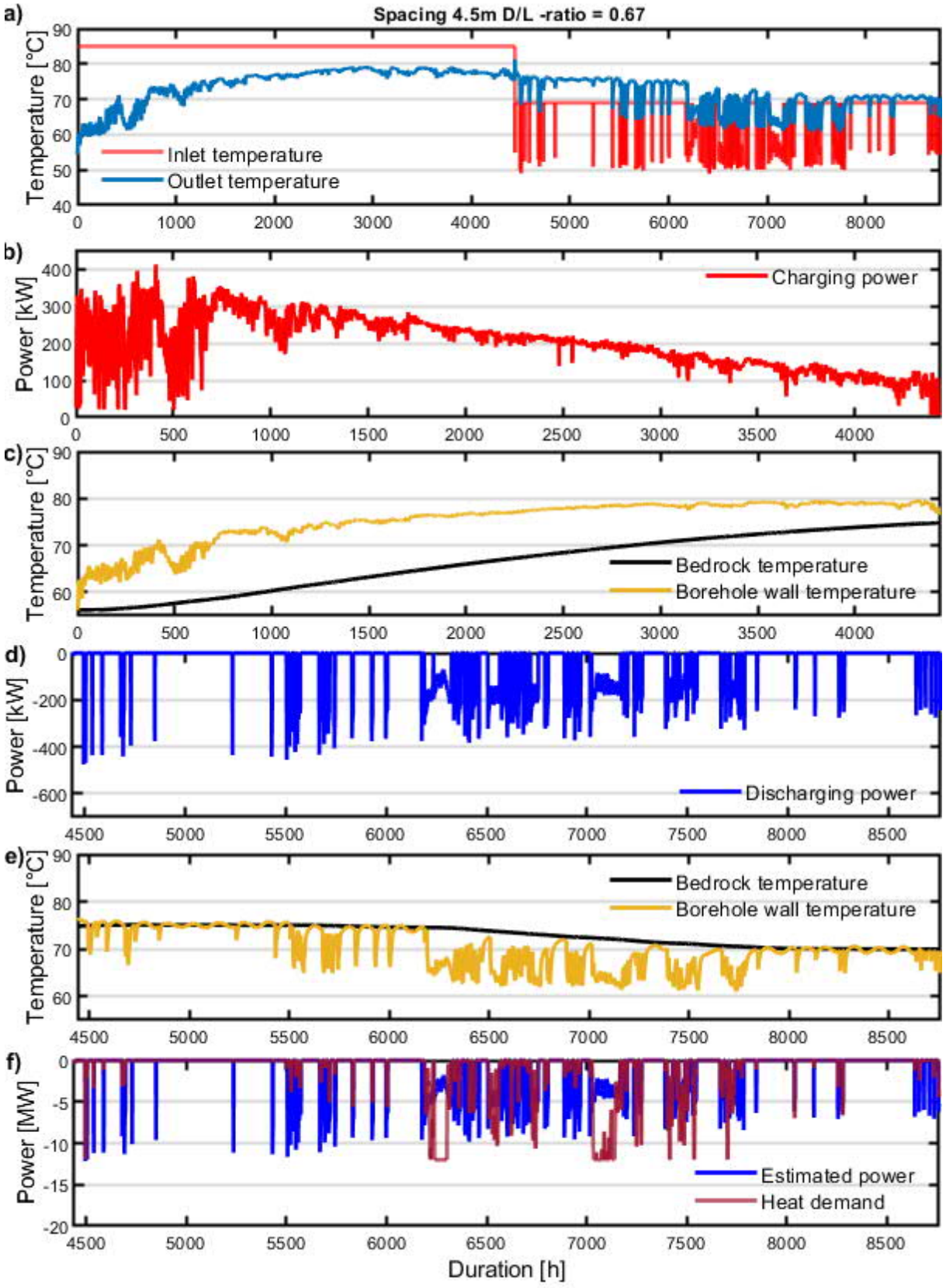
a)
Spacing 4.5m D/L -ratio = 0.67
Temperature [°C]
Inlet temperature
Outlet temperature
b)
Power [kW]
Charging power
c)
Temperature [°C]
Bedrock temperature
Borehole wall temperature
d)
Power [kW]
Discharging power
e)
Temperature [°C]
Bedrock temperature
Borehole wall temperature
f)
Power [MW]
Estimated power
Heat demand
Duration [h]

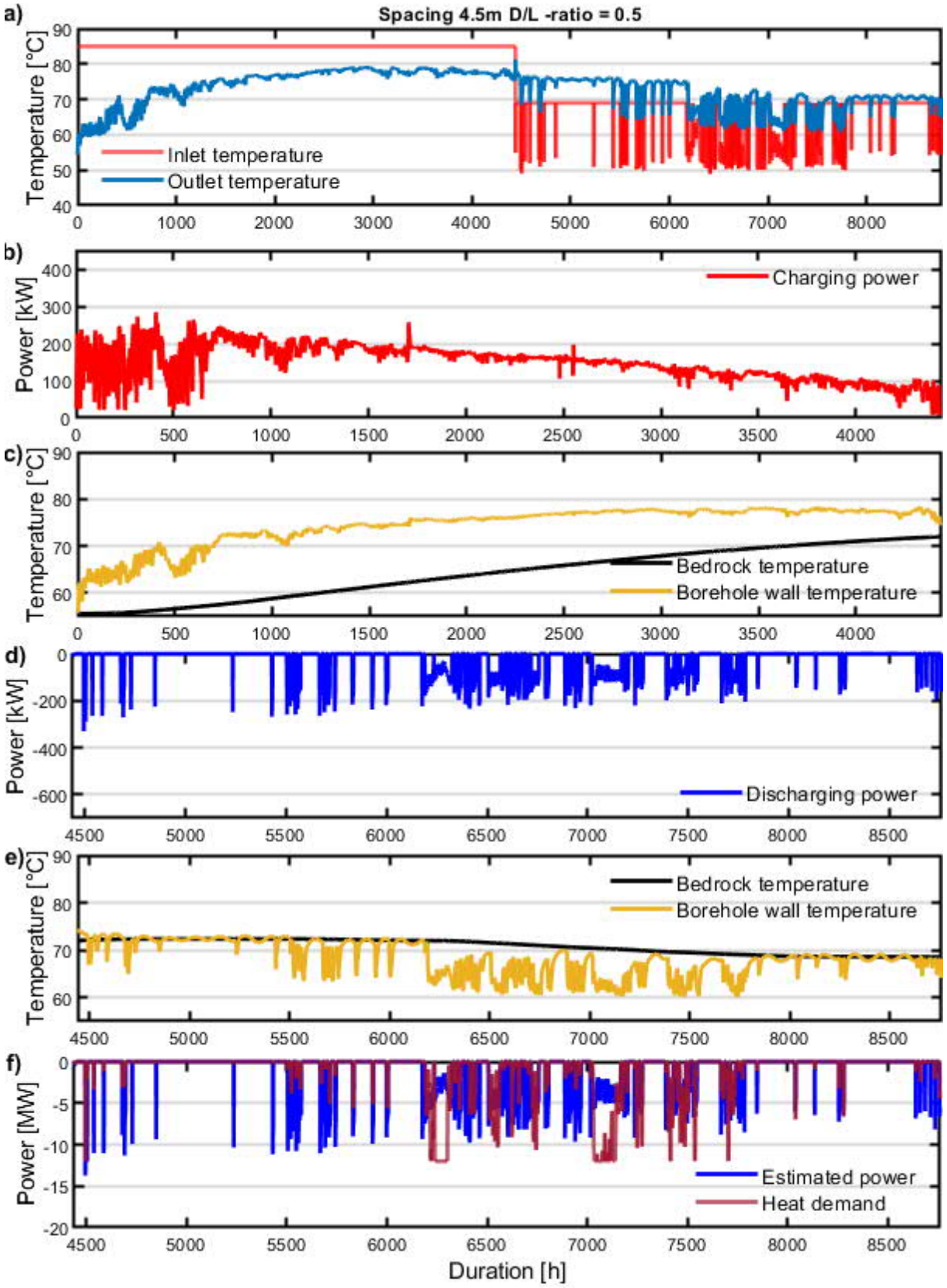
a)
Spacing 4.5m D/L -ratio = 0.5
Temperature [°C]
Inlet temperature
Outlet temperature
b)
Power [kW]
Charging power
c)
Temperature [°C]
Bedrock temperature
Borehole wall temperature
d)
Power [kW]
Discharging power
e)
Temperature [°C]
Bedrock temperature
Borehole wall temperature
f)
Power [MW]
Estimated power
Heat demand
Duration [h]

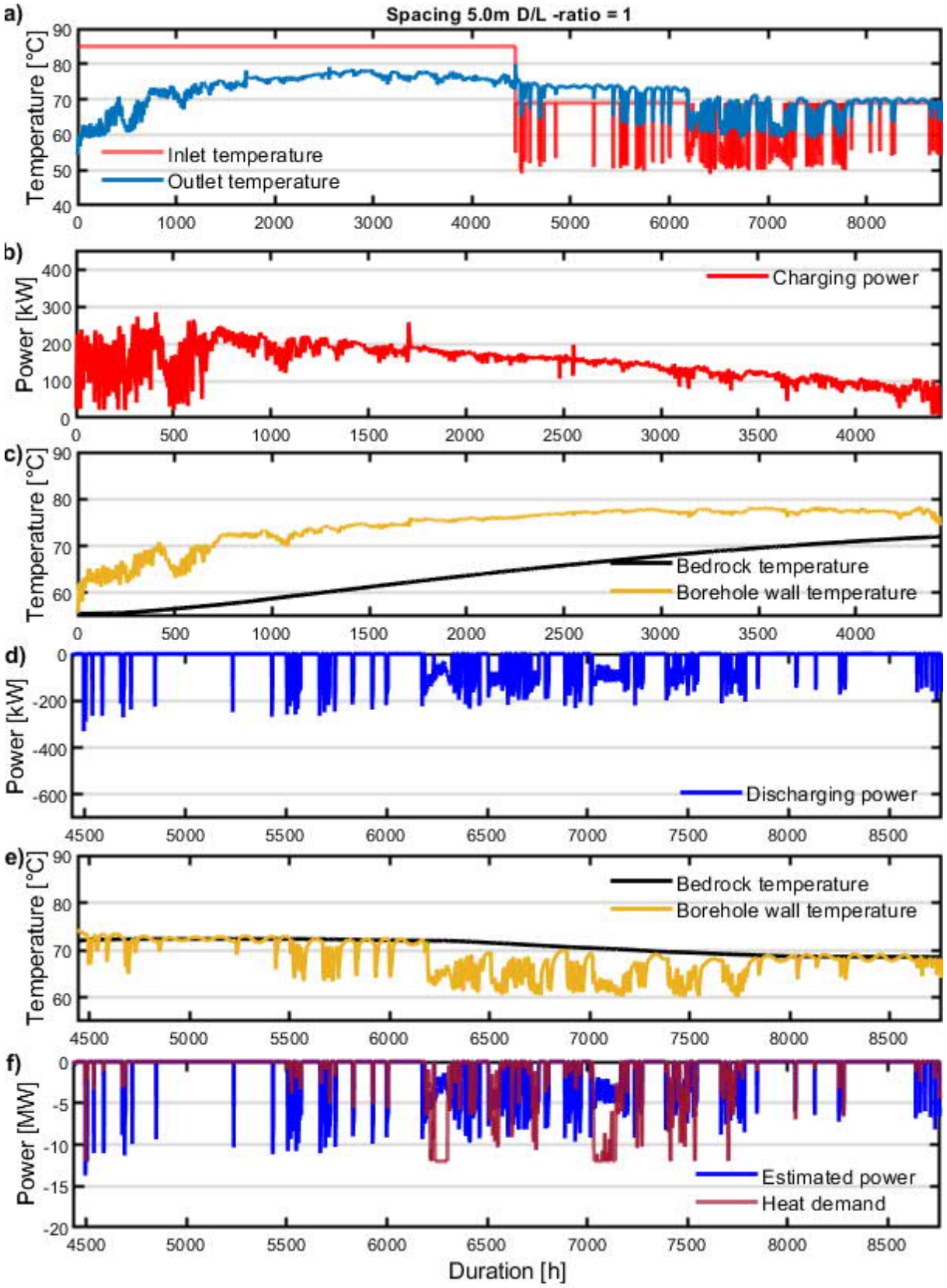
a)
Spacing 5.0m D/L -ratio = 1
Temperature [°C]
Inlet temperature
Outlet temperature
b)
Power [kW]
Charging power
c)
Temperature [°C]
Bedrock temperature
Borehole wall temperature
d)
Power [kW]
Discharging power
e)
Temperature [°C]
Bedrock temperature
Borehole wall temperature
f)
Power [MW]
Estimated power
Heat demand
Duration [h]

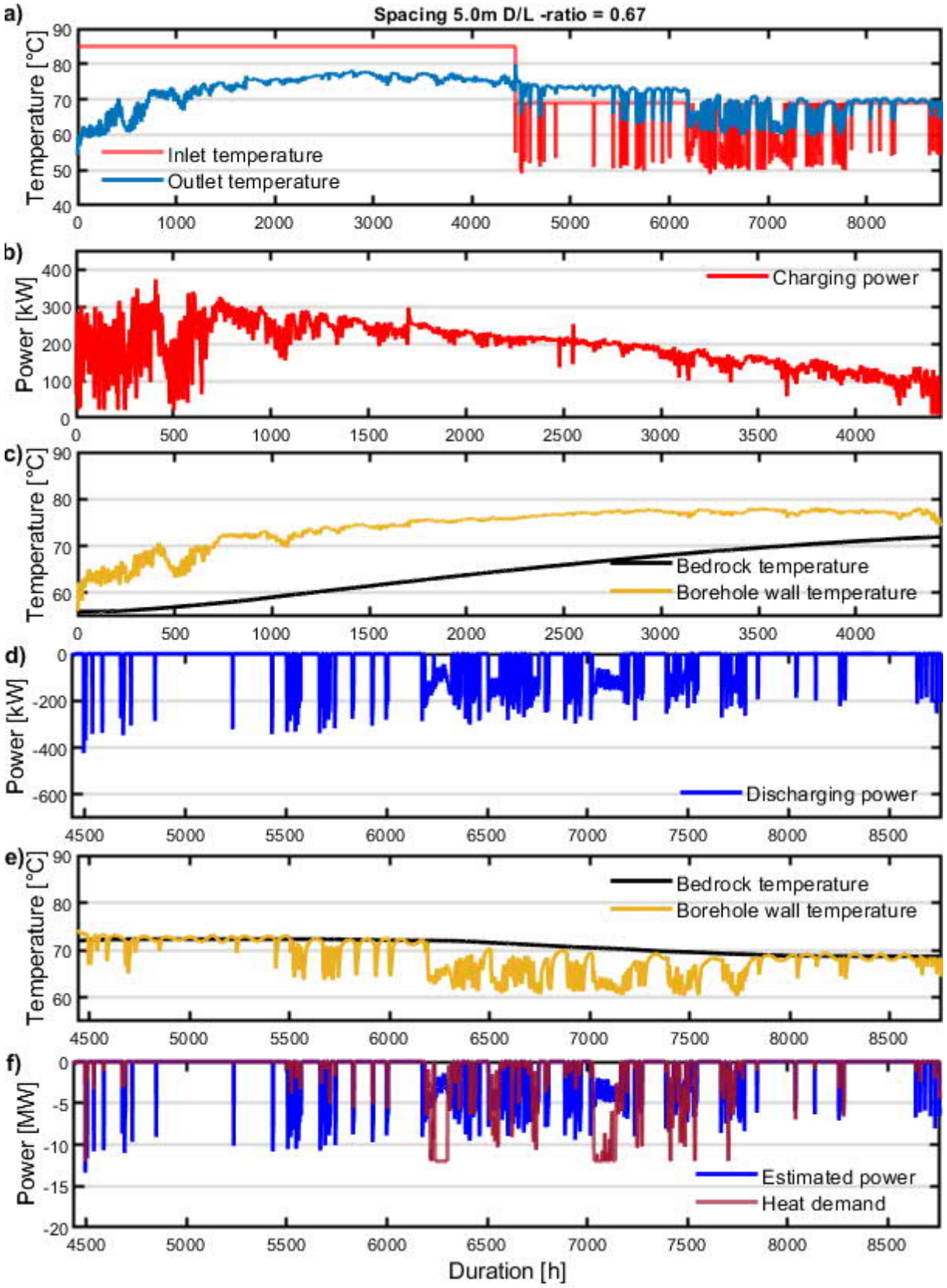
a)
Spacing 5.0m D/L -ratio = 0.67
Temperature [°C]
Inlet temperature
Outlet temperature
b)
Power [kW]
Charging power
c)
Temperature [°C]
Bedrock temperature
Borehole wall temperature
d)
Power [kW]
Discharging power
e)
Temperature [°C]
Bedrock temperature
Borehole wall temperature
f)
Power [MW]
Estimated power
Heat demand
Duration [h]

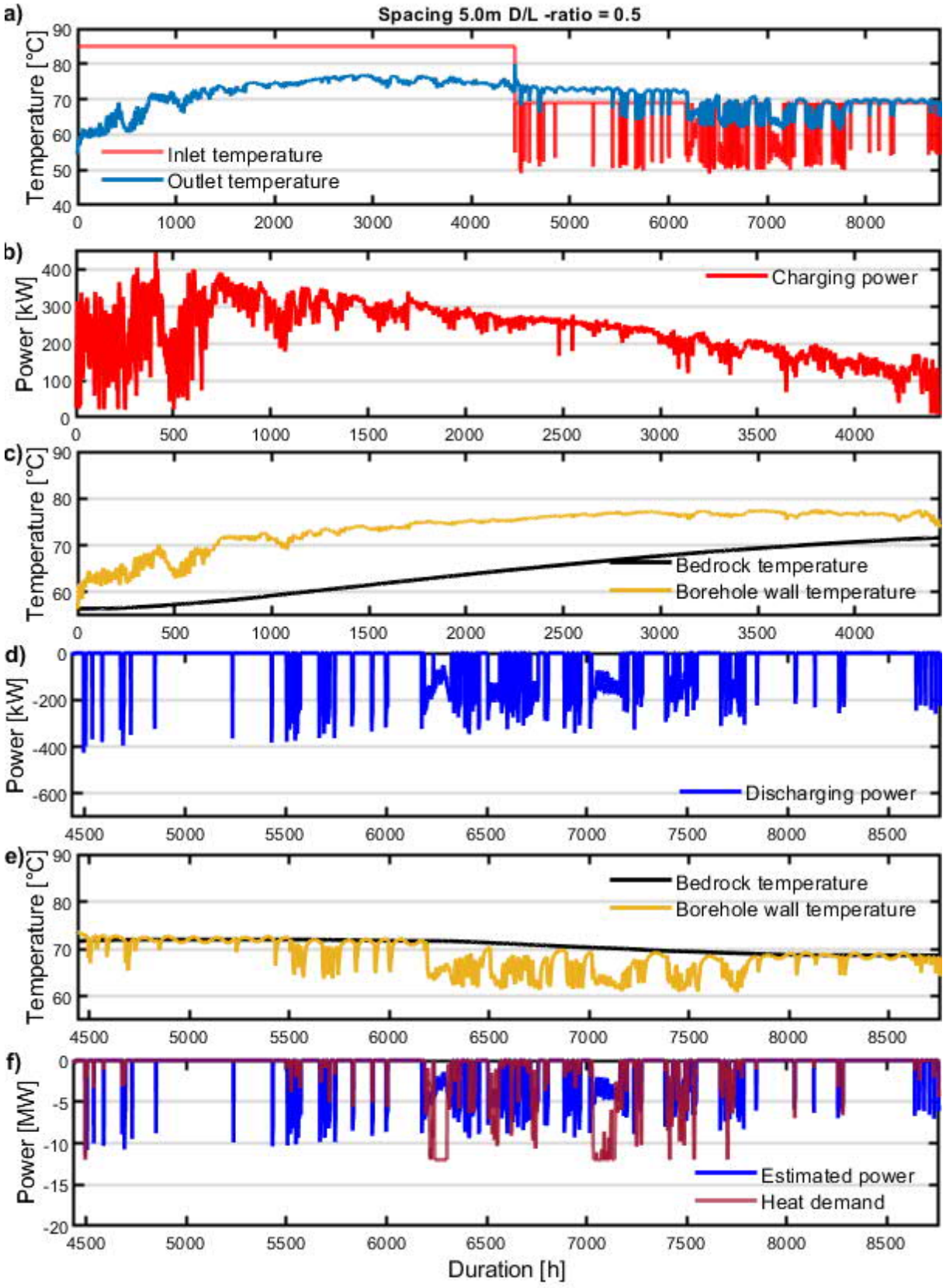
a)
Spacing 5.0m D/L -ratio = 0.5
Temperature [°C]
Inlet temperature
Outlet temperature
b)
Power [kW]
Charging power
c)
Temperature [°C]
Bedrock temperature
Borehole wall temperature
d)
Power [kW]
Discharging power
e)
Temperature [°C]
Bedrock temperature
Borehole wall temperature
f)
Power [MW]
Estimated power
Heat demand
Duration [h]

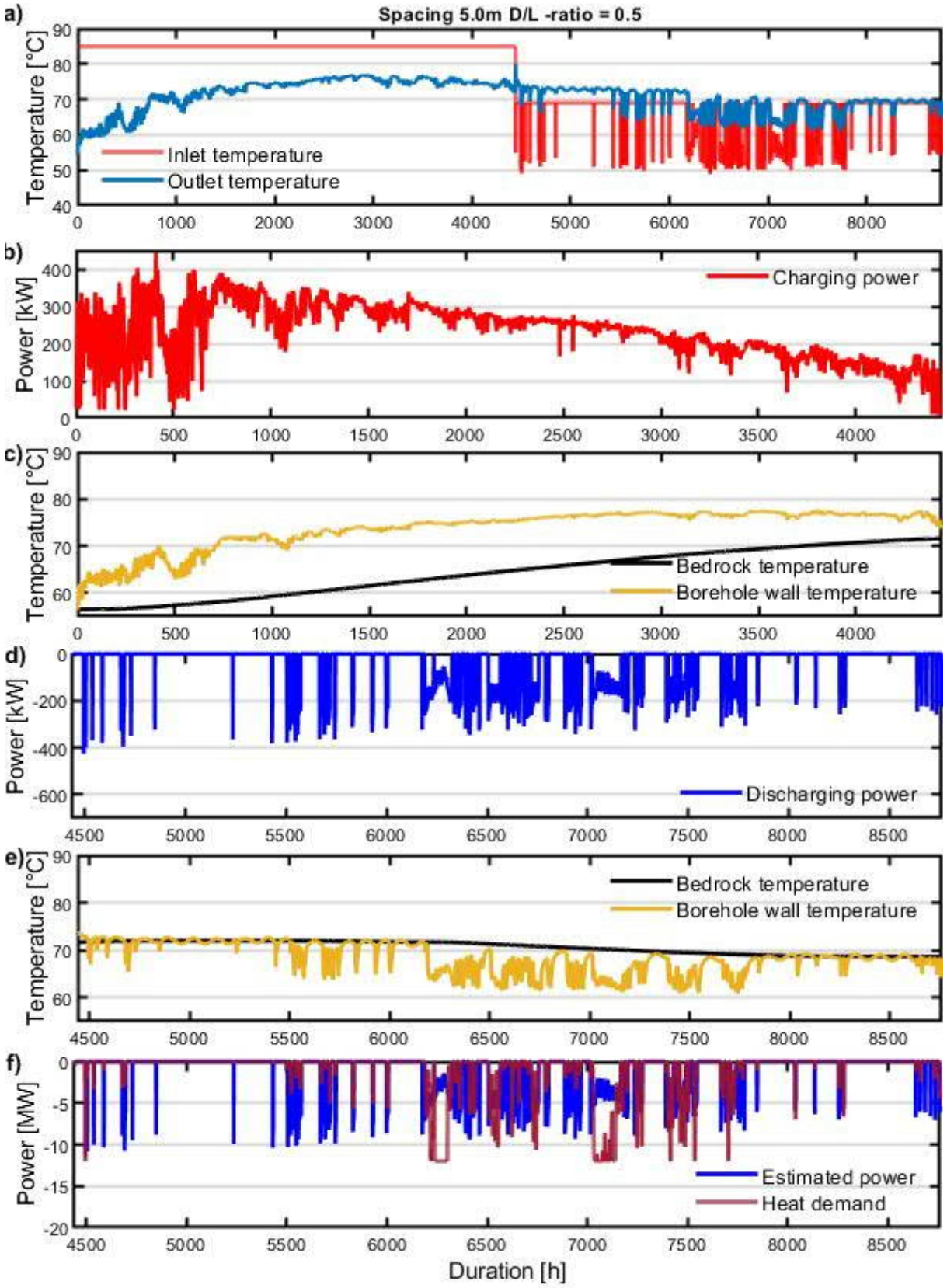
a)
Spacing 5.0m D/L -ratio = 0.5
Temperature [°C]
Inlet temperature
Outlet temperature
b)
Power [kW]
Charging power
c)
Temperature [°C]
Bedrock temperature
Borehole wall temperature
d)
Power [kW]
Discharging power
e)
Temperature [°C]
Bedrock temperature
Borehole wall temperature
f)
Power [MW]
Estimated power
Heat demand
Duration [h]